A STUDY OF VARIABILITY OF OPTICAL DEPTH AND RADIATIVE FORCING OF AEROSOLS IN DELHI NCR

Thesis submitted to Jawaharlal Nehru University

for the award of the Degree of

DOCTOR OF PHILOSOPHY

SUMANT KUMAR

SCHOOL OF ENVIRONMENTAL SCIENCES

JAWAHARLAL NEHRU UNIVERSITY

NEW DELHI-110067, INDIA

2016

जवाहरलाल नेहरू विश्वविद्यालय
Jawaharlal Nehru University
SCHOOL OF ENVIRONMENTAL SCIENCES
New Delhi - 110067, INDIA

July, 2016

CERTIFICATE

This is to certify that the research work embodied in this thesis entitled **"A study of variability of Optical depth and Radiative forcing of Aerosols in Delhi NCR "** has been carried out at the School of Environmental Sciences, Jawaharlal Nehru University, New Delhi in partial fulfillment for the award of the degree of Doctor of Philosophy. The work is original and has not been submitted in part or full, for any other degree or diploma in any institute or university.

Sumant Kumar.
Sumant Kumar

(Candidate)

Dr. Arun Srivastava

(Supervisor)

21/7/2016
Prof. S. Mukherjee

(Dean)

Prof. Saumitra Mukherjee
Dean
School of Environmental Sciences
Jawaharlal Nehru University

TEL 26741557, 26742575, 26742676 SES : 26741538 (Direct) 26704302, 4303, 4304

ACKNOWLEDGEMENTS

*I have great pleasure in presenting the thesis entitled "**A study of variability of Optical depth and Radiative forcing of Aerosols in Delhi NCR**" under the generous guidance and constant supervision of Dr. Arun Srivastava, School of Environmental Sciences (SES), Jawaharlal Nehru University, New Delhi.*

I express my deep sense of obligation and gratitude to Dr. Sagnik Dey (IIT, Delhi), who spared his valuable time in providing me his help, expert advices, constant encouragement and scintillating discussions. His love for research will be a never ending source of inspiration for me.

I would also like to thank all my teachers, who supported me at the time of course work. I am especially grateful to the members of my doctoral committee, Dr. Paulraj and Dr. Madhav Govind for their useful inputs throughout my Ph.D. I owe a special sense of gratitude to our dean Prof S. Mukherjee and all the teachers of SES. I would like to thank the office staff of SES for their cooperation and help. I am thankful to University Grant Commission for providing fellowship throughout the tenure of my work.

No words of thanks will be sufficient for Rajneesh Dwivedi, Ashwani, Ajay, Rupa, Ritu, Aniket and Navneet Kumar for their invaluable, consistent and unconditional support and suggestions throughout my research work. I would like to express special thanks to my senior Amit Kumar singh and labmates Himanshu and Rajesh for their support. I would like to thanks my juniors; Bipasha, Sunita, Naba, Akash, Anshul, Richa and Dundun Mehta for making the lab environment congenial. Om Prakash Jee need a special mention and thanks for maintaining the lab so well.

I thank my fellow classmates and friends Sonam Wangmo, Alok Pandey and Ram Pravesh for the stimulating discussions and all the fun we have had in the last several years. I would like to express special thanks to my friend Awadhesh Kumar Jha and also to my hostel juniors Gautam, Rakesh Kumar Singh, Rakesh, Sudisht and Sanjeet for his unconditional support, the present work would have not been possible in present shape without his valuable help.

The blessings of my parents, love of my elder brother Hemant Kumar, bhabhi Swati, younger brother Basant kumar and nephew Utshav, affection of all my near and dear ones was a source of immense strength that cannot be expressed in words. I am highly thankful to them for their unconditional love and emotional support throughout my life.

Sumant Kumar

Table of contents

S. No.	Chapters	Page No.
	List of Figures	
	List of Tables	
1	**Introduction**	1-28
	1.1 Climate system	1
	1.2 Earth's radiation budget	2
	1.2.1 Radiative forcing	4
1.3	1.3 Aerosols	5
	1.3.1 Aerosols characteristic	7
	1.3.2 Aerosol Impact on climate	10
	1.3.3 Aerosol Impact on Air Quality and Health	11
	1.4 International studies	14
	1.4.1 Ground-based studies	15
	1.4.2 Satellite-based studies	16
	1.4.3 Campaign- based studies	19
	1.5 National scenario of Aerosol	23
	1.6 Objective of the study	28
	1.7 Thesis structure	28
2	**Data and Methodology**	29-40
	2.1 Study Area	29
	2.2 Meteorological conditions	30
	2.3 Instrumentation	32
	2.3.1 MICROTOP-II, Sunphotometer	32
	2.3.2 Aethalometer	36
	2.4 Data	37
	2.5 Analysis	38
	2.5.1 Computation of aerosol optical properties	38
	2.5.2 Radiative transfer calculations	40
3	**Aerosol Climatology and Variation of AOD and BC and their**	41-53

	relation with Meteorological Parameters	
	3.1 Monthly climatology of MODIS derived AOD and intercomparision between deep blue and dark target approach	41
	3.2 Evaluation of deep blue and dark target AODs with MICROTOP-II at Delhi	43
	3.3 Monthly climatology of OMI derived UV index from 2005 to 2014	45
	3.4 Monthly climatology OMI derived Singly scattering albedo (SSA)	46
	3.5 Daily variation of AOD and BC	47
	3.6 Relation of AOD and BC with meteorological parameters	49
4	**Modulation of Aerosol Radiative Forcing during Extreme Events**	54-63
	4.1 General	54
	4.2 Aerosol characteristics during the campaign period	55
	4.3 Aerosol Direct Radiative Forcing (ADRF)	60
5	**Retrieval of $PM_{2.5}$ from AOD using Regression Approach for Air Quality application**	64-76
	5.1 General	64
	5.2 Regression Model adequacy check and validation studies	66
	5.3 Descriptive statistics	67
	5.4 Estimation of $PM_{2.5}$ using linear regression models	71
	5.5 Estimation of $PM_{2.5}$ using logistic regression models	74
6	**Aerosol characteristic during the festival period of Diwali**	77-85
	6.1 Variation of $PM_{2.5}$ concentrations	77
	6.2 Variation of BC and PM	78
	6.3 Variation of AOD and Angstrom Parameter	83
7	**Conclusion**	86-88
	References	89-104
	Publication	

List of figures

Figure No.	Figure Title	Page No.
1.1	Components of global climate system, their processes and interactions and some aspects that may change.	2
1.2	Earth's radiation budget	4
1.3	Radiative forcing due to gases, aerosols, clouds and external forces	5
1.4	Atmospheric cycling of aerosols	6
2.1	Map of the sampling site	30
2.2	Daily variation of wind speed (km/hr), temperature (^{0}c) and relative humidity (%) during the campaign period (2012)	31
2.3	Mean value of temperature, relative humidity, and wind speed four days before and after Diwali from 2009 to 2014.	32
2.4	MICROTOP-II Sunphotometer	34
2.5	Aethalometer (microAeth® Model AE51)	37
3.1	Monthly mean pattern of MODIS derived deep blue AODs at 550 nm wavelength	42
3.2	Monthly mean pattern of MODIS derived dark target AODS at 550 nm wavelength	43
3.3	Scatter plot between deep blue and MICROTOP-II	44
3.4	Scatter plot between dark target and MICROTOP-II.	45
3.5	Monthly mean pattern of MODIS derived UV index from 2005 to 2014	46
3.6	Monthly mean pattern of OMI derived SSA	47
3.7	Daily variation of average AOD_{500} for the year 2014	48
3.8	Daily variation of average BC concentration over JNU for the year 2014	49
3.9	Linear regression analysis of AOD with meteorological parameters	51
3.10	Linear regression analysis of BC with meteorological parameters	53
4.1	Mass fraction of various aerosol species during the 'relatively clean', 'normal' and 'extreme' aerosol days at Delhi NCR	55
4.2	Box plot of AOD at 500 nm wavelength during the 'relatively clean',	56

	'normal' and 'extreme' aerosol days at Delhi NCR	
4.3	Relative contribution of aerosol species to AOD at 500 nm wavelength during the 'relatively clean', 'normal' and 'extreme' aerosol days at Delhi NCR	57
4.4	SSA spectrum during the relatively 'clean', 'normal' and 'extreme' aerosol episodes at Delhi NCR	58
4.5	CALIOP-retrieval during its overpass on 28th March 2012 indicates presence of thick layer of aerosols over Delhi NCR spread up to 5 km. Aerosol sub-type identified is 'dust' and 'polluted dust'	59
4.6	Mean aerosol DRF at the TOA, surface and atmosphere during relatively 'clean', 'normal' and 'extreme' aerosol days	61
4.7	Relative contribution of aerosol species to total surface ADRF during relatively 'clean', 'normal' and 'extreme' aerosol days	62
5.1	Box plot of AOD at 550 nm wavelength from 2005 to 2014 at Delhi NCR	69
5.2	Observed $PM_{2.5}$ (2007-2012) and estimated $PM_{2.5}$ (2005-2014) during different months	70
5.3	Residual plots of linear regression model of set I	74
5.4	Residual plots of log linear regression model of set II	76
6.1	Box plot of $PM_{2.5}$ from 2009 to 2013 four days before and four days after Diwali	77
6.2	Daily average value of BC with standard deviation	78
6.3	Diurnal variation of BC from 21st to 25th October	80
6.4	Daily variation of fine and coarse particles	81
6.5	Percentage contribution of fine and coarse particles	82
6.6	Linear regression between BC and PM (a) fine and (b) coarse particles	82
6.7	Daily average value of AOD_{500}, α and α' with standard deviation	84
6.8	AOD variability at different wavelength	85

List of Tables

Table No.	Table Title	Page No.
1.1	Specific air pollutants and associated health effects	13
1.2	Effects of heavy metal constituent of particulate matter on human health	14
2.1	Specifications Of MICROTOP –II Sunphotometer	33
5.1	Descriptive Statistics of the of the data for Delhi capital	67
5.2	Descriptive statistics AOD_{MODIS}, $PM_{2.5}$ and $PM_{2.5}$/AOD at Delhi from the years 2005 to 2014	71
5.3	Statistical result of linear regression models	72
5.4	Statistical result of logistic regression models	75
5.5	Brief comparison of regression and validation results	76
6.1	Ambient aerosol mass concentrations of PM_{10} and $PM_{2.5}$ in $\mu g/m^3$at various locations measured by CPCB in 2014, on Diwali day	83

Dedicated to My

Beloved Parents and brothers

1.1 Climate system

The climate system is composed of five major components: the atmosphere, the hydrosphere, the cryosphere, the land surface and the biosphere. The climate system is influenced by various external factors, in which the most important is the Sun. In addition, direct effect of human activities on the climate system is considered an external forcing. The components of global climate system, their processes and interactions are shown in Figure 1.1. Among five major components most unstable component is atmosphere which is changes very rapidly. The atmosphere is composed of nitrogen (78.1% volume mixing ratio), oxygen (20.9% volume mixing ratio), and argon (0.93% volume mixing ratio). These gases do not interact with the incoming solar radiation and outgoing infrared radiation emitted by the Earth. Beside these gases, atmosphere also contains trace gases such as carbon dioxide (CO_2), nitrous oxide (N_2O), methane (CH_4) and ozone (O_3), which absorb and emit infrared radiation. These are called greenhouse gases, with total volume mixing ratio of less than 0.1% by volume, which play significant role in Earth's radiation budget. Furthermore the atmosphere also contains water vapor, which has volume mixing ratio highly variable and is in the order of about 1%. These greenhouse gases absorb the infrared radiation emitted by the Earth's surface and reemit radiation up and down and thus increase the temperature near the Earth's surface. Besides these gases, the atmosphere also contains solid and liquid particles, known as 'aerosols', and clouds, which interact with the incoming and outgoing radiation in a very complex and variable manner. Due to variable nature of interaction (physical, chemical and biological) among the various components of the Earth's climate system on spatial and temporal scales, making the system extremely complex. Any change in it, whether natural or anthropogenic (man made), in the component of Earth's climate system and their interactions, or in the external forcing, may possibly result in climate variations.

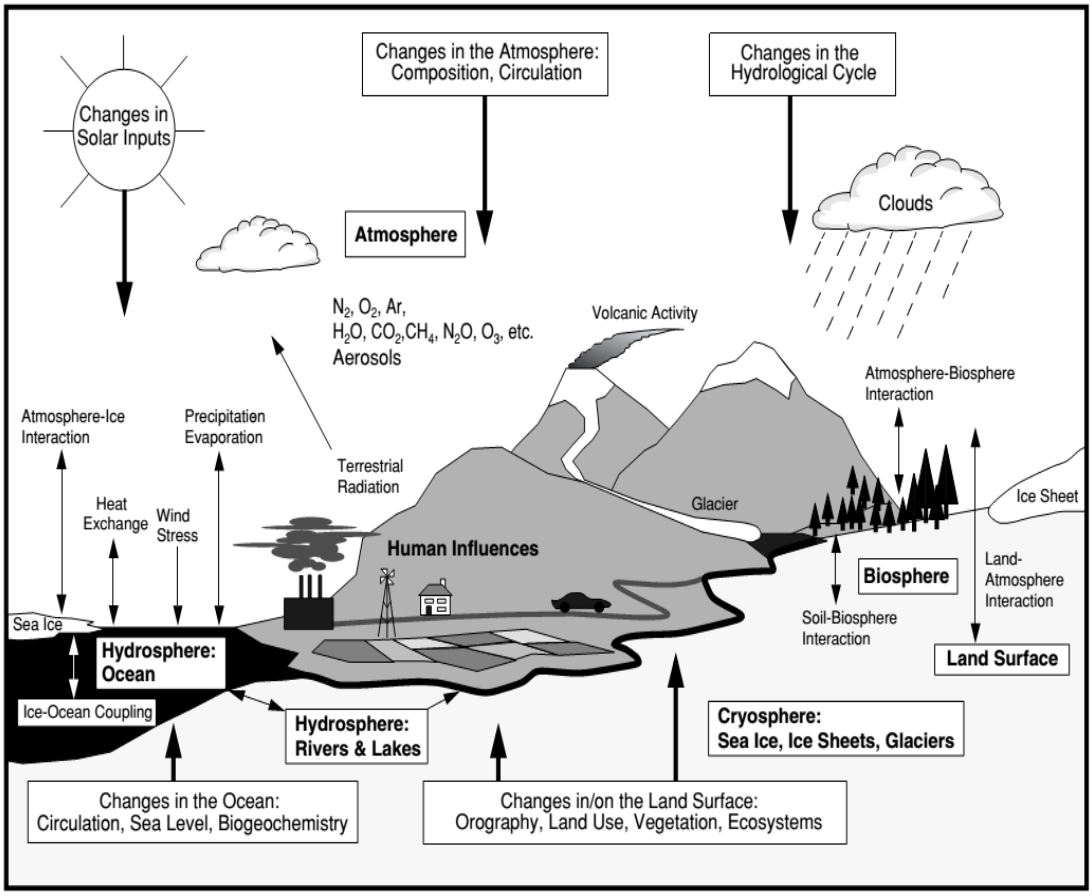

Figure 1.1 Components of global climate system (bold), their processes and interactions (thin arrows) and some aspects that may change (bold arrows).

1.2 Earth's radiation budget

The source of energy that drives the climate system is radiation from the Sun. In total radiation half of the radiation is in the visible (0.4-0.7 μm) short-wave part of the electromagnetic spectrum. The other half is mostly in the near-infrared, with some in the ultraviolet part of the spectrum. The mean annual radiation budget of the Earth's climate system is shown in Figure 1.2 (adopted from (Kiehl and Trenberth, 1997)). Each square meter of the Earth's surface outside the atmosphere receives an average of 342 W/m^2 of solar radiation throughout the year, out of which 31% is immediately reflected back into space by clouds, by the atmosphere, and by the Earth's surface. The rest 235 W/m^2 is partly absorbed by the atmosphere but mostly 168 W/m^2 warms the Earth's surface: the land and the ocean. Then, warm Earth's surface returns that heat to the atmosphere,

partly as infrared radiation partly as sensible heat and as water vapor which releases its heat when it condenses higher up in the atmosphere. This exchange of energy between surface and atmosphere maintains global mean temperature near the surface of 14^0C, which decreasing rapidly with height and reaching a mean temperature of -58^0C at the top of the atmosphere. To maintain balance in the Earth's climate system, the incoming radiation must be equal to the outgoing radiation. Earth's surface can not emit that much amount of energy in the infrared region. The Earth's surface temperature should become -19^0C to emit that much amount of energy, but it is not the reality in the present condition. To understand why this is happening, we must have to know the radiative properties of the atmosphere in the infrared part of the spectrum. The atmosphere contains several trace gases which absorb infrared radiation emitted by Earth's surface, the atmosphere and the cloud called greenhouse gases. These greenhouse gases trap heat within the atmosphere. This mechanism is called greenhouse effect. The net result is an upward transfer of infrared radiation from warmer lower level to higher level in the atmosphere. Clouds also play an important role in Earth's radiation budget, particularly in greenhouse effect. Clouds warm the Earth's surface by absorbing and re-emitting the infrared radiation and cooling effect on the atmosphere by reflecting back the infrared radiation. The net average effect of Earth's cloud cover is slight cooling, which compensate partly the greenhouse warming. However this effect is highly variable and depends on parameter like height, type and optical properties of clouds. On the other hand, aerosols produce net cooling effect on the Earth's surface as well as warm the atmosphere through scattering and absorption of solar and infrared radiation.

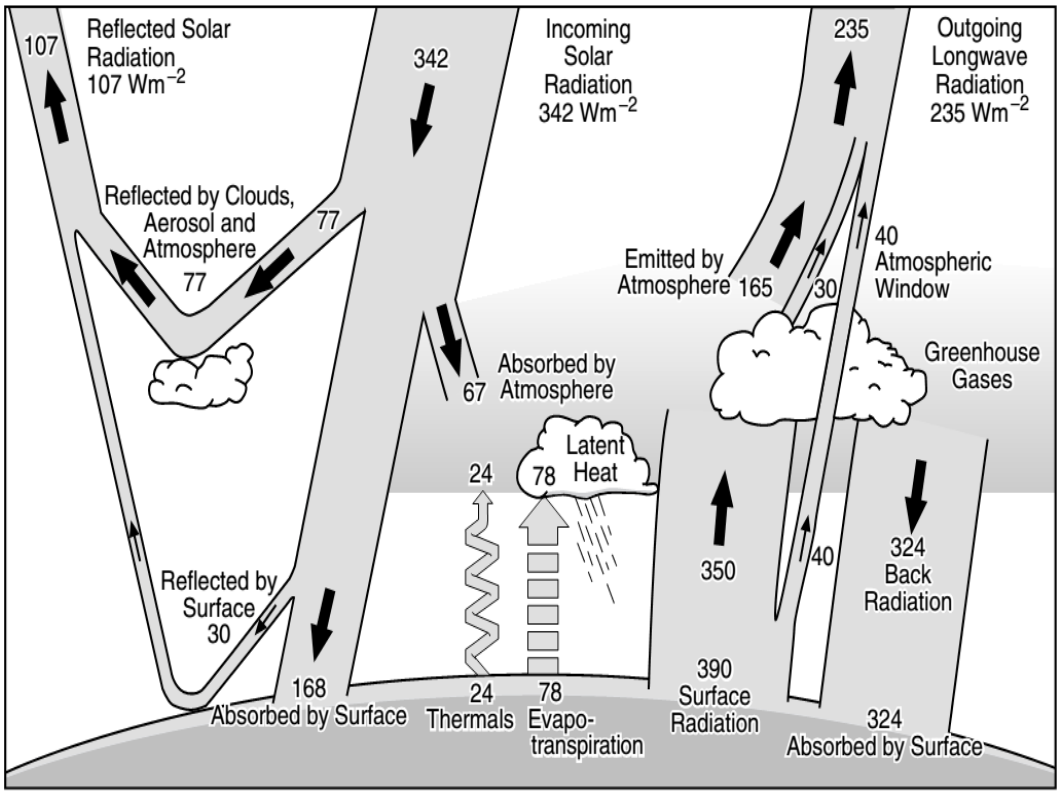

Figure 1.2 Earth's radiation budget (source: *Kiehl and Trenberth*, 1997).

1.2.1 Radiative forcing

When Earth's climate is in equilibrium, the net radiation (up minus down), at the top of the atmosphere (TOA) is zero. Any change in climate system altered the Earth's radiation budget is called radiative forcing. The word radiative arises because any factor that change the energy balance between incoming solar radiation and outgoing infrared radiation within Earth's atmosphere. The term forcing indicates that Earth's radiative balance is being pushed away from its normal state. Radaitive forcing is measured in W/m^2. When radiative forcing from a factor or group of factors is evaluated as positive, the energy of the Earth-atmosphere system will ultimately enhance, leading to warming of the system is called positive radiative forcing. In contrast, the energy will ultimately decrease; leading to a cooling of the system is called negative radiative forcing. It is difficult to quantify exact radiative forcing because physical, chemical and optical properties due to different component are extremely heterogeneous in time and space. Figures 1.3 illustrate the estimates of global mean TOA radiative forcing due to various

gases and aerosols present in the Earth's atmosphere (Ramaswamy et al., 2001). It is clear from figure that the warming effect (i.e. positive forcing) is caused by green house gases and tropospheric ozone and which is partly compensated by the aerosols and stratospheric ozone (negative forcing). Also, black carbon emitted from fossil fuel burning is causes positive forcing.

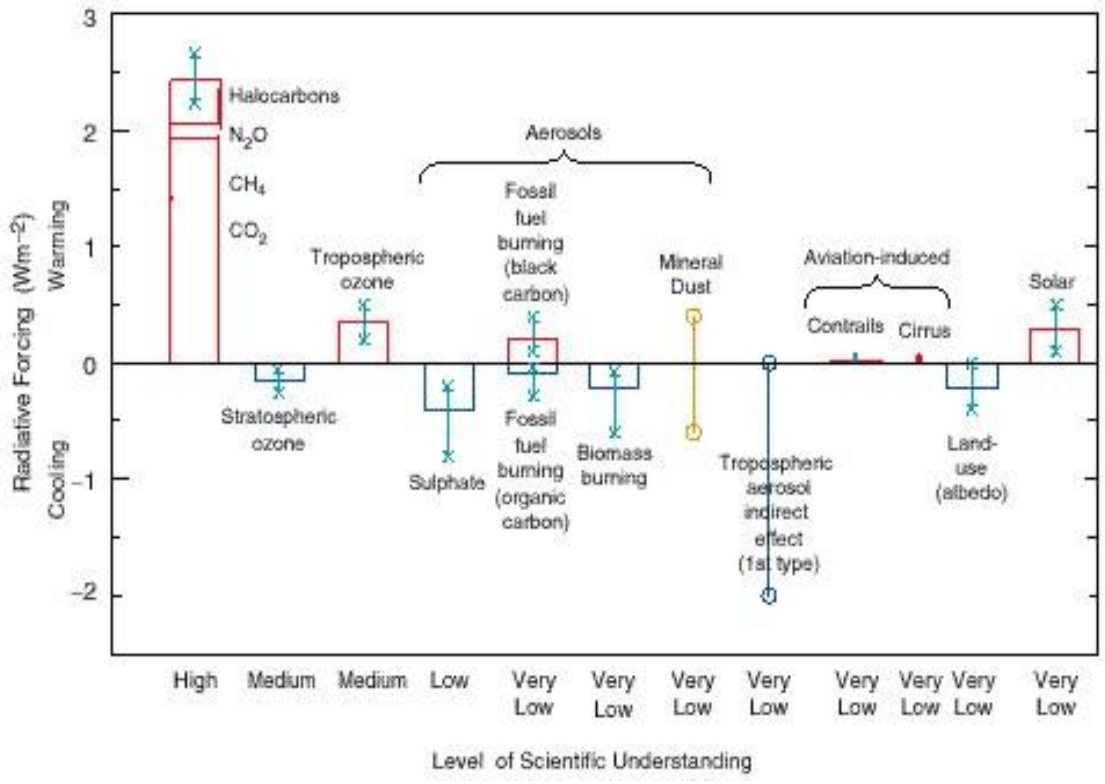

Figure 1.3 Radiative forcing due to gases, aerosols, clouds and external forces (source: *IPCC report*, 2001).

1.3 Aerosols

Aerosols are solid or liquid particles suspended in the air. Aerosols are emitted in to the atmosphere by natural (sea salt and wind borne dust) and anthropogenic activities (fossil fuel combustion [diesel and coal], open biomass burning, and cooking with bio-fuel etc). Based on the formation processes, aerosols are divided into primary and secondary. Primary aerosols (sea-salt emission from ocean surface, mineral dust emission from arid regions, and fly ash emission from the industrial activities) are emitted directly at the sources and secondary aerosols (sulfate aerosols from dimethyl sulfide emitted by

oceanic phytoplankton) are formed from gaseous precursors through various gas and aqueous phase reactions. Figure 1.4 illustrated the atmospheric cycling of aerosols. As illustrated in Figure 1.4, airborne particles undergo various physical and chemical transformations that change the particle size, structure, and composition (coagulation, restructuring, gas uptake, chemical reaction). Aerosols are removed from the atmosphere through dry and wet deposition and its life time in the atmosphere depends on size of the particles. The life time of the aerosols in the atmosphere is few minutes to several weeks. Aerosols are important atmospheric components both due to their impact on air quality and climate.

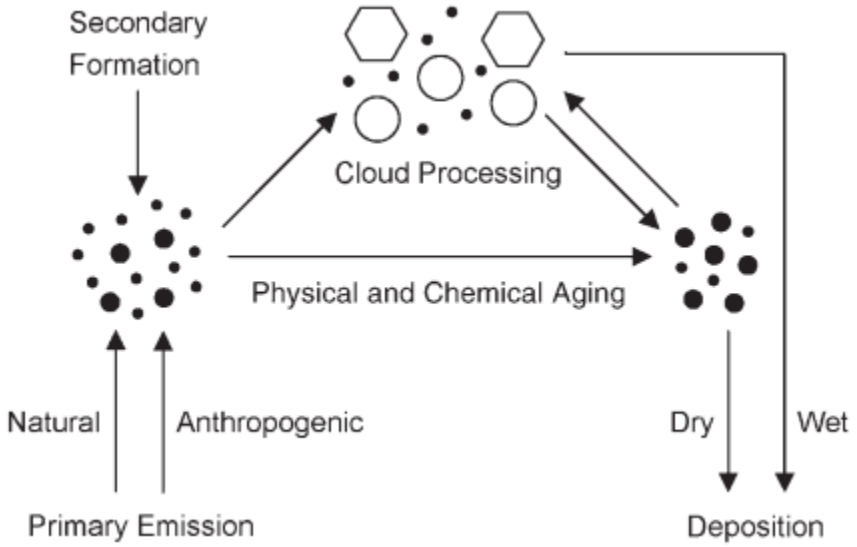

Figure 1.4 Atmospheric cycling of aerosols.

A category of aerosols, black carbon (BC), is optically absorbing and graphitic form of carbonaceous aerosols which is emitted into the atmosphere by various combustion processes such as industrial pollution, outdoors fires, traffic, and household burning of coal and biomass fuels. BC doesn't exist freely in the atmosphere; it is always bonded with some other aerosols particles such as sulphates, organics etc. Atmospheric aerosols containing BC can absorb in so far as 20-25% of the incoming solar radiation which leads to heating of the particles and local warming of the boundary layer of the atmosphere (Herrmann and Hänel, 1997) and thus most likely changing the temperature profile in the troposphere, which in turn affects the cloud microphysical properties and there by rainfall mechanism (Menon et al., 2002). It has been also reported that when BC become

hydrophilic it acts as a cloud condensation nuclei (Twomey, 1977) and therefore affects cloud cover and lifetime. Thus, the fraction of BC in total aerosol load in the atmosphere is critical to the aerosol radiative forcing at the Earth's surface and also at different level in the atmosphere. When atmospheric BC suspended near clouds then it contribute to cloud evaporation, termed as 'semi-direct effect' (Hansen et al., 1997). The enhancement in BC fraction can also change the surface albedo and the single scattering albedo (SSA) of the atmosphere, which leads to change in sign of aerosol radiative forcing (Solomon, 2007). When BC is deposited on snow then after receiving radiation it promotes snow-melt (Flanner et al., 2007) and further contributes to warming. Recently, BC has been used as an indicator of exposure to diesel soot (Fruin et al., 2004), which has been classified as a toxic air contaminant and a suspected carcinogen.

1.3.1 Aerosol characteristic

Aerosol is characterized by its optical, physical and chemical properties. The interaction of aerosols with radiation is studied by using three optical parameters: aerosol optical depth (AOD, τ), the single scattering albedo (SSA) and the phase function. Among these, one of the most important properties of aerosols is the Aerosol optical depth (AOD). It is dimensionless quantity that quantifies how efficiently a beam of radiation is weakened. It is defined as attenuation of solar radiation when passing through the atmosphere by scattering and absorption due to aerosols.

When a beam of light is attenuated, it is called attenuation extinction. Extinction is an outcome of scattering plus absorption. When aerosols scatter and absorb the light then attenuation due to aerosol is called aerosol extinction. Aerosol extinction weakens the light intensity from $I\lambda$ to $I\lambda + dI\lambda$ after traversing a thickness ds in the direction of its propagation. Where λ represents the wavelength. The following equation is obtained finally:

$$dI = -k\lambda\rho I\lambda \, ds$$

Where ρ is represents the density of the material, and $k\lambda$ denotes the mass extinction cross section (in units of area per mass). $K\lambda\rho$ is referred to as the aerosol extinction coefficient whose units are represented in term of length (cm^{-1}). The aerosol extinction

coefficient is aerosol scattering coefficient plus aerosol absorption coefficient. The aerosol extinction coefficient is a function of space (X-Y-Z), time (T) and wavelength. The aerosol optical depth τ is a vertical integral of the aerosol extinction coefficient from the earth surface (Sfc) to the top of the atmosphere (TOA), as follows:

$$\tau_\lambda = \int_{Sfc}^{TOA} k\lambda\rho dz$$

AOD is not a function of height. AOD is AAOD (Absorption Aerosol Optical depth) plus SAOD (Scattering Aerosol Optical Depth). AAOD (τ_a) is the vertical integral of the aerosol absorption coefficient. In other words AOD is column-integrated aerosol amount in an optical sense. When aerosol mass amount is doubled, AOD should also be doubled. It helps in deriving information of the optical properties and size distribution of particles as well as studying the diurnal and seasonal variability of aerosols by measuring AOD at different spectral wavelengths. AOD value is used to estimate aerosol radiative forcing. The largest contribution to global annual average AOD (0.12 at 550 nm) is from natural (58%), fossil fuel (26%) and biomass burning (16%).

Single scattering albedo is defined as the ratio of scattering coefficient to the extinction coefficient, measuring the relative importance of scattering and absorption. The effect of aerosol on the TOA radiative budget switches from net cooling to net warming at a certain value of SSA, depends on the surface albedo (Hansen et al., 1997). The SSA determines the degree of absorption and is a very important parameter in term of their radiative effects.

The angular distribution of scattering radiation is described by the phase function. It is a ratio of the scattered intensity at a specific direction to the integral of the scattered intensity in all directions. The phase function is defined in terms of asymmetry parameter (g). The value of g is 1 for completely forward scattering and 0 for symmetric scattering (e.g. Rayleigh scattering). Its value lies in the range of 0.5 to 0.8. It is most important input parameter for radiative transfer calculations.

The optical properties aerosol varies with the wavelength of radiation. The wavelength – dependence of aerosol optical depth is represented by Angstrom exponent. The high

value of Angstrom exponent indicates small size particles and low value indicates large size particles. Generally, at visible wavelength, for non dust aerosols the SSA decreases with wavelength and for dust aerosols increases with wavelength (Dubovik et al., 2002). The asymmetry parameter decreases with wavelength because of decrease in scattering-effective particle size (Hansen and Travis, 1974). Aerosol optical properties also depend on the size distribution i.e. any factors that affect size distribution will impact the optical properties. Among which relative humidity (RH) is one critical factor. Some aerosols are hygroscopic in nature i.e. they grow as they take up water vapor. As a result, their size increases then their refractive indices change which in turn leading to change in their optical properties. When RH increases twice, then the scattering cross section of sulfate-dominated aerosols doubles, whereas it increases by only 10-40% for same RH ranges (Kaufman et al., 1998b). For hygroscopic aerosol, SSA increases with RH and g increases with RH and particle size.

The physical characteristic of aerosols depends on concentration and size distribution. The concentration is expressed in number, area volume and mass concentrations. Aerosols particles present in the atmosphere have widely variable shape and their dimension is characterized by particle diameter. One of the most important parameters which describes the behavior of aerosols, affecting their life time, physical and chemical properties is particle size. The distribution of aerosol particles is defined by their number, surface or volume. On the basis of particle distribution, atmospheric particles are divided into nucleation mode, accumulation mode and coarse mode. Aerosol particles which have diameter below 0.1 μm constitute the nucleation (Aitken) mode. The smallest range of particles which have diameter below 0.01 μm is called ultrafine, produced by homogeneous and heterogeneous nucleation process. These particles are produced during gas-to particle conversion or during condensation of hot vapor in combustion process. The lifetime of these particles is very short (minutes to hours) due to their rapid coagulation or random impaction onto surfaces. The larger aerosol particles which have diameter in the size range 0.1 to 1 μm is called accumulation mode. The lifetime of these particles in the atmosphere is 7 to 10 days due to which it is transported to long distance from their sources. These particles are mainly formed by coagulation process or coagulation of vapors onto existing particles. They are also emitted into atmosphere from

different sources, mainly from incomplete combustion. They are removed by wet deposition. The aerosol particles which have diameter greater than 1.0 μm are called coarse mode particles. These particles are emitted into atmosphere during mechanical process from both natural and anthropogenic sources (e.g. sea-salt particles from ocean surface, soil and mineral dust, biological materials). They have short atmospheric lifetime due to relatively large mass and because of this rapid sedimentation.

The chemical composition of atmospheric aerosol is very complex and variable in nature. Each particle has individual composition due to various sources of emission and transformation. Generally, it is composed of sulphate, nitrate, ammonium, sea salt, crustal elements and carbonaceous compounds (elemental and organic carbon) and other organic materials. Fine particles predominantly have sulphate, nitrate, ammonium, elemental and organic carbon and certain trace metals (e.g. lead, cadmium, nickel, copper etc.). The primary components of coarse particles have dust, crustal elements, nitrate, sodium, chloride and biogenic organic particles (e.g. pollen, spores, plant fragments etc.).

1.3.2 Aerosol Impact on climate

Aerosols impacts on climate are generally classified as direct or indirect with respect to radiative forcing of the climate system. Aerosols scatter and absorb the solar and thermal infrared radiation, thus alter the radiative balance of the Earth-atmosphere system is termed as direct effect (Haywood and Boucher, 2000). Direct radiative forcing is defined as change in net radiative balance due to the perturbation by aerosols holding all atmospheric variables fixed (Haywood and Boucher, 2000). The difference between the TOA forcing and the surface forcing is known as atmospheric forcing.

Aerosols modify the microphysical and hence the radiative properties and life time of clouds is called aerosol indirect effect. Aerosol indirect effect is split into two effects: the first indirect effect and the second indirect effect. In first indirect effect (Twomey effect), whereby an increase in aerosols causes an increase in droplet concentration and a decrease in droplet size for fixed water content (Twomey, 1974). In second indirect effect, whereby decrease in cloud droplet size affects the precipitation efficiency, tending to increase the water content, the cloud life time and the cloud thickness (Pincus and

Baker, 1994). The first and second indirect effects are also known as 'cloud albedo' and 'cloud lifetime'. A latest review article (Lohmann and Feichter, 2005) have described the overview of indirect aerosol effects, climatic implications estimated their magnitude. The third assessment report of IPCC find out that the Twomey effect of anthropogenic aerosol particles amounts to 0 to -2 W/m^2 in the global mean (Ramaswamy et al., 2001). Absorbing aerosols, particularly BC impact climate after deposition to bright surfaces. When BC deposited onto snow and ice surfaces, it reduces the albedo of snow through which causes additional warming of climate (Hansen and Nazarenko, 2004). Earlier (Flanner et al., 2007) had reported that the snow-albedo forcing and associated feedbacks from all anthropogenic BC emission result in global warming (annual mean temperature) of between 0.1 and 0.15^0K, while (Jacobson, 2004) find out that fossil and biofuel sources individiually result in a warming of 0.03 to 0.11^0 K. On the whole impact of anthropogenic aerosol is cooling impact on climate. The fourth assessment report of IPCC estimated that total forcing of 1.2 W/m^2 from anthropogenic aerosol, partly satiating the warming of 2.6 W/m^2 from long lived greenhouse gases (Forster et al., 2007).

1.3.3 Aerosol Impact on Air Quality and Health

Aerosol impact on air quality has become matter of concern for everyone. According to the reports, aerosols play very crucial role in air quality. The impact of gaseous and particulate pollutant is measured by the effect on pollution receptors. For example, deposition of acidic pollutants on building can deteriorate its material, harm vegetation, damage the aquatic ecosystem, cause breathing problems and increase mortality rate among humans (Seinfeld and Pandis, 2016). Atmospheric aerosols reduce visibility. Fine aerosols which have diameter between 0.3 to 1.0 μm cause visibility reduction (Eldering et al., 1993; Trijonis et al., 1991). From 13^{th} to 20^{th} December 1952, high concentration of sulphur oxide and soot particles was responsible for 'London Smog', which led to over 4000 deaths (Noble and Prather, 1998). Moreover, the discovery of photochemical smog in the Los Angeles area in the mid-1940s have made high concentration of ozone and photochemical products and their impact on human health a major issue worldwide (Finlayson-Pitts and Pitts, 2000).

In pollution studies, particulate matter has recently become an issue due to its noticeable effects on human health. Coarse particles (2.5 µm < dp 10 µm) are efficiently removed in the upper respiratory track while fine particles (dp < 2.5 µm) are deposited on the bronchi walls in the bronchi trees (Akeredolu, 1996). Particles (dp <0.1 µm) get deposited in the bronchi through Brownian motion while particles with diameter 0.1- 1µm get deposited in the lungs as they are too large for Brownian motion and too small to be trapped in the upper part of the trachea, thus increasing airways resistance (Akeredolu, 1996). Aerosols impacts on health consist of both long-term acute symptoms like asthma and bronchitis and short-term chronic irritation and inflammation of the respiratory track, which can potentially lead to cancer. Fine particles get deposited in the lungs and causes lung cancer and cardiopulmonary mortality (Dockery et al., 1993; Pope III et al., 2002). The major health effects of particulate matters are breathing and respiratory symptoms, the aggravation of existing respiratory and cardiovascular diseases, the alteration of body's defense against foreign materials, damage to lung tissue, carcinogenesis and premature mortality. These types of health effects are more noticeable in the elderly and children than other age groups. The specific air pollutants including the particulate matter and their associated health effects is shown in table 1.1 (source: (Stern et al., 1984)) while table 1.2 (source: (Kimani, 2007)) shows the effects of heavy metal constituents of particulate matter on human health.

Table 1.1 Specific air pollutants and associated health effects

Pollutants	Effects
CO	Reduction in the ability of the circulatory system to transport O_2 Impairment of performance on tasks requiring vigilance Aggravation of cardiovascular diseases
NO_2	Increased susceptibility to respiratory pathogens
O_3	Decrement in pulmonary function Coughing; chest discomfort Increased asthma attacks
Peroxyacyl nitrates, Aldehyde	Eye irritation
SO_2/particulates	Increased prevalence of chronic respiratory disease Increased risk of acute respiratory disease

Source: Stern *et al.* (1984).

Table 1.2 Effects of heavy metal constituent of particulate matter on human health

Heavy metal	Environmental sources	Minimum risk level	Chronic exposure toxicity effects
Lead	Industrial and vehicular emissions, paints and burning of plastics, paper etc	Blood lead levels below 10 micrograms per deciliter of blood	Impairment of neurological development, Suppression of the hematological system (anemia), kidney failure, immunosuppression etc
Mercury	Electronic and Plastic wastes, pesticides, pharmaceutical and dental waste.	Below 10 microgram per deciliter of blood; oral Rfd 4 mg/kg/day	Gastrointestinal and respiratory tract irritation, renal failure, neurotoxic
Cadmium	Electronic, Plastic, batteries - diet and water.	Below 1 microgram per deciliter of blood	Local irritation of the lungs and gastrointestinal tract, kidney damage and abnormalities of skeletal system.
Arsenic	Herbicides and pesticides, electronics, burning of waste containing the element, contaminated water.	Oral exposure of 0.0003 mg/kg/day	Inflammation of the liver, peripheral nerve damage - neuropathy, cancer of the liver, skin and lungs, irritation of the upper respiratory system- pharyngitis, laryngitis, rhinitis, anemia, cardiovascular diseases.

Source: Kimani (2007)

1.4 International studies

Since the last two decades, the aerosol research has gained remarkable attention, once its importance in modifying the local, regional and global climate has been recognized. The data being collected from various platforms such as satellite, aircraft, ground- based instrument and campaign based study to know the different aerosol properties. Since aerosol characteristic vary globally, so purpose for the measurements is to feed the data into global models to reduce the uncertainty. A detail review of aerosol direct radiative forcing (DRF) and indirect radiative forcing came from (Haywood and Boucher, 2000), where authors summarized the workdone before the year 2000. After

that detail review on DRF came from (Yu et al., 2006), where they summarized the results focusing on satellite and ground-based measurements and modeling in DRF.

1.4.1 Ground- based studies

Ground based studies are most essential in estimating microphysical and optical properties of the aerosols in a particular region (Kaufman et al., 1994) and to validate the satellite measurements. It was carried out either in the continuous mode in fixed locations across the globe through various networks for a shorter period of time.

Various instruments have been developed to measure AOD directly with high precision, among which Aerosol Robotic Network (AERONET) was the first one, established with an aim to measure the optical properties in various environments across the globe continuously (Holben et al., 2001). AERONET network is a federated remote sensing network of well-calibrated photometers and radiometers. AERONET network includes about 200 sites around the world, which covers all major tropospheric regimes (Holben et al., 2001). AERONET network measures spectral AOD at 440, 670, 870 and 1020 nm wavelengths and provide inversion-based-algorithm retrievals of a variety of effective, column-mean properties such as SSA, and size distributions, phase function and asymmetry factor (Dubovik et al., 2002; Holben et al., 2001). The data from AERONET constitute a high-quality, ground-based aerosol climatology and, as such, have been widely used for aerosol process studies, as well as for evaluation and validation of model simulation and satellite remote sensing applications (Chin et al., 2002; Remer et al., 2005). AERONET networks cover urban areas, deserts, biomass-burning sites, maritime locations to retrieve aerosol optical properties at certain interval of time through direct and diffuse radiation measurement.

Besides AERONET, several other networks have been established with less geographical and spatial coverage or temporal coverage. These networks are AEROCAN, the Canadian counterpart of sunphotometer network (http://ccrs.hrcan.gc.ca/optic/aeroca_e.php), SKYNET, the Japanese network (http://atmos.cr.chiba-u.ac.jp/, (Kim et al., 2005), Multiwavelength Radiometer (MWR) network of Indian Space Research Organisation (Moorthy et al., 1999). The Integracy

Monitoring of Protected Visual Environment (IMPROVE) network measured spatial and temporal trend of visibility, composition and extinction of near-surface aerosol in rural areas and national parks of the US (Malm et al., 1994). Several multifilter rotating shadowband radiometer (MFRSR) quantify the direct solar beam extinction and horizontal diffuse flux at multiple wavelengths (Harrison et al., 1994). The European Aerosol Lidar Network (EARLINET) was used to characterize the horizontal, vertical, and temporal distribution of aerosols on a continental scale (Matthias et al., 2004). The Asian Dust Network (AD-Net) (Murayama et al., 2001) was used to monitor the transport of Asian dust distribution lidar systems in East Asia. In the Asian continent under Asian 'Atmosphere Brown Cloud' (Ramanathan and Crutzen, 2003), separate network of various instruments were used for the measurement of optical properties and surface radiative flux.

1.4.2 Satellite- based studies

The characterization of aerosols on a global scale can only be achieved through satellite remote sensing because of short lifetime of aerosols, complex chemical composition and interaction in the atmosphere that result in large spatial and temporal heterogeneities. Aerosols monitoring from space has been performed over two decades (King et al., 1999). The ability of satellite is to distinguish fine mode fraction from coarse ones is great advantage as it gives further information about the relative proportion of natural and anthropogenic contribution to the regional aerosol loading. Direct measurements and models gives information that anthropogenic aerosols mostly belongs to fine mode, whereas the natural aerosols dust and maritime belongs to coarse mode with significant fine mode fractions (Kaufman et al., 2005; Tanré et al., 2001). The primary aerosol parameter measured by satellite is the AOD. Early monitoring of aerosol through satellite used data from sensors that were designed for other purposes, e.g., Advanced Very High Resolution Radiometer (AVHRR) and Total Ozone Mapping Spectrometer (TOMS), among others. However, both of them provide multi-decadal climatology of AOD, which help in the understanding of aerosol distribution (Husar et al., 1997; Torres et al., 1998). Satellites have been measuring aerosols since the launch of TOMS in 1978. Previously it was used for ozone monitoring, which used two channels in

the ultraviolet wavelength region. Recently, it was found that TOMS are sensitive to aerosol absorption and not too sensitive to surface interferences, even over land (Torres et al., 1998). It is extremely successful in monitoring of biomass burning and smoke (Herman et al., 1997) and retrieving aerosol SSA (Torres et al., 2005). A new sensor which has improved over such advantage is OMI, aboard Aura.

Another satellite, AVHRR projected as a weather satellite, which monitor radiance in visible and near infrared wavelength that are sensitive to aerosol properties over the ocean. The first AVHRR was a 4-channel radiometer, carried on TIROS-N (launched on October 1978) then subsequently improved to 5-channel instrument and now its latest version is AVHRR/3, with 6-channel, onboard NOAA-15 launched in May 1998. Recently, new satellites measure the polarization and radiance at multiple wavelengths in the UV through the IR at fine temporal and spatial resolution. These satellites retrieved not only optical depth at one wavelength, but spectral optical depth and particle size over ocean and land as well as more direct measurements of polarization and phase function. Examples of such new and enhanced sensors are Polarization and Directionality of earth's Reflectance (POLDER), Moderate Resolution Imaging Spectroradiometer (MODIS), and Multiangle Imaging Spectroradiometer (MISR). POLDER is a special type of aerosol sensor that has wide field-of-view imaging Spectroradiometer capable of measuring multi-spectral, multi-directional, and polarized radiances. The observed multi-angle polarized radiance can be used to better separate the atmospheric contribution over both land and ocean (Deuzé et al., 2001). POLDER onboard the Japanese Advanced Earth Observation Satellite (ADEOS-1 and -2) has an ability to collect aerosol data over both land and ocean (Boucher and Tanré, 2000). A similar type of POLDER onboard the PARASOL satellite launched in December 2004. POLDER has limitation to coarse spatial resolution of about 6 km, which affects the ability to account for scene heterogenesis. Also, it is unable to retrieved larger aerosol particles such as desert dust quantitatively because unable to polarize the sunlight. MODIS onboard NASA'S twin satellite Terra and Aqua (cross the equator in opposite direction at about 10:30 and 13:30 local time respectively), retrieving near global AOD with higher spatial and temporal resolution. MODIS has separate algorithms over land and ocean (Remer et al., 2005; Tanré et al., 1997) and retrieved AOD with high accuracy of $\pm 0.05 \pm 0.2\tau$ over land (Chu

et al., 2002; Remer et al., 2005). MODIS has not only retrieving AOD with larger accuracy of ± 0.03 ± 0.05τ over ocean (Remer et al., 2005), but also retrieving quantitative aerosol size parameters (e.g. effective radius and fine-mode fraction of aerosols) (Remer et al., 2005). The standard deviation of MODIS effective radius is ± 0.11 μm in comparison to AERONET retrievals. MISR onboard Terra measures solar radiance in four spectral bands and at nine view angles which spread out in the forward and aft directions along the flight path (Diner et al., 2002). It also measures the daily global AOD over land and ocean. Its global coverage is about once per week.

The advantage of satellite derived aerosol product is that, it measures global distribution of aerosols in a snapshot. The main purpose of satellites is to provide continuous dataset of columnar aerosol properties in spatial and temporal scale in order to reduce the uncertainty in estimating their effect on radiation budget. So it is essential to validate the aerosol products with ground-based observations.

(Kaufman et al., 2000) gave detail overview and reported the use of satellite data to study the aerosols in climate system. Now, new satellite has capability to differentiate various aerosol types, e.g. biomass-burning aerosols, mostly absorbing and at fine mode mineral dusts, absorbing at the UV wavelength and mostly at coarse mode, maritime aerosols, scattering and mostly at coarse mode etc. (Bellouin et al., 2005) have used state-of-the-art based measurements of aerosols and surface wind speed to evaluate the clear-sky DRF over land and ocean for year 2002. They find out that clear-sky, global, annual average direct radiative forcing at the TOA is -1.9W/m^2 and standard deviation ±0.3. Natural aerosols (mineral dusts) and anthropogenic aerosols (biomass-burning) were identified for MODIS accumulation mode fractions (AMFs) between 0.35 ± 0.05 and 0.83 ± 0.05 and simultaneous TOMS AAI (aerosol absorbing index) greater than 1.0 ± 0.15. (Chung et al., 2005) has estimated anthropogenic aerosol DRF by using satellite data in combination with ground-based and model-based measurements on global scale. Their finding was that anthropogenic aerosol SSA varies in between 0.85 to 0.88, indicating absorbing nature of aerosols. They estimated global annual average anthropogenic aerosol DRF at TOA, surface and atmosphere were -0.35, -3.4 and + 3 W/m^2, respectively. The reduction of surface solar radiation was 10 times larger than that of

TOA. Asia and Africa account for 33.8% and 28.5% of the total reduction of solar radiation at surface, followed by South America (12.7%), North America (8.3%), Europe (6%) and the rest of the world (10.7%) (Chung et al., 2005).

1.4.3 Campaign-based studies

Many intensive field campaigns have been conducted worldwide to study physical, chemical, optical properties and radiative effects of aerosols in different aerosol regimes. These campaign based study have been designed for aerosol research and serve as a complement to the ground- based continuous measurements. Among these major campaigns and their finding are listed below.

Aerosol characterization experiment, ACE1 and ACE2 were designed to focus on natural aerosols and anthropogenic aerosols in remote marine atmosphere. ACE was designed to study how atmospheric aerosol particles affect the Earth's climate system (Bates et al., 1998; Seinfeld et al., 2004). ACE1 was conducted from November 15 to December 14, 1995 over southern hemisphere mid-latitudes, focused on maritime aerosol, relatively free of anthropogenic aerosols (Bates et al., 1998). The main goal of ACE was to understand the properties and controlling factors of aerosols in the remote marine atmosphere that are relevant to radiation balance and climate (Griffiths et al., 1999). ACE2 was conducted during July 1997 in the northeast Atlantic Ocean and focused to study the influence of anthropogenic pollution on the maritime aerosol radiative effect (Verver et al., 2000). The presence of maritime aerosols and absence of anthropogenic aerosol in ACE1 result in very high SSA (0.99 ± 0.01) (Quinn et al., 2000). In respect of natural aerosols, anthropogenic pollution (specifically absorbing black carbon, BC), result in lower SSA (0.9 ± 0.03).

In ACE2 concentration of submicron non-sea-salt sulfate during continental flow was higher by an order of magnitude than concentration during maritime flow. Also, marine aerosol concentration in ACE2 was larger by factor of four than concentration in ACE1. Hence the impact of sea-salt aerosols on composite aerosols properties is much smaller in ACE2.

Aerosol Characterization Experiment-Asia, ACE-Asia took place in the eastern Asia and Pacific region during spring of 2001 to characterize aerosol optical and radiative effects. ACE-Asia identified the range of clean, polluted, and duty aerosol conditions. During this campaign 40 field instruments have been used to measure aerosol chemical, physical and optical properties simultaneously (Kahn et al., 2004). For ACE-Asia a optical model is developed which reports for sulfate, organic carbon, black carbon, mineral dust and sea salt and then after aerosol DRF was estimated (Conant et al., 2003). The average surface forcing efficiency during that period was – 65 W/m^2 for dust which was pure and – 60 W/m^2 for clear skies pure pollution aerosol. During ACE-Asia Chemical Weather Forecast System (FORS) model was developed with radiative transfer model to calculate radiative forcing under clear and cloudy skies. Net DRF was – 3 W/m^2 at the TOA and – 17 W/m^2 at the surface. The forcing observed was alike to INDOEX. The efficiency of surface forcing during INDOEX (Ramanathan et al., 2001b) was – $72W/m^2T^{-1}$, compared to moderate forcing during Ace-Asia. ACE-Asia had low value of surface/TOA (clear-sky) forcing ratio (2.2/3) in comparison to INDOEX. This variation can be due to smaller fraction of BC aerosol present in the ACE-Asia. The all-sky (clear + clouds) average surface forcing during ACE-Asia was – 17 W/m^2 which is equivalent to – 14 W/m^2 surface forcing observed during INDOEX. The major difference between the radiative forcing of ACE-Asia and INDOEX was that the ACE-Asia is characterized by larger influence of dust and greater influence of high-level, midlevel clouds that reduce aerosol absorption as compared to predominant low level clouds in INDOEX that enhanced aerosol absorption as well as complex distribution vertically due to midlatitude frontal systems. Another important finding from this campaign is that mixing of anthropogenic components with natural dusts in form of coating (Conant et al., 2003). The coating of dust particles on BC was very common and this type of mixing has not significantly reduced the BC impact on total absorption.

Tropospheric Aerosol Radiative Forcing Observational Experiment, TARAFOX intensive campaign was conducted from July 10-31, 1996 in the Atlantic Ocean, where huge plumes of industrial haze comes from the continent (Russell et al., 1999). The measurements were carried out by satellites, aircraft and a modified (Cessna), ships and land sites. TARFOX measured an aerosol radiative forcing as well as chemical, physical

and optical properties of the aerosol. TARFOX determined the radiative forcing of various aerosol episodes, having mid-visible optical depths ranges from 0.07 to 0.6. TARFOX determined the forcing by using general circulation model (GCM) and find out that day time aerosol direct radiative forcing is in the range of – 50 to – 190 W/m^2 per unit mid-visible optical depth. The magnitude of forcing was about fifteen to hundred times the global-average of direct forcing. The reason behind the larger forcing during TARFOX was due to larger optical depths and the focus on cloud-free conditions during day time over the dark Ocean surface. The key finding of TARFOX was:

- Unexpected high concentration of carbonaceous compound in the U.S. mid-Atlantic haze plume and its carbonaceous mass fraction increasing with altitude (Novakov et al., 1997).
- Greater humification factors than earlier reported in aerosol climate effect measurements.
- Closure chemical mass equivalence between total aerosol and water, carbonaceous compound (organic and inorganic) and sulfate (Hegg et al., 1997).
- Near similar optical depth measured by MICROTOPS and computed airborne Nephelometer (Hegg et al., 1997).
- Chemical apportionment suggests dominant importance of water condensed on aerosol followed by carbonaceous material and sulfate (Hegg et al., 1997).
- Near similar value of radiative forcing computed through measured aerosol properties and those from aircraft measured (Hignett and Taylor, 1997).
- Internal closure was assessed by comparing in situ measured aerosol properties with those from chemical characterization and size distributions (Remer et al., 1997; Tanré et al., 1997).

Smoke, Clouds and Radiation-Brazil Experiment, SCAR-B was conducted in the Brazilian Amazon and cerrado region in August-September 1995 as collaboration between Brazilian and American scientists. SCAR-B was conducted to characterize the biomass burning, emphasized measurements of surface biomass, fires, smoke aerosol and trace gases, clouds, and radiation and their climatic effects. In this study aircraft and ground-based in situ measurements were used for characterization of smoke emission

factors and the composition, sizes, and optical properties of the smoke particles; studies of the formation of ozone; the transport and evaluation of smoke; smoke interaction with water vapor and clouds (Kaufman et al., 1998a). The key finding of SCAR-B was:

- Fires: For the measurements of size distribution MODIS air borne simulator (50 m resolution) and satellite sensors (e.g., AVHRR and MODIS with 1 km resolution) were used. MODIS Airborne simulator show that most of the fires are small (e.g. 0.005 km^2) but satellite sensors detect fires in Brazil are responsible for 60- 85% of the burned biomass.
- Aerosol: Smoke particles emitted from fires increases their radius by 60% during first three days in the atmosphere due to condensation and coagulation and reaching a mass median radius of 0.13-0.17 μm.
- Radiative forcing: Global radiative forcing was estimated to be – 0.1 to – 0.3 W/m2, based on the properties of smoke measured. Its value was smaller than previously modeled due to lower SSA (0.8 to 0.9), smaller scattering efficiency, and low humification factor.
- Effect on clouds: Approximately linear relationship was found between cloud condensation nuclei (CCN) and smoke volume concentration, thus an increase in the smoke emission is expected to affect cloud properties.

Southern African fire-Atmosphere Research Initiative, SAFARI was used to study the radiative effects of biomass generated aerosols and role of clouds in modifying the clear-sky aerosol DRF was also investigated. During this campaign AERONET data was used to study the aerosol optical properties (Eck et al., 2003). The aerosols emitted from burned biomass were found to exist in an elevated layer (1.8-3.7 km) and the BC mass fraction of 4.9% in the plume resulted in $SSA_{0.55}$ of 0.9 (Keil and Haywood, 2003). In clear sky condition, TOA and surface aerosol DRFs were found to be -13 and -24 W/m^2. When cloud layer altered by liquid path then in this condition the TOA aerosol DRF was +13W/m^2 and surface aerosol DRF was reduced to - 4.9 W/m^2, increasing the atmospheric absorption by 6 W/m^2.

Experience sur Site pour COntraindre les Mode 'les de Pollution atmospherique et de Transport d' Emission, ESCOMPTE campaign was initiated to generate data set for

testing and evaluating regional pollution models in Europe with an emphasis to produce more accurate emission inventory for the pollutants (Cros et al., 2004). From the size segregated chemical composition microphysical and optical properties were derived, which were further used to evaluate the mixing state of the aerosols in the region (Mallet et al., 2003). Comparison of the modeled derived SSA with the AERONET-retrieved values indicated external mixing to be the most probable mixing state.

Chesapeake Lighthouse and Aircraft Measurements for Satellite Experiment, CLAMS campaign was conducted to validate several satellite data products including aerosol and cloud parameters and radiative fluxes using data collected from ground-based and aircraft measurements (Magi et al., 2005). MODIS (Remer et al., 2005), MISR and Clouds and Earth's Radiant Energy System, CERES (Jin et al., 2005) data were used to inspect the critical role of aerosols in perturbing the Earth's climate system.

1.5 National scenario of Aerosol

The measurements of aerosols in India started in 1985, when multi wavelength radiometer (MWR) was developed and employed in Trivandrum (Moorthy et al., 1999). The instruments measured AOD at 0.38, 0.40, 0.45, 0.50, 0.60, 0.65, 0.75, 0.85, 0.932 and 1.025 μm wavelengths. In last 20^{th} century, the measurements in Indian subcontinent were mostly restricted in measuring spectral AOD using MWR network. After INDOEX (Ramanathan et al., 2001) results came out that huge pollutant transported from the south Asian land mass to the nearby oceanic regions affect the regional forcing considerably, and then after it is essential to focus on characterization of the aerosols over the south Asian region including Indian land mass and adjacent oceans has intensified. There are various publications on the aerosol radiative effects in this region, but most of them were restricted to the oceanic regions. It is impossible to list all studies, rather than important finding from all these studies and the present status in the understanding of the aerosol radiative effects are assessed.

In Delhi region, recently (Kumar et al., 2016) have quantified the ADRF during 'extreme aerosol days' in summer 2012. They have found that ADRF at the TOA increases from 21.2 W/m^2 (relatively clean to 56.6 W/m^2 (extreme), while enhancement in surface

ADRF is from -99.5 W/m^2 (clean) to -153.5 W/m^2(extreme). The dust of coarse mode contribution is 60.3% in the examined surface ADRF during 'extreme' days. Also, in same region by using satellite data (MODIS and MISR) aerosol characteristic have been reported (Srivastava et al., 2014). They found that a large difference in the direct radiative forcing efficiency at the TOA (by 25 W/m^2 per unit AOD) during the winter and pre-monsoon seasons as compared to other seasons. The ubiquitous presence of dust (fraction of non-spherical particle to AOD) is observed throughout the year. Long term (11.5 year) climatology of spectral AOD and its relation to the seasonal air mass have also been reported in Delhi (Lodhi et al., 2013). The pattern of climatology in Delhi shows that mean of monthly AOD at shorter wavelength peaks twice in June and November, as at longer wavelength peak once in June. The coarse mode particles dominate during summer and monsoon seasons, whereas fine/accumulation mode enhances during post-monsoon and winter seasons. The range of daily mean value of AOD_{500} was greater at Mukherjeenagar and Patelnagar (0.67-0.98) as compared to JNU (0.32-0.77) during the period of pre-monsoon have also reported in Delhi (Mishra et al., 2013). The diurnal variation of AOD_{500} and Angstrom exponent at JNU was affected with rush hours of traffic and find out that emission from vehicle as a major source of pollution. Aerosol radiative forcing during dust events over Delhi is also reported (Pandithurai et al., 2008). They reported aerosol optical properties, Angstrom exponent as well as real and imaginary refractive indices in the spectral channels. During this study period there was a continuous enhancement in AOD and SSA in pre-monsoon, indicates mixture of anthropogenic and desert dust absorbing aerosols. They also quantified surface forcing which was consistently increases from March (-39 W/m^2) to June (-99 W/m^2). The heating rate was also increases in same way. The heating rate in the lower atmosphere (up to 5 km) was 0.6, 1.3, 2.1and 2.5 k/d from March to June. The clear-sky aerosol radiative forcing over Delhi is also reported (Singh et al., 2010). They have found that monthly average AOD throughout the year vary in the range 0.56 to 1.22 with Angstrom exponent vary in the range of 0.38 to 0.96. A monthly average BC concentration in the range 4-15 μg/m^3 led to the monthly average SSA vary in the 0.90 ± 0.4 to 0.74 ± 0.3 during the year. The monthly average clear-sky DARF at surface was in the range of -46 ± 8 W/m^2 to -110 ± 20 W/m^2 and DARF at the TOA vary in the range of

-1.4 ± 0.4 to 21 ± 2 W/m^2, whereas in the atmosphere it was in the range of 46 ± 9 W/m^2 throughout the year. Ganguly et al. (2006b) have reported winter time aerosol properties during foggy and non foggy days over urban center Delhi. They found that average clear-sky aerosol optical depth value is 0.91 ± 0.48. The increases in AOD on hazy and foggy days are found to be spectrally non uniform. The diurnally average BC concentration during clear was 15 µg/m^3 and during hazy days 65 µg/m^3. The SSA at 525 nm wavelength varied between 0.6 to 0.8 with an average value of 0.68 for the entire period. The ADRF at the surface varied between – 40 to – 86 W/m^2 and at the TOA varied between – 2 to + 3 W/m^2. Srivastava et al. (2007) have reported contribution of anthropogenic aerosol in direct radiative forcing over Delhi. They estimated ADRF at the surface and atmosphere for composite aerosols to be about – 69, - 85, and – 78 W/m^2 and about +78, +98, and +79 W/m^2 during winter, summer and post-monsoon, respectively. The contribution of anthropogenic aerosols total surface forcing was ~ 90%, ~ 53%, and 84% and to total TOA forcing was ~ 93%, 54%, and 88% to the total aerosol atmospheric forcing during the above respective period. Bano et al. (2011) have found that BC concentration nearly double during cloudy-sky conditions as compared to clear-sky conditions at megacity Delhi. The seasonal variation showed that maximum average concentration of BC during the winter (25.5 µg/m^3) and minimum during the monsoon season (7.7 µg/m^3), with post- and pre-monsoon values at 13.7 and 9.4 µg/m^3, respectively.

The Indo-Gangetic basin (IGB) is the major polluted location inside the global, wherein anthropogenic and natural aerosols have distinct seasonal feature and mixing state (Dey and Tripathi, 2008; Singh et al., 2004). In IGB except anthropogenic pollutants, natural aerosols (normally dusts) also make a contribution to the nearby aerosol loading within the summer time months (Dey et al., 2004), which alter the aerosol optical properties and radiative effects. Di Girolamo et al. (2004) have reported that AOD at 0.55 µm remains high (>0.4) in the eastern part of the IGB during winter season. They also concluded that there is highest aerosol loading in IGB, but the nature of aerosols is different in winter (dominance of anthropogenic aerosol) and summer (dominance of natural aerosol) e.g. dust). Prasad et al. (2006) have reported that AOD in the major locations of the IGB is increased in the last few years. Singh et al. (2004) have reported that Angstrom exponent

(α) reveals two modes, α>1 for fine mode dominated aerosols, mostly in the season of winter and post-monsoon and α<1 for the coarse-mode dominated aerosols in the season of pre-monsoon and monsoon. The spectrally decreasing trend of SSA along with lower value (<0.9) in various seasons shows that the winter season is dominated by absorbing aerosols and increasing trend of SSA with wavelength in the pre-monsoon and monsoon season implies that dominance of dust aerosol. IGB was affected by several dust storms in the pre-monsoon season every year (Dey et al., 2004; Sikka, 1997). Dey et al. (2004) have examined the influence of dust events on the aerosol optical properties by using AERONET, satellite and surface based measurements of PM_{10} data. The dust events are responsible for increase in $AOD_{0.5}$ by 50-100% with reduction in α by 70-90%. The introduction of dusts increases the PM_{10} concentration by ~150 μg/m^3. The source of dust events in IGB are Thar desert of Rajasthan, western India, Gulf regions and arid regions of Pakistan and Afghanistan based on the air mass back trajectories analysis. Tripathi et al. (2007) analyzed the MODIS data over the Indo-Gangetic plain (IGP) to study the effect of AOD on the water (R_{eff}, w) and ice (R_{eff}, i) cloud effective radius for the period 2001-2005 and found that R_{eff}, w and R_{eff}, i shows reverse trend as that of AOD for most of time. The intensity of positive indirect effect is highest in winter, when the role of meteorology is least (Tripathi et al., 2007). The positive indirect effect in winter, pre-monsoon, monsoon and post-monsoon seasons is significant in 43%, 37%, 68% and 54% of area of water clouds; whereas the corresponding values for ice clouds are 42%, 35%, 53%, for the four seasons respectively. Dey and Tripathi (2007) have estimated the aerosol optical properties and radiative effects in the Ganga basin, during winter time and found that spectral variation of SSA in the coarse mode fraction suggests mixing of BC and dust particles. The mean shortwave clear sky TOA and surface forcing over Kanpur was estimated to be -13 ± 3 and -43 ± 8 W/m^2, respectively. The long wave forcing was 3.6 ± 0.7 and 2.9 ± 0.6 W/m^2, respectively. There are few studies on the measurements of aerosols parameters and estimation of radiative forcing over the Indian sub-continent exists in the literature. Ganguly et al. (2006a) have reported the aerosol physical optical properties and subsequently estimated the aerosol DRF for the period of 2002- 2005. They have reported high surface DRF during post-monsoon (-63 ± 10 W/m^2) and winter (-54 ± 6 W/m^2) seasons, whereas slightly less values in the monsoon (-41 ± 11 W/m^2)

and pre-monsoon (-41.4 ± 5 W/m^2) seasons. In respect of surface forcing, the TOA forcing during the post-monsoon (-22 ± 3 W/m^2) and winter (-26 ± 3 W/m^2) were negative, while positive during monsoon (+14 ± 4 W/m^2) and pre-monsoon seasons (+8 ± 2 W/m^2). Similar result were reported for DRF over Pune (Pandithurai et al., 2004), Banglore (Babu et al., 2002) and south India (Jayaraman et al., 2006). Latha et al. (2004) have reported that BC concentration is high during 6:00- 9:00 h and 19:00- 23:00 h at Hyderabad. Weekly variations of BC suggest that the day average BC concentration gradually increases from Monday to Wednesday and gradually decreases from Thursday to Sunday. The fraction of BC to total mass concentration has been observed to be 7%. Babu and Moorthy (2001) have reported the impact of extensive anthropogenic activity, associated with Indian festival event (Diwali), on the mass concentration of BC. They found that large increase in BC concentration by a factor of over 3 above the unperturbed background level. Ramachandran et al. (2006) have found that AOD is higher (0.63) in summer as compared to winter (0.31). SSA varies from ~0.7 during winter and post-monsoon to 0.93 in monsoon over Ahmedabad. The ADRF at surface and atmosphere in pre-monsoon and monsoon are ~50% lower than during winter and post-monsoon despite higher AODs. Atmospheric forcing is more positive for lower SSA and AOD; in contrast it is less positive for higher AOD and SSA. BC aerosol alone contributes 60% and 25% to shortwave and long wave atmospheric forcing. Seasonal mean heating rates higher than 1.5 k/d in winter and post-monsoon. A land campaign (LC I) was conducted by ISRO GBP across various locations in southern and peninsular India during February 2004 (Moorthy et al., 2005). Their results showed that high aerosol concentration (>50 µg/m^3) along the coastal regions and adjacent to the urban locations and lower mass concentration (<30 µg/m^3) in the semi-arid inner continental regions.

The studies over oceanic regions adjacent to Indian subcontinent was began in 1996 (Jayaraman et al., 1998; Krishnamurti et al., 1998). During INDOEX campaign measured average AODs were greater than 0.3 (Ramanathan et al., 2001) and anthropogenic sources from South Asia contributed as much as 75% to the AOD (Satheesh and Ramanathan, 2000). The average chemical compositions of the aerosols by mass were sulfate (32%), ammonia (8%), organics (26%), nitrates (10%), BC (14%), fly ash (5%), dust (10%), and potassium (2%). The measured SSA was 0.9 due to highly absorbing

hazes (Ramanathan et al., 2001). INDOEX campaign also revealed that reduction in surface solar radiation (surface forcing) is three times as large as the reflected solar radiation at TOA for clear skies, due to haze (Satheesh and Ramanathan, 2000). The surface forcing have been estimated -16 W/m^2, a consequence of large atmospheric absorption. There were lots of campaigns have been conducted after the INDOEX, over the Bay of Bengal, Arabian Sea and tropical Indian Ocean in various seasons and measured optical properties were used to estimate the aerosol DRF.

1.6 Objective of the study

In this thesis long term data of MODIS is used to know the aerosol climatology of Delhi region and aerosol properties are studied and DRF is estimated during extreme event. Also, a regression model is developed for the estimation of $PM_{2.5}$ regarding health related issue. Finally, aerosol characteristic is studied during the period of Diwali. To be precise, the objectives of this study are as follows:

I. Temporal variations of AOD and BC and their relation with meteorological parameter.
II. Estimation of aerosol radiative forcing.
III. Long term trend of aerosol loading over Delhi from satellite (TOMS/OMI).
IV. Impact on air quality using hybrid approach.

1.7 Thesis structure

This thesis begins with review of the major relevant works in aerosol DRF in global and regional scale, with special focus on the Delhi region in this chapter. Chapter 2 deals with the current work, including data analysis and methodology. Chapter 3 explain the long term loading of aerosol (aerosol climatology) in Delhi region by using MODIS and OMI data and its validation by ground-based measurement of the year 2014. Chapter 4 deals with the quantification of enhancement in ADRF during 'extreme aerosol days' in summer by using ground-based measurement of the year 2012. In chapter 5 a regression model is developed for the estimation of $PM_{2.5}$ for air quality application. In chapter 6 aerosol characteristic is studied during the festival period of Diwali.

2.1 Study Area

The study area is Delhi (28.6^0 N and 77.3^0 E), the capital city of India. It borders the Indian states of Uttar Pradesh on East and Haryana on west, north and south. It lies almost entirely in the Gangetic plains. Two prominent feature of geography of Delhi are the Yamuna flood plains and the Delhi ridge. It originates from the Aravilli Range in the south and encircles the west, northeast and northwest parts of the city. Yamuna is the only major river flowing through Delhi. Most of the city, including New Delhi, lies west of the river. East of the river is the urban area of Shahdra. Delhi falls under seismic zone-IV, making it vulnerable to major earthquakes. It is one of the densely populated cities in Asia (10,340 person's km^{-2}) and it is situated 160 km south of the Himalayas at altitude of 238 m above mean sea level. It is to be found in a semi-arid region and bounded by the Thar-Desert of Rajasthan in the west and plains of central India in the South. Its summer temperature reaches up to 45^0C during daytime and lowest temperature reaches up to 1^0C during winter in night. It has extreme temperatures range from -0.6^0C to 47^0C. The annual mean temperature is 25^0C; monthly mean temperatures range from 14^0C to 33^0C. The monsoon season is from July to September when there is a high humidity level. The city receives an average amount of rainfall approximately 611.8 mm. During pre-monsoon (March-June), recurrent dust storms from desert regions increases aerosol load which is responsible for reduction in visibility. During winter winds are mostly Westely or North-Westerly and Easterly and South-Easterly in monsoon. Delhi is notorious for its heavy fog during the winter season. In December, reduced visibility leads to disruption of road, air and rail traffic. The city has a pleasant climate from February to March and from September to November. Beside windblown dust in pre-monsoon this cities has vehicular load more than 10 times the average density of the country with more than 5.5 Million vehicles and its vehicular load increasing at a rate of 8 to 10%. In total population of Delhi, industry and domestic use contribute 12 and 8%, respectively. The site of study is JNU campus (latitude 28.21'to 28.53' N and longitude 76.20/ to 77.37/ E) which is shown in Figure 2.1. JNU is located at outskirts of southern part of Delhi. It is partly vegetative area and it is away from industrial activity and heavy traffic, thereby providing a site representative of regional aerosol characteristics, not influenced heavily by local pollution.

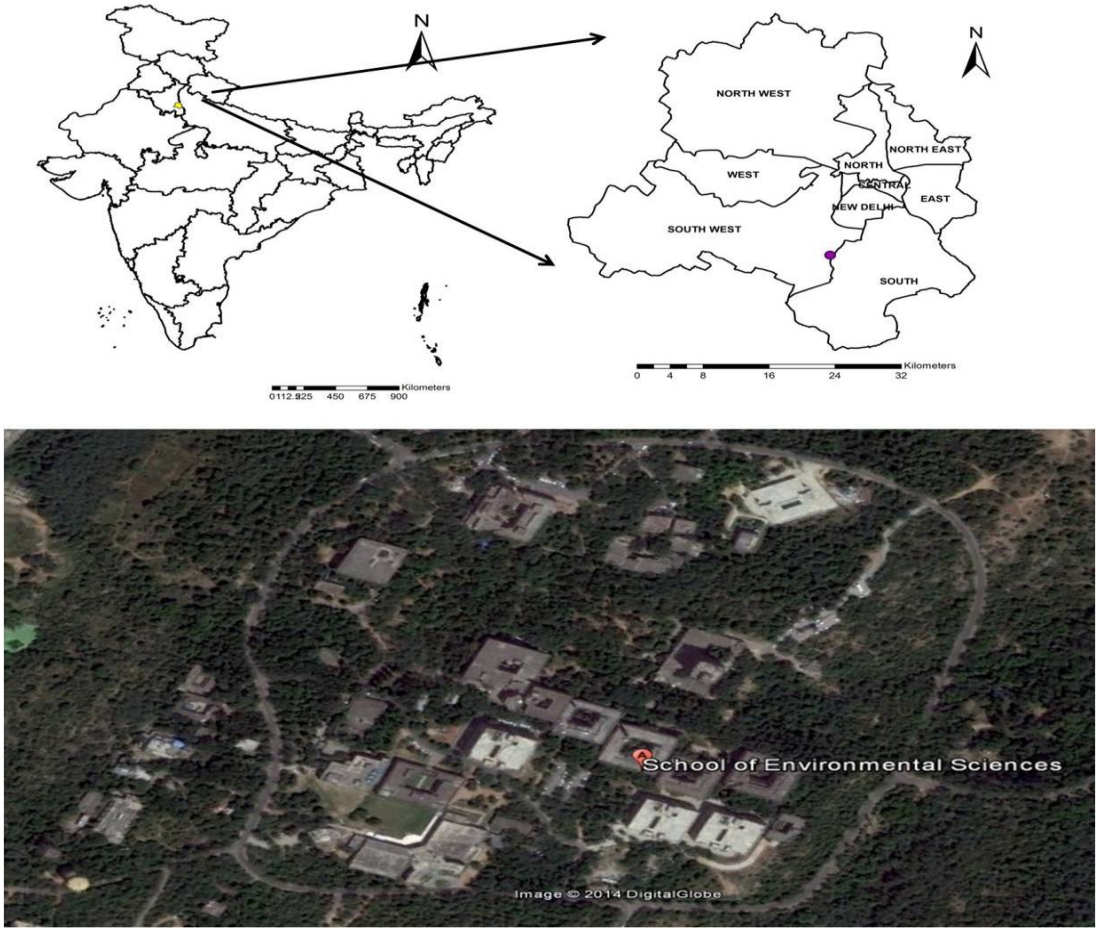

Figure 2.1 Map of the sampling site.

2.2 Meteorological conditions

The temperature (T), relative humidity (RH) and wind speed (WS) during the campaign period in pre-monsoon (2012) varied from 29° to 39°c, 14 % to 58 % and 1.9 to 13.4 km/hr respectively (Figure 2.2). The mean value of temperature, relative humidity and wind speed four days before and after the festival period of Diwali from 2009 to 2014 is shown in Figure 2.3.

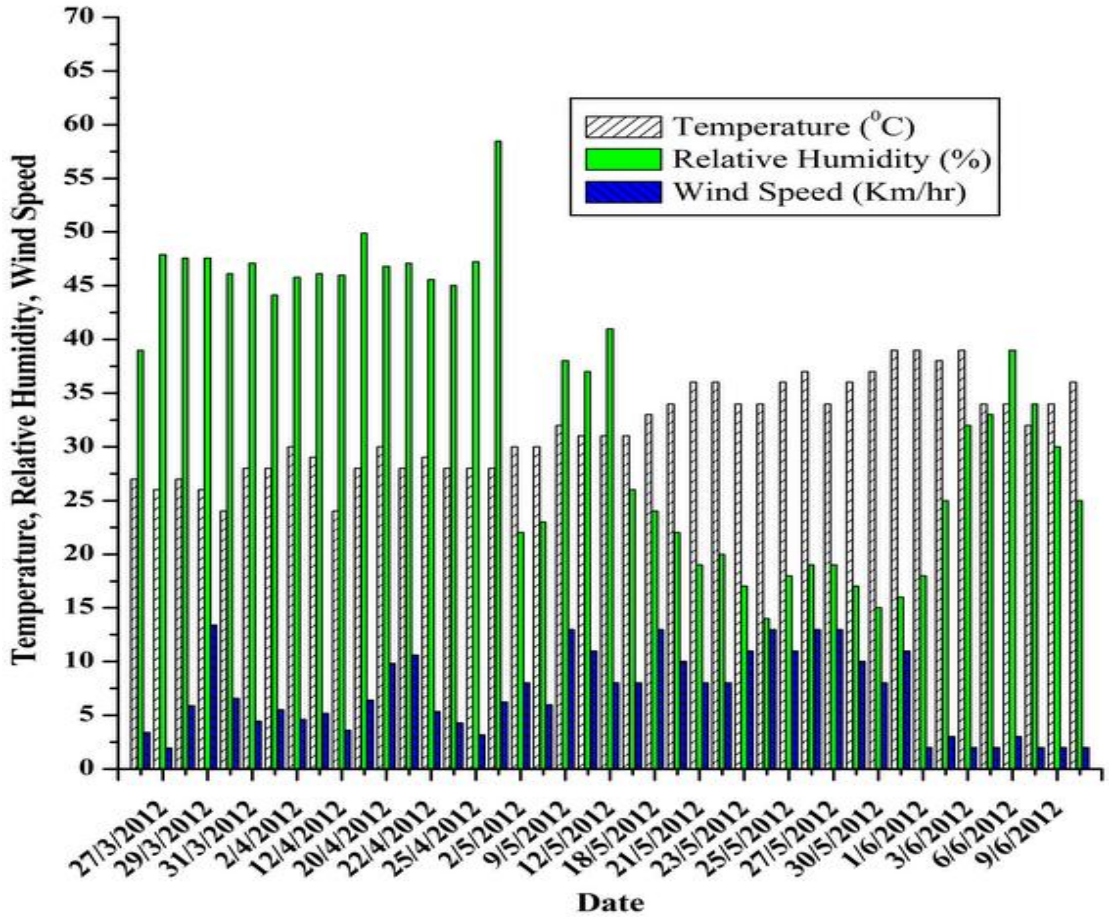

Figure 2.2 Daily variation of wind speed (km/hr), temperature (^{0}c) and relative humidity (%) during the campaign period (2012).

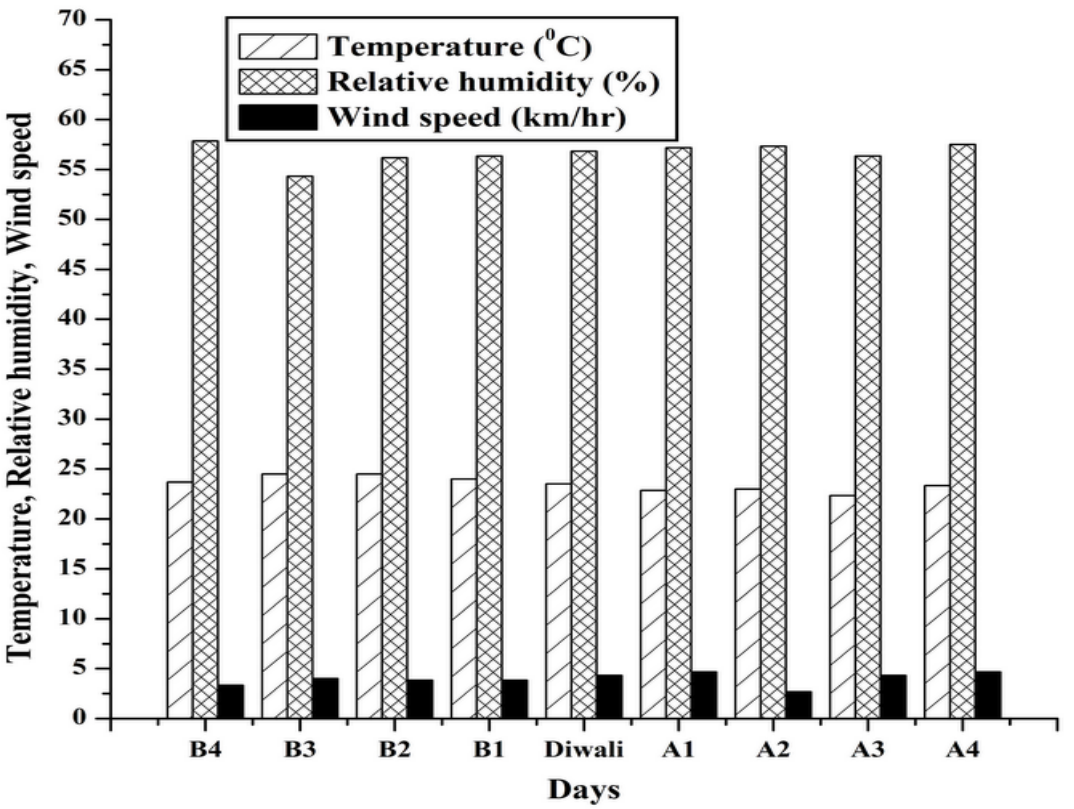

Figure 2.3 Mean value of temperature, relative humidity and wind speed four days before and four days after Diwali from 2009 to 2014.

2.3 Instrumentation

2.3.1 MICROTOP-II Sunphotometer

For this thesis, the aerosols optical depths (AOD) were measured with recently calibrated MICROTP-II Sunphotometer (Solar light Co., USA) at five wavelengths, 380, 500, 675, 936 and 1020 nm using narrow band of interference filters (Figure 2.4). It has an error margin of 0.002-0.021 in the visible to infrared wavelength range (Singh et al., 2010). Complete details about instrument and measurement technique can be found in users guide, MICROTOP-II Sunphotometer version 5.5, Solar Light Company Inc. The specification of the instrument is shown in the table 2.1.

Table: 2.1 Specifications of MICROTOP-II Sunphotometer

Optical channels	305.0±0.3nm, 2.4±0.4nm FWHM 312.5±0.3nm, 2.4±0.4nm FWHM 320.5±0.3nm, 2.4±0.4nm FWHM OPTIONAL 936±1.5nm, 10±1.5nm FWHM 1020±1.5nm, 10±1.5nm FWHM
Max. out-of-band sensitivity, rel. to peak transmission	305.0nm: 10^{-7} 312.5nm: 10^{-6} 320.5nm: 10^{-5} 936, 1020 nm: 10^{-4}
Angle of view	2.5°
Dynamic range	$>3*10^{5}$
Precision	1-2%
Non-linearity	Max. 0.002%
Operating environment	0-50°C, no precipitation
Computer interface	RS232
Data storage	800 records
Power source	4xAA alkaline batteries
Battery life	50hrs min. continuous operation (10 min. inactivity shutdown)
Weight	21oz (600 grams)
Size	4"W x 8"L x 1.7"D (10 x 20 x 4.3cm)

Figure 2.4 MICROTOP-II Sunphotometer

Theory of Sunphotometer:

Solar transmittance is calculated with the Beer- Bouguer- Lambert law:

$$I = I_0 \exp(-\tau m) \quad (1)$$

Where I_0 is the spectral irradiance value outside the atmosphere, τ is the total optical depth of the atmosphere and m is the optical mass, which is defined as the ratio of vertical total optical depth and the optical depth in specific direction.

Eq. (1) can be rearranged using voltages:

$$V = V_0 \exp(-\tau m) \quad (2)$$

To know the optical mass, consider the atmosphere to be plane (not spherical), which makes it easy to write this parameter as a function of solar zenith angle (θ) as,

$$m = 1/\cos(\theta) \quad (3)$$

Because of the Earth's curvature, refraction in air and multiple scattering, Eq. (3) fails beyond 60^0 of solar zenith angle. So, it is better to use other equation like (Kasten, 1965)

$$m = 1/ [\cos\theta + 0.50572 (1.46468-\theta)^{-1.6364}] \quad (4)$$

According to Beer-Bouguer-Lambert law, the total depth of the atmosphere is given by:

$$\tau = - (1/m). \ln (I/I_0) \quad (5)$$

The aerosol optical depth (AOD) is the essential parameter to know the aerosol optical properties. It indicates vertical distribution of aerosol in the atmospheric column. Its measuring range does not cover the other contribution like Rayleigh particles and gases; therefore τ represents the AOD in present Sunphotometer. The Sunphotometer was calibrated by Langley method, which is based on Beer-Bouguer-Lambert law. Since its measurement is obtained for each wavelength, so it is specified on the corresponding equation as a λ subscript, so:

$$I_\lambda = I_0 \exp(-\tau_\lambda m) \quad (6)$$

Where I_λ is the measured irradiance at the surface, $I_{0\lambda}$ is the extraterrestrial irradiance, corrected from the eart-sun distance, τ_λ is total optical depth of the atmosphere and m is the optical mass. Now eq. (6) can be written as:

$$\ln = \ln (I_{0\lambda}) - \tau_\lambda m \quad (7)$$

When, we keep total optical depth constant and the logarithm of measured irradiance is represented against the optical mass for a certain wavelength along a series of measurements, the result is straight line whose slope is the optical depth, and the ordinate at the origin corresponds to the extraterrestrial irradiance for that wavelength. This value will give the calibrating coefficient for that specific wavelength. If the extra terrestrial

signal in voltage or digital counts and the extraterrestrial irradiance are compared, then calibrating coefficient can be obtained to convert raw signal into physical units. These coefficients, as obtained from Langley fit depend on the earth-sun distance.

To calibrate initial hypothesis, the total optical depth is kept constant; in fact, the ideal conditions to perform a Langley calibration require a minimal variation in the total optical depth. These variations come out because of aerosols; thus, in order to obtain the least variation, places having low amounts of aerosol are sought where their variations are less in absolute terms.

2.3.2 Aethalometer

The Aethalometer (AE-51) manufactured by Magee Scientific, Barkley, California, USA is an instrument that provides real-time measurement of the concentration of the BC aerosol in an air stream (Figure 2.5). The Aethalometer measures BC using light beams from a high- intensity LED lamp at 880 nm wavelengths by measuring the attenuation of light transmitted through particles that accumulate on a quartz fiber filter paper. A vacuum pump draws air inside the instrument so that particles continuously accumulate on the filter paper. The optical attenuation, ATN, is defined as:

$$ATN=100*In\ (I_o/I)$$

Where I_o is the intensity of the light transmitted through the filter paper. I is the intensity of light transmitted through the portion of the filter on which the aerosol deposit is collected (Hansen et al., 1984). With an Aethalometer it is assumed that the ATN only increases due to light absorption by the accumulation of BC on the filter. Therefore, the BC concentration reported from the Aethalometer is calculated from the rate of change of attenuation, as below;

$$BC\ (Aethalometer) = A*\Delta ATN/\sigma_{ATN}*Q*\Delta t$$

Where, A is a collecting spot area, σ_{ATN} is the optical absorption cross section ("specific attenuation") of BC (m^2g^{-1}). ΔATN the change in attenuation during the time interval Δt. Q the volumetric flow rate ($1min^{-1}$), Δt is the sampling time (min.). The specific attenuation coefficient is the most important parameter for optical BC determination

using an Aethalometer (Petzold et al., 1997). The amount of BC deposited on the filter paper was derived at 5 min integrating time interval with flow rate of 100 ml/min. The instrument has been factory calibrated and the manufactures reports that error in the instrument is ±2%. More details about the instrument can be found in elsewhere (Hansen et al., 1984).

Figure 2.5 Aethalometer (microAeth® Model AE51)

2.4 Data

Remote sensing technologies in the recent days have provided tremendous advantage, to obtain numerous atmospheric and surface parameters globally. MODIS onboard NASA Terra/Aqua satellite retrieves AOD with 1 km spatial resolution in the visible to infrared region. In this thesis MODIS retrieved, Level 2 data product (1^0X1^0) is used for the analysis. MODIS derived AOD at 550 nm wavelength of deep blue and dark target is used for the period of 10 years (2005-2014). UV index which is an indicator of absorbing particle in the atmosphere is also used for the 10 years. The SSA at 388 nm wavelength

(2005-2014), total column ozone and surface albedo have been taken from Ozone monitoring instrument (OMI) Level 2G data products and water vapor has been taken from MODIS.

In- situ measured data of AOD for campaign based study in pre-monsoon (March to June) have been taken in 2012 at JNU. AOD and BC data is also taken in 2014. The measurement of AOD is done for every one hour during the day time from 09:30 to 17:30 h. The data is continuously taken to three times by ponting the instrument towards the Sun. Out of these measurements the one with minimum value of AOD at 500 nm wavelength was used for analysis. This was done for better pointing accuracy of MICROTOPS towards the Sun as minimum value of AOD corresponds to better accuracy at given time. The measurement of BC is also done from 09:30 to 17:30 h.

$PM_{2.5}$ data is obtained from ground-based air quality station of Income Tax office (ITO) from the website of CPCB (http://www.cpcb.nic.in). I have used daily 1hr means of $PM_{2.5}$ data when Aqua MODIS overpass the Delhi for the development of the model. Meteorological data has been taken from weather woundergound (www.woundergound.com).

2.5 Analysis

In this thesis for the calculation of ADRF two computational programs, namely Optical Properties of Aerosols and Clouds (OPAC) and Santa Barbara DISORT Atmospheric Radiative Transfer Model (SBDART) are used. The OPAC calculates the optical properties of aerosols, which is used as an input to SBDART, to calculate the ADRF. The details are described below.

2.5.1 Computation of aerosol optical properties

The Optical Properties of Aerosols and Clouds, OPAC package (Hess et al., 1998) is used for the calculation of aerosol optical properties. OPAC has two parts. The first part provides dataset of microphysical properties and gives optical properties of cloud and aerosols components at different wavelengths under different humidity conditions. The second part is a FORTRAN program which extracts data from dataset, to calculate

additional optical properties, and to calculate optical properties of mixtures of the stored clouds and aerosol components. The optical properties are calculated on the basis of the microphysical data (size distribution and spectral refractive index) considering spherical particles in case of aerosols and cloud droplets and hexagonal columns in case of cirrus clouds. OPAC also allows calculation of derived optical properties like mass extinction coefficient and Angstrom coefficients. The optical properties are calculated using Mie theory (Quenzel and Müller, 1978) for water droplets, aerosols particles, ice crystals in the terrestrial spectral range and with ray tracing for ice crystals in the solar spectral range (Hess and Wiegner, 1994), which are written in FORTRAN source code. The dataset provides the microphysical and optical properties for six types of water clouds, three ice clouds, and 10 aerosol components. OPAC allows calculation of the aerosol and water clouds optical properties at 61 wavelengths between 0.25 and 40 μm and at 8 R.H. (0, 50, 70, 80, 90, 95, 98, and 99%) values. The user can select any particular type of component out of total 19 aerosol and cloud components, each marked with definite numbers. If user want to create own mixtures, they can choose maximum up to 5 components. The number density is required for the calculation of optical properties. But few aerosol types have fixed number density, such as continental clean, continental average, continental polluted, urban, desert, maritime tropical, Arctic and Antarctic. For the calculation of AOD, the vertical profile of aerosol has to be defined by setting the lower and upper limit of mixing layer, mineral transported layer for long-range transport of mineral dust, free troposphere, stratosphere and cloud, along with aerosol scale height. Aerosol scale height and thickness of aerosol layer at delhi during the observation periods are taken from CALIOP retrieval aerosol vertical profiles for the corresponding period following (Srivastava et al., 2014). Mean aerosol scale height for the simulation is considered to be 1.9 km. Aerosol composition was fixed during this iterative process when the root-mean square error of simulated AOD at four wavelengths closest to the wavelengths at which AOD is measured (380, 500, 675, 936 and 1020 nm) drops below 0.025 to ensure a robust match relative to measured AOD spectrum (Dey and Tripathi, 2008). Through OPAC various optical parameters can be computed like b_{ext}, b_{sca}, b_{abs}, SSA, g, AOD, spectral turbidity factor, lidar ratio, phase function, mass extinction cross section, mass absorption cross section, normalized extinction coefficient, Angstrom

exponent, spectrally weighted coefficient, visibility and composite refractive index. However for radiative transfer calculations, b_{ext}, b_{sca}, b_{abs}, SSA, g and AOD are the essential parameters.

2.5.2 Radiative transfer calculations

Radiative transfer is calculated by using Santa Barbara DISORT Atmospheric Transfer Model (SBDART), which is developed by (Ricchiazzi et al., 1998). SBDART is a software tool that estimates plane- parallel radiative transfer in clear and cloudy conditions within Earth's atmosphere and at surface. In the SBDART, the radiative transfer equations are numerically integrated with Discrete Ordinate Radiative Transfer (DISORT) module (Stamnes et al., 1988). DISORT module uses numerically stable algorithm to solve the equations of plane-parallel radiative transfer in vertically inhomogeneous atmosphere (Ricchiazzi et al., 1998). Generally, six physical models are required as inputs to perform radiative transfer calculations using DISORT. These are atmospheric profiles, surface albedo, clouds, molecular absorption, aerosols and Rayleigh scattering.

In this thesis, we have used the aerosol spectral properties (SSA, asymmetry parameter and AOD) simulated by OPAC as input to SBDART. Other input parameters- total column ozone and surface albedo data have been taken from OMI Level 2G data products and water vapor has been taken from MODIS. Finally, diurnally averaged ADRF has been has been estimated following standard procedure demonstrated by numerous researchers e.g. (Dey and Tripathi, 2008; Srivastava et al., 2011).

3.1 Monthly climatology of MODIS derived AOD and intercomparision between deep blue and dark target approach

Box plot of MODIS derived monthly mean values of AOD at 550 nm wavelength of deep blue and dark target is shown in figure 3.1 and 3.2. Since the values were taken from 2005 to 2014 (10 years), the database is so robust to generate the climatological pattern. AODs of deep blue shows that highest values during post-monsoon period of October- November (0.96), decreases throughout the winter (December- February) (0.69) to reach low value in March (0.35) and increase continuously up to pre-monsoon (March-Jnue) (0.68) and reaches to lowest values in September (0.33) of monsoon season (July-September) (0.65). The high value of AOD during post-monsoon is due to inreased anthropogenic activities associated with festivals periods (Dushera and Diwali) which are responsible for the emission of fine/accumulation mode particles in the atmosphere. During that time, a period of second half of October to the first week of November, the extensive burning of fireworks and crackers produces large amount of aerosols in the atmosphere (Attri et al., 2001). The lowest value of AOD during monsoon is due to intense spells of rainfall which reduces the aerosol burden in the atmosphere. The impact of aerosol is more during winter due to poor horizontal and vertical distribution which hindered the removal mechanisms. This causes fine/accumulation mode particles dominated in the atmosphere. But during pre-monsoon when land gets dry due to intense solar heating, the atmosphere become conductive to pick dust from arid and semiarid regions of central and western India. The dust storm came from that region causes dominance of coarse- mode aerosol in the atmosphere which are responsible for reduction in visibility and radiation flux reaching the Earth surface during summer (Pandithurai et al., 2008; Singh et al., 2005). The desert dust came mainly from Iran, Afganistan, Arabian Peninsula, pakistan and Thar desert of India which changes the optical and radiative properties of aerosols over IGP region during summer (Dey et al., 2004; Gautam et al., 2009). This is responsible for high value of AOD during pre-monsoon specially from May to June.

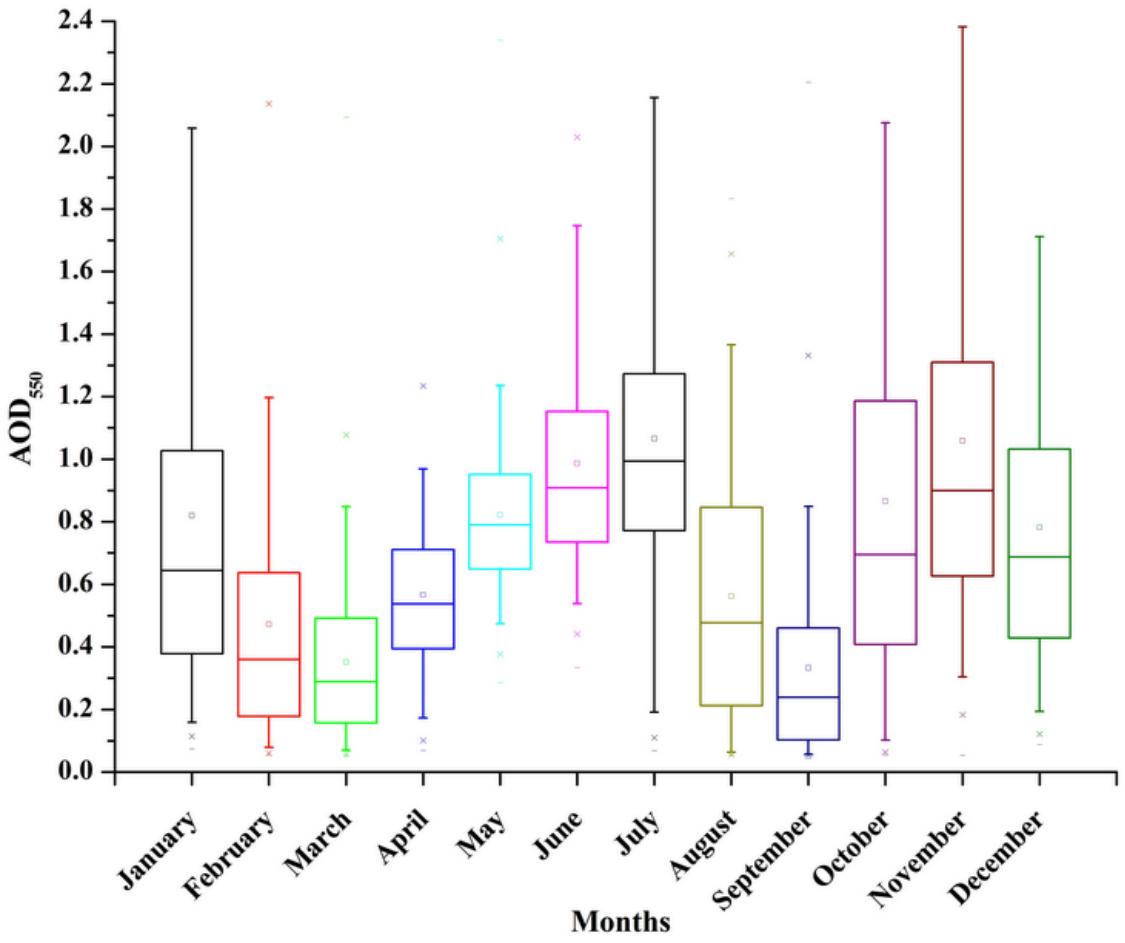

Figure 3. 1. Monthly mean pattern of MODIS derived deep blue AODs at 550 nm wavelength.

The climatological pattern of AODs at Delhi shows that the atmosphere is highly turbid thoughout the year which inform that contribution from local sources (either generated locally or confined to northwest India and IGP) plays a critical role in columnar aerosol loading (Dey et al., 2004; Gautam et al., 2007). Among the local sources, the emission from vehicle as well as frequent dust storms, specially in northwest India including western IGP are the major contributors of aerosol loading during the summer.

The similar monthly pattern is also observed through dark target (land only) at 550 nm wavelength but climatological pattern was different from deep blue. The AODs value of dark target shows maximum values during monsoon (0.82), minimum values during winter (0.63). The AODs value during pre-monsoon is 0.73 and during post-monsoon is 0.77, respectively.

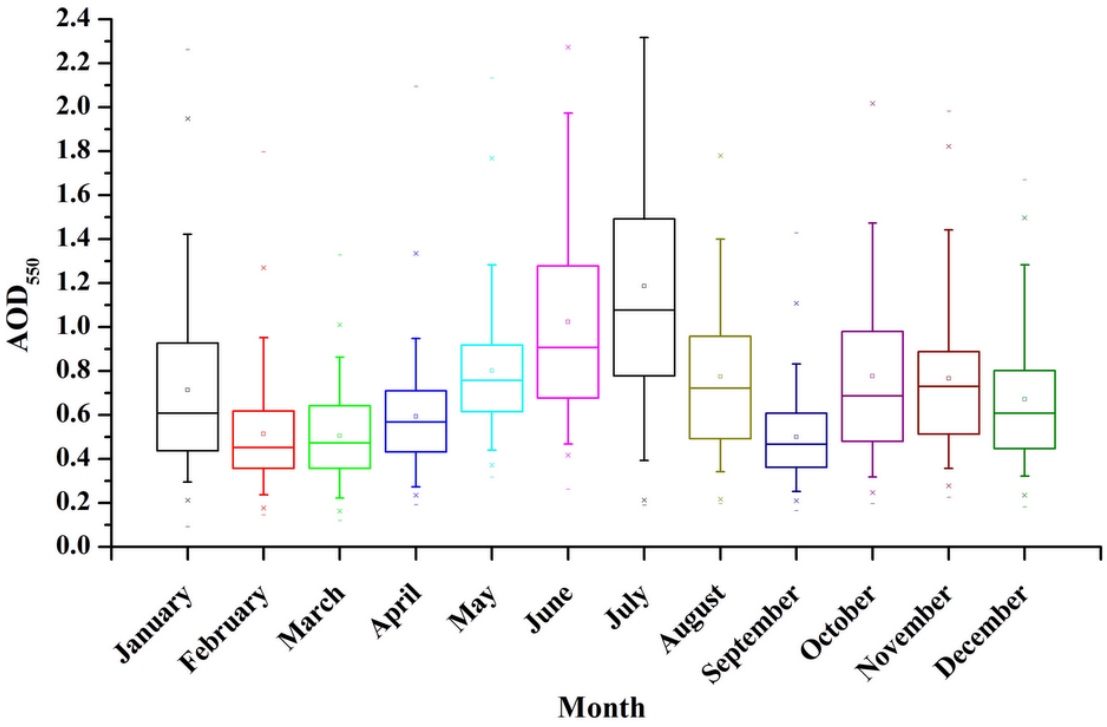

Figure 3.2. Monthly mean pattern of MODIS derived dark target AODS at 550 nm wavelength.

3.2 Evaluation of deep blue and dark target AODs with MICROTOP-II at Delhi

Since deep blue has better algorithm than dark target. To check which one is better between deep blue and dark target, we have plotted scatter diagram with measured MICROTOP-II values of AOD at 500 nm wavelength for the data of year 2014. Figure 3.3 and 3.4 shows the scatter plot between deep blue and dark target with MICROTOP-II. The coefficient of corelation (R^2) of deep blue and dark target with measured

MICROTOP-II values was 0.73 and 0.55, respectively. This shows that deep blue has better algorithm than dark target.

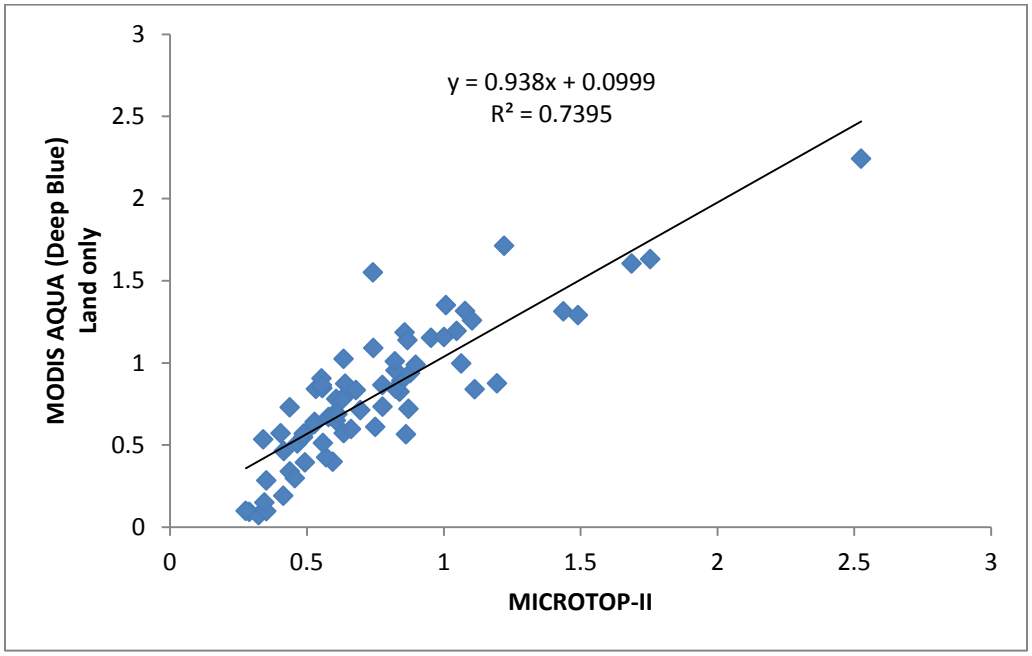

Figure 3.3. Scatter plot between deep blue and MICROTOP-II.

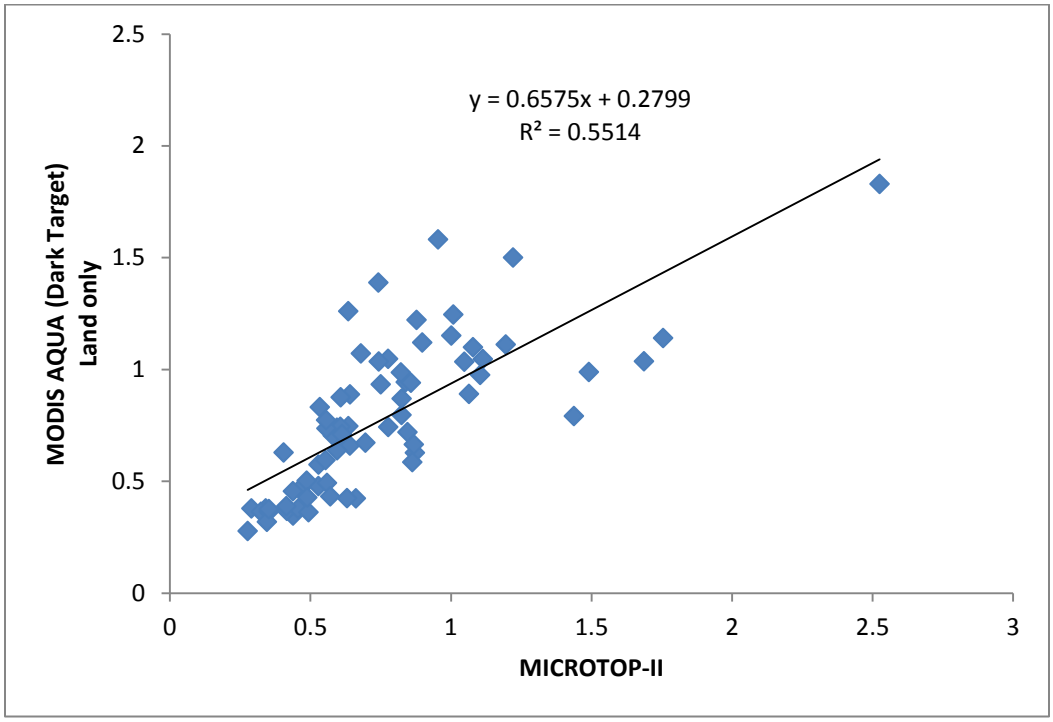

Figure 3.4. Scatter plot between dark target and MICROTOP-II.

3.3 Monthly climatology of OMI derived UV index from 2005 to 2014

UV Index which is an indicator of absorbing particle in the atmosphere. Box plot of monthly mean values of UV index from 2005 to 2014 is shown in figure 3.5. The climatological pattern shows that its mean value was maximum during pre-monsoon (1.67) and minimum during monsoon (0.92). The values during post-monsoon and winter was 1.41 and 0.99, respectively. The greater values of UV index in pre-monsoon is due to forest fire in nearby area. The lowest value during monsoon is due to intense spells of rainfall which reduces aerosol loading. Monthly pattern shows that its mean value was maximum in the month of May (2.08) and minimum in the month of September (0.79).

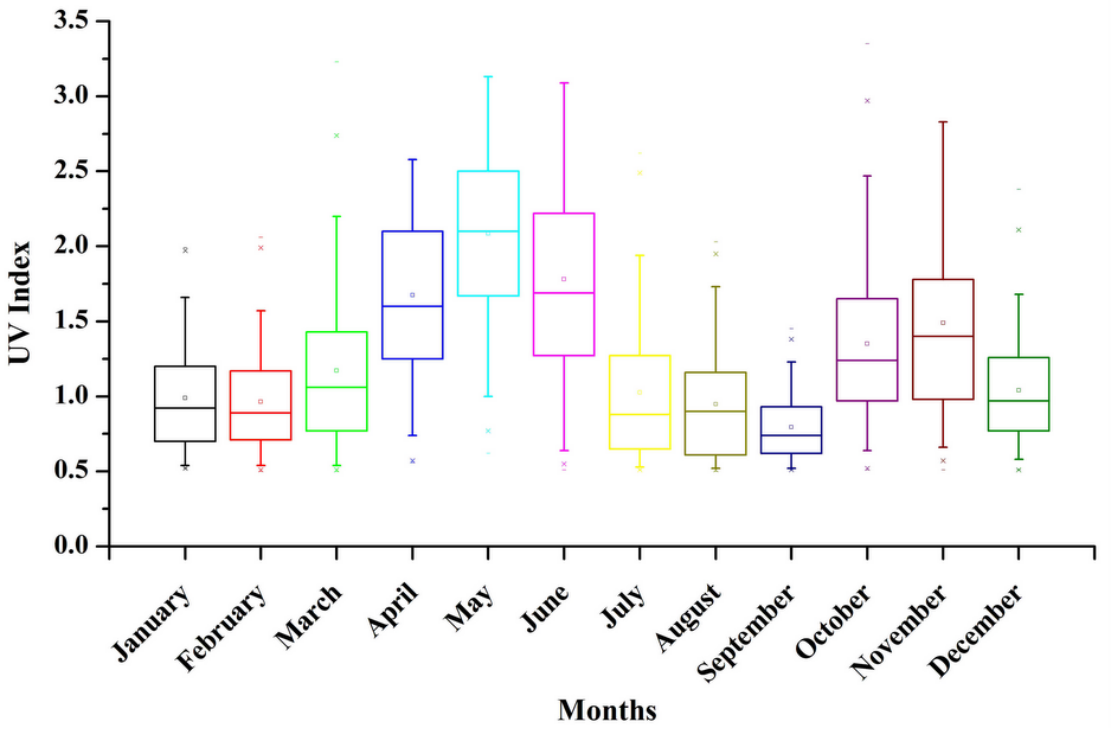

Figure 3.5. Monthly mean pattern of MODIS derived UV index from 2005 to 2014.

3.4. Monthly climatology OMI derived Single scattering albedo (SSA)

Figure 3.6 shows the monthly mean pattern of single scattering albedo (SSA) at 388 nm wavelength which was derived from Ozone monitoring instrument (OMI). Aerosol SSA is defined as ratio of scattering efficiency (Q_{scat}) to the extinction efficiency (Q_{ext}) and extinction efficiency is ($Q_{scat} + Q_{abs}$). The scattering and absorption cross sections per unit area of the particle are called scattering and absorption efficiencies. The climatological pattern shows that mean values of SSA was maximum during monsoon (0.981) and minimum during pre-monsoon (0.939) and during post-monsoon and winter it was 0.940 and 0.976, respectively. The monthly mean pattern shows that its value was maximum during the month of September (0.980) and minimum during the month of May (0.920). The high value of SSA during monsoon is due to low concentration of BC and atmosphere has more water soluble particles which have higher SSA. But we have seen that there is no specific pattern of OMI derived SSA during these time period because value of SSA is more than 0.9 in every months. Since satellite derived SSA does not give exact value. So OPAC model is being used to derive the SSA by using measured AOD value.

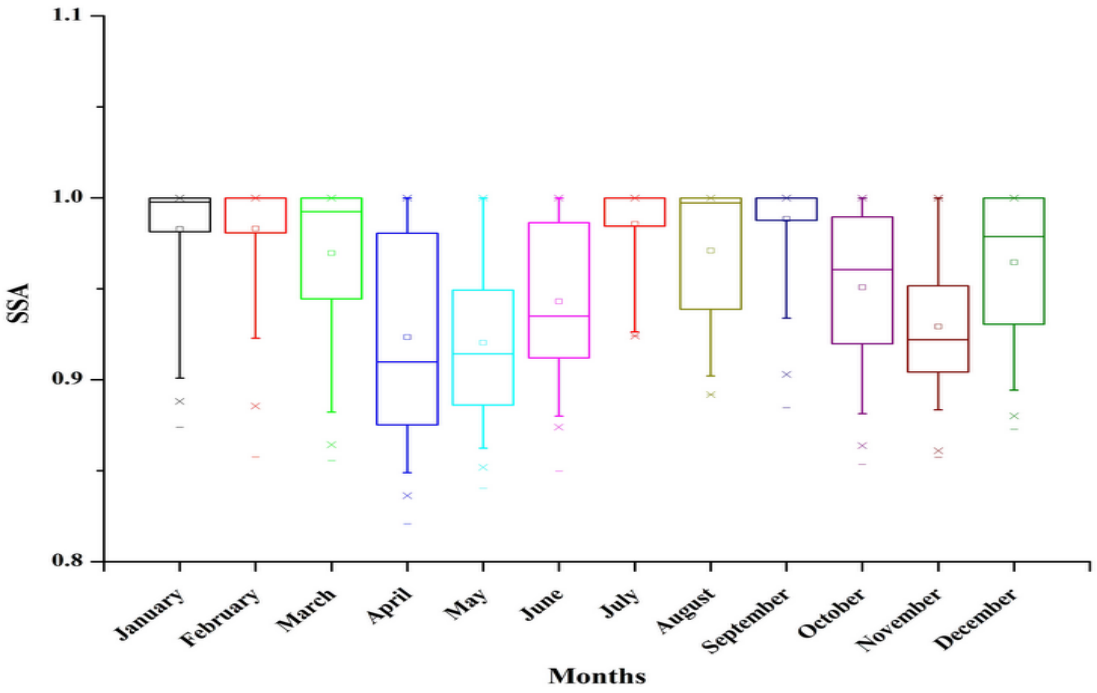

Figure 3.6 Monthly mean pattern of OMI derived SSA.

3.5 Daily variation of AOD and BC

Daily variation of AOD_{500} of the year 2014 is shown in figure 3.7. The AOD is measured at five wavelengths 380, 500, 675, 936 and 1020 nm by using MICROTOP-II Sunphotometer. During that period maximum value of AOD_{500} is obtained on 25th October (2.52) and minimum value is obtained on 24th September (0.276). From 21st October to 25th October measurement of AOD has been carried out at Laxminagar (residential site) during the period of Diwali. Diwali was celebrated on 23rd October and after two days maximum value of AOD_{500} is obtained. It was due to burning of fireworks and crackers which releases large amount of pollutant in the atmosphere and it persist in the atmosphere after two days. Also, Laxminagar is a highly densely populated with heavy traffic density all around it as well as Gas Turbine Power Station (~ 6 km distance from site of measurement). But at JNU maximum value of AOD_{500} is obtained on 26th October (1.195). It was due to same reason celebration practices during that period.

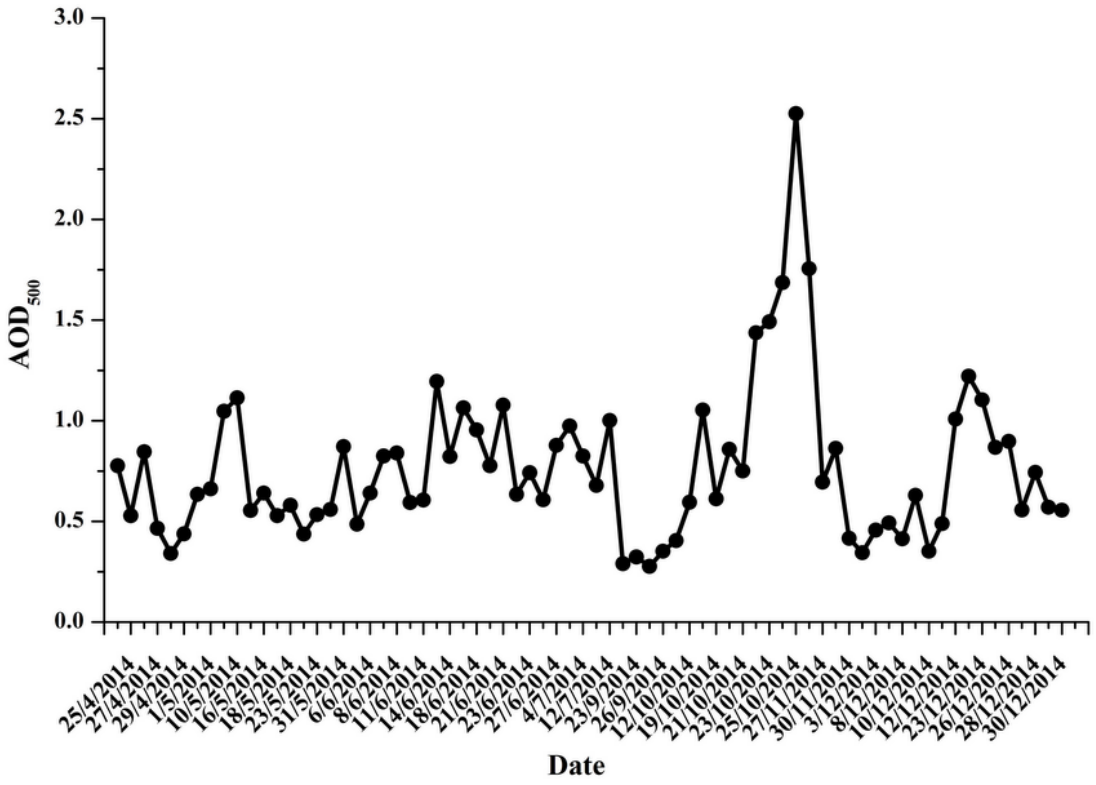

Figure 3.7 Daily variation of average AOD_{500} for the year 2014.

There was a consistent increase in average value of AOD_{500} as month progress from April to June (0.575, 0.684 and 0.796). It was due to local anthropogenic activities, long range transport of aerosols and dust event during that period (Singh et al., 2010). Generally, aerosol loading increases from March to June over the IGB during the period of pre-monsoon (Singh et al., 2005; Srivastava et al., 2011). During that period maximum average value of AOD 500 is obtained in the month of October (1.197). It was due to festival season of Diwali celebration practices was at peak which made atmosphere smoky and its persistence for more than a week over Delhi (Attri et al., 2001).

Daily variation of average BC concentration for the year 2014 is shown in figure 3.8. During that period maximum concentration of BC is obtained on 19th December (19.32 μg/m^3) and 22nd December (18.65 μg/m^3). It was due to local anthropogenic activities and bone fire by the people during that period. The minimum concentration of BC is obtained on 25th September (0.86 μg/m^3) and 26th September (0.68 μg/m^3). It was due to monsoon season because intense spells of rainfall washout the pollutant from the atmosphere.

During these period maximum average BC concentration is obtained in the month of December (8.18 μg/m^3) and January (9.82 μg/m^3) and lowest in the month of September (1.07 μg/m^3). Singh et al (2010) have also reported maximum average BC concentration in the month of December (16.7 μg/m^3) and January (~ 14 μg/m^3) and minimum in the month of August (~ 2.4 μg/m^3). The very low amount of BC concentration is obtained at JNU because it is vegetative area and far away from heavy traffic and local anthropogenic activities.

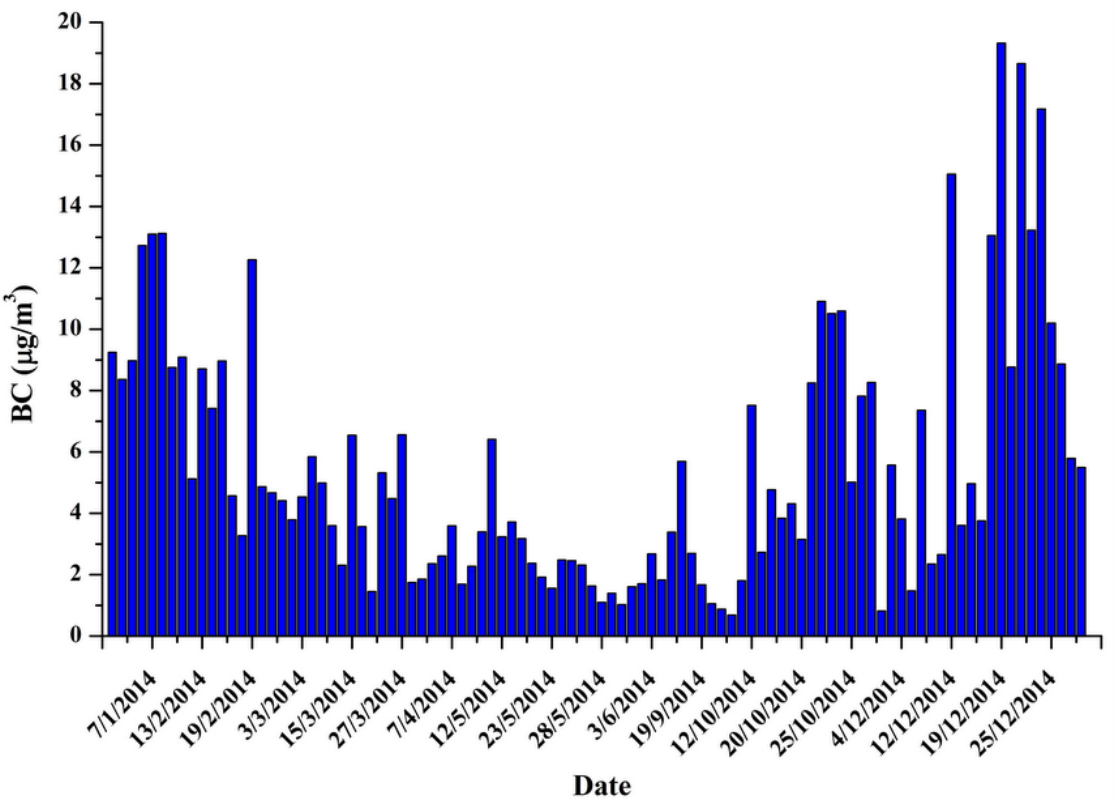

Figure 3.8 Daily variation of average BC concentration over JNU for the year 2014.

3.6 Relation of AOD and BC with meteorological parameters

Linear regression analysis of AOD with temperature, wind speed and relative humidity (RH) is shown in figure 3.9. AOD decreases with temperature and wind speed but varies slightly with RH. The coefficient of correlation (R^2) of AOD with temperature, wind speed and RH are 0.0002, 0.0041, and 0.0435, respectively. The negative

correlation of AOD with temperature shows that higher temperature decrease the value of AOD because higher temperature increases the mixing layer height and disperse the aerosol in the atmosphere. Result is also similar with wind speed (negative correlation) because high wind speed disperses the aerosol and shortens the residence time of aerosol in the atmosphere. The positive correlation of AOD with RH shows that RH increases the value of AOD also increases. It is because at high RH aerosol becomes hygroscopic which enhances the scattering efficiency of the aerosols (Malm and Day, 2001). The components of aerosol which are hygroscopic like organic carbon, ammonium nitrate and ammonium sulfate, increase in size under higher RH condition and consequently increases the light extinction efficiencies (Malm et al., 2000). The increase in AOD with RH is also reported by (Clarke and Kapustin, 2002).

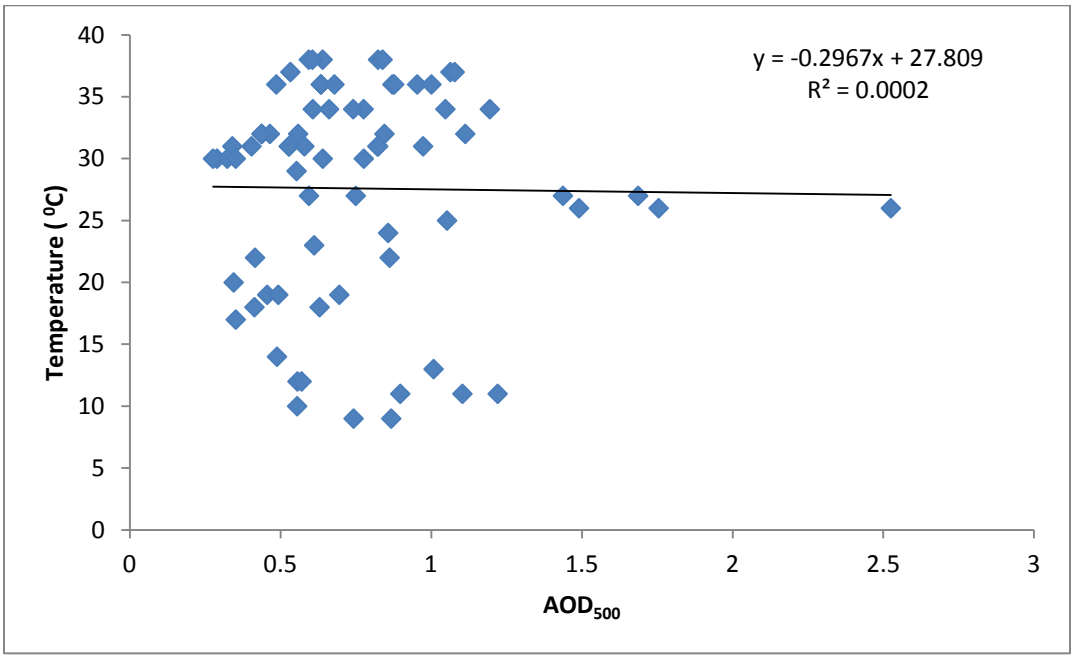

(a)

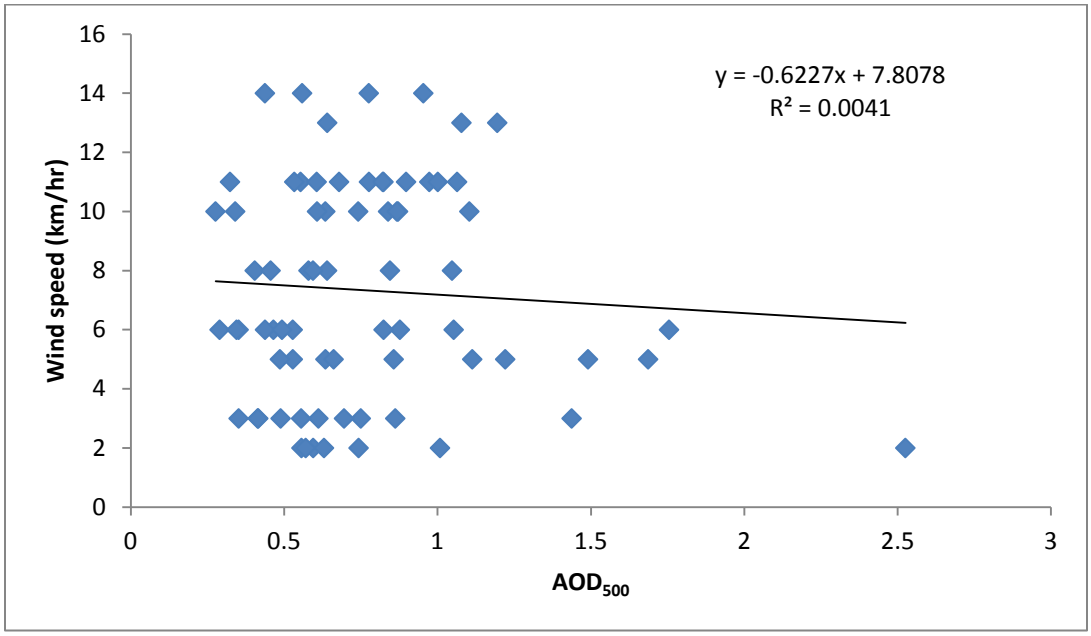

(b)

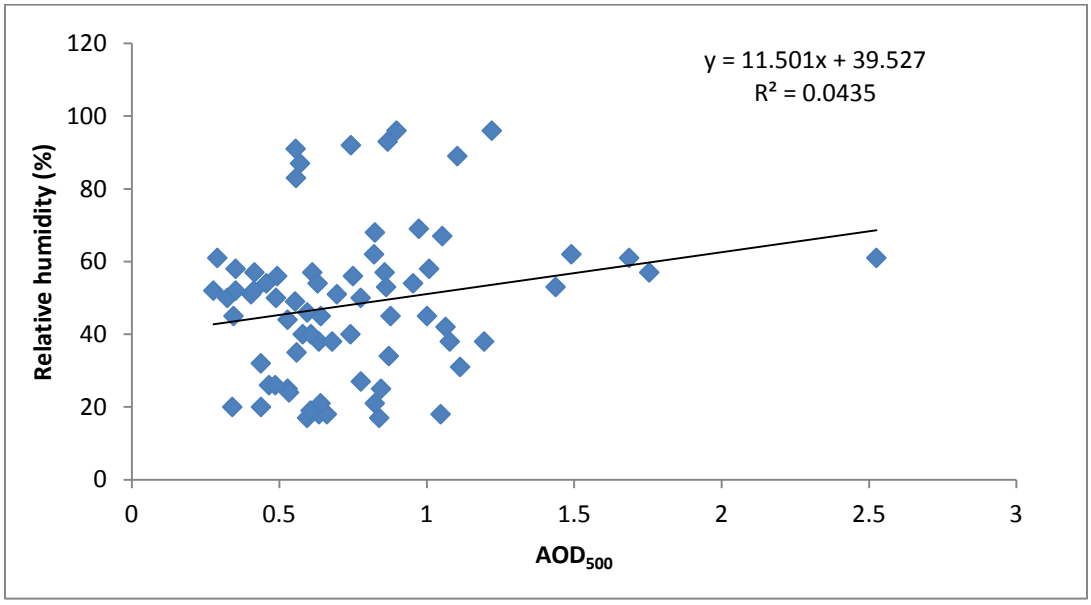

(c)

Figure 3.9 Linear regression analysis of AOD with meteorological parameters.

Linear regression analysis of BC with temperature, wind speed and RH is shown in figure 3.10. The coefficient of correlation of BC with temperature, wind speed, and RH are 0.3941, 0.2148, and 0.4116, respectively. The value of coefficient of correlation shows that there is significant inverse relation between BC and temperature. It is due to coal burning during low temperature condition at site along with more stable atmosphere. Also, when surface temperature increases which enhance the convective activity due to which pollutant get dispersed as boundary layer height increases, thus the concentration of BC decreases. Cao et al. (2005) reported that residential coal burning contributes ~ 44% of total carbon at Xi'an in China during winter. BC also shows inverse relation with wind speed but less significant than temperature. The result suggests that major contribution from the local sources when wind speed is low (winter and post-monsoon). Approximately, similar result of BC with temperature (r = - 0.64) and wind speed (r = - 0.53) had reported by Tiwari et al. (2013) in Delhi at Indian Institute of Tropical Meteorology and Ramachandran and Rajesh (2007) at Ahmedabad. BC shows direct relation with RH and good significant than temperature and wind speed. Positive correlation of BC with RH shows that RH increases the BC concentration is also increases.

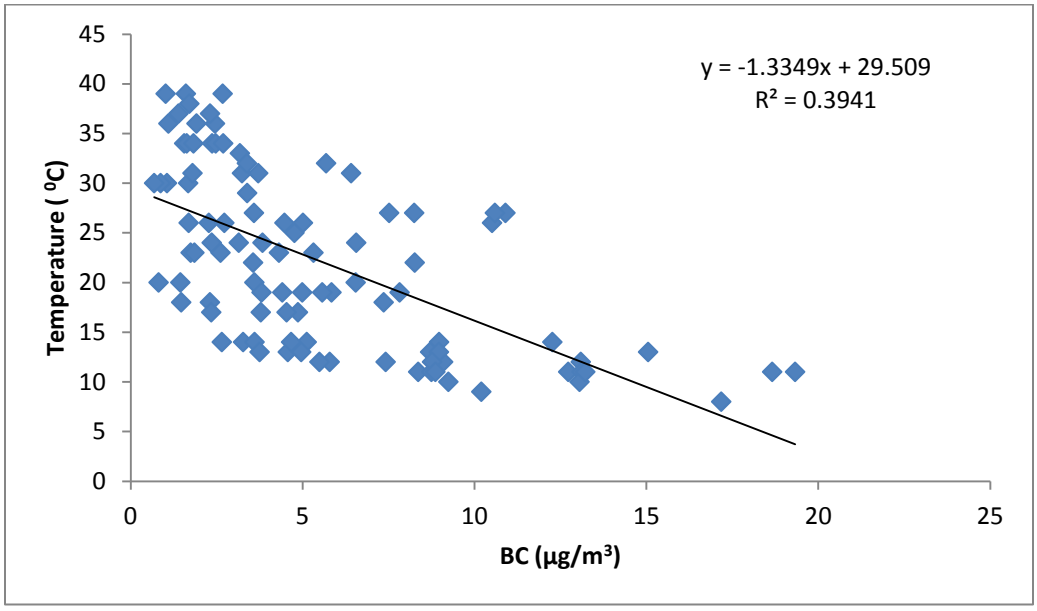

(a)

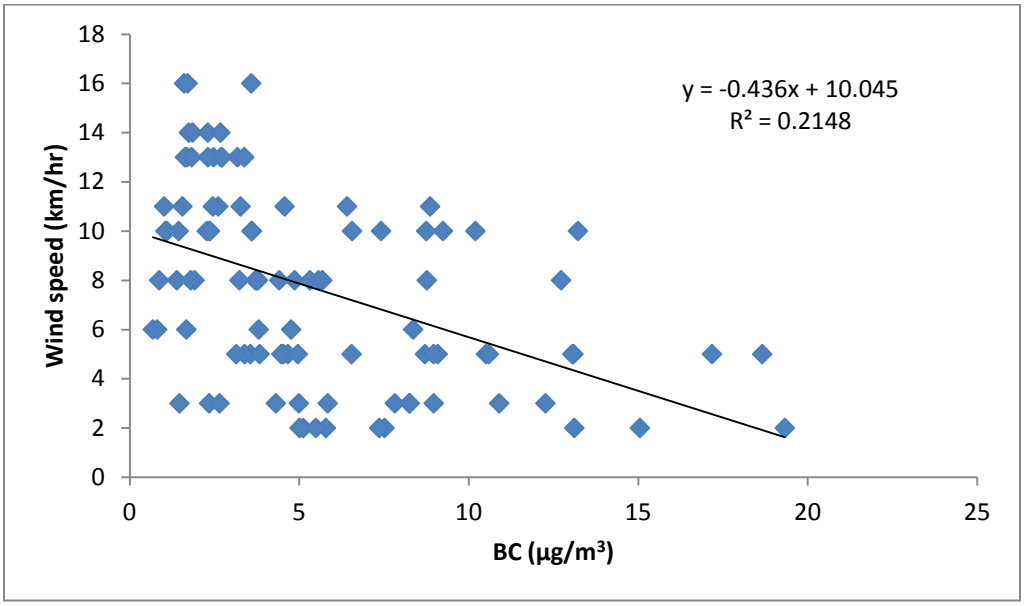

(b)

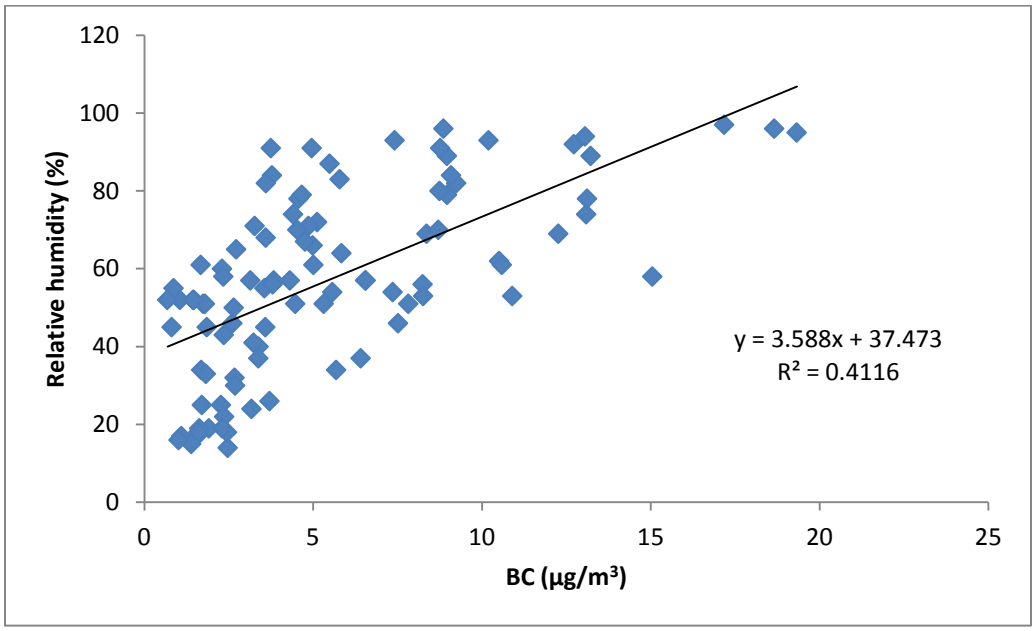

(c)

Figure 3.10 Linear regression analysis of BC with meteorological parameters.

4.1 Introduction

We have classified the aerosol days during the measurement period following the AOD climatology reported by Lodhi et al. (2013) for the period 2001-2012 at Delhi. These AOD data were also collected using the same instrument, thereby causing minimal instrumental bias in our analysis. When our measured daily AOD exceeds 12-year mean AOD + 1 standard deviation (σ) for the corresponding month reported by (Lodhi et al., 2013), we categorize it as 'extreme' aerosol days. Days with AOD values smaller than 12-year mean AOD - 1σ are classified as 'relatively clean'. This condition represents background aerosol concentration of Delhi for that corresponding month. Days with AOD values between 12-year mean AOD - 1σ and 12-year mean AOD + 1σ are classified as 'normal' aerosol days. We classified 33.3%, 40.5% and 26.2% days as 'relatively clean', 'normal' and 'extreme' aerosol days during the observation period.

Aerosol composition was inferred from the measured AOD spectra and BC concentration using OPAC model. We choose five aerosol species to be externally mixed – BC, water-soluble, insoluble, dust in accumulation mode and dust in coarse mode. These species are chosen because previous studies Singh et al. (2010) have identified these as the major aerosol species in Delhi during this time period. Number concentration of BC is derived from the measured mass. Number concentrations of the remaining four species are set through iterative method by matching the AOD spectrum simulated by OPAC with the measured AOD spectrum. Aerosol scale height and thickness of aerosol layer during the observation period are taken from CALIOP-retrieved aerosol vertical profiles for the corresponding period following Srivastava et al. (2014). Mean aerosol scale height for the simulation is considered to be 1.9 km. Aerosol composition was fixed during this iterative process when the root-mean square error of simulated AOD at four wavelengths closest to the wavelengths at which AOD is measured (380, 500, 675, 936 and 1020 nm) drops below 0.025 to ensure a robust match relative to measured AOD spectrum (Dey and Tripathi, 2008).

4.2 Aerosol characteristics during the campaign period

Insoluble component contributes only 0.1% to total mass, while water-soluble and BC contributions remain confined witin 1-2% during the measurement period (Figure 4.1). Bulk of the aerosol mass is contributed by accumulation mode and coarse mode dust. Mass fraction of accumulation mode dust decreases from 19.5% during 'clean' days to 1.5% to 'extreme' aerosol days. This decrease is compensated by coarse mode dust, whose mass fraction increases from 76.8% to 96.8%.

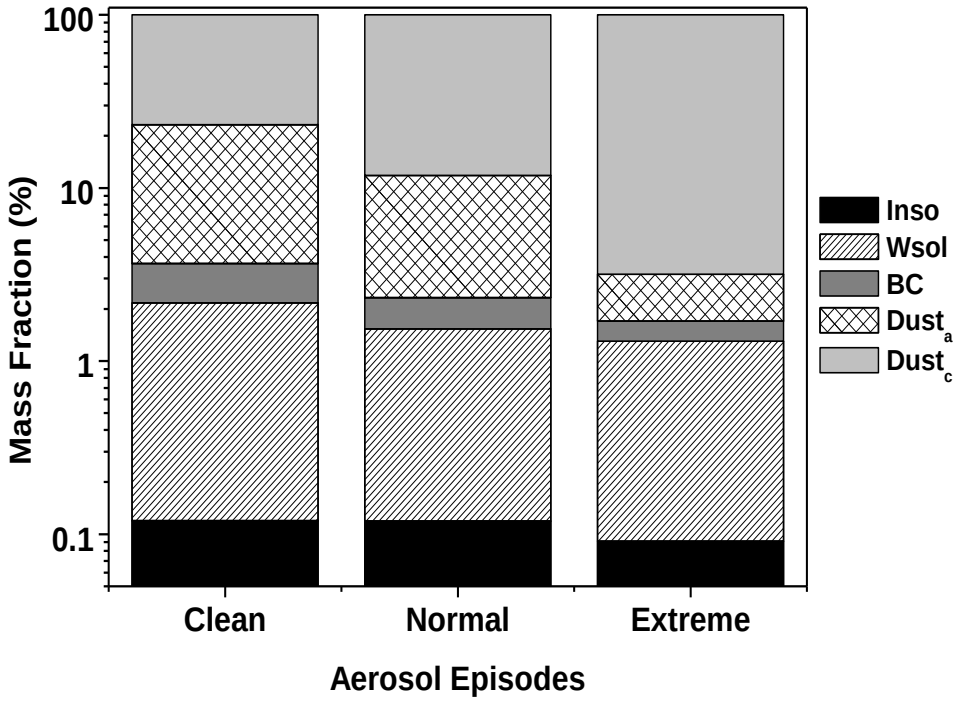

Figure 4.1. Mass fraction of various aerosol species during the 'relatively clean', 'normal' and 'extreme' aerosol days at Delhi NCR.

Box plot of AOD at 500 nm wavelength during the 'clean', 'normal' and 'extreme' aerosol days is shown in Figure 4.2. Median AOD during the 'clean' days is observed to 0.51, which increases by ~45% to 0.74 during the normal days. During the 'extreme' pollution days, it increases further by 60.8% to reach a median value of 1.2. On some given days during the 'extreme' events, AOD rises even above 1.8. This increase in AOD is accompanied by a consistent reduction in angstrom exponent, a first order indicator of aerosol size. Mean angstrom exponent of 0.54±0.09 during the 'clean' days implies dominance of large size particles, consistent with large mass fraction of coarse mode dust. Angstrom exponent further reduces to 0.35±0.08 during 'normal' days, when mass fraction of coarse mode dust increases. During 'extreme' events when coarse mode dust contributes 96.8% to total aerosol mass, mean angstrom exponent drops to 0.22±0.12.

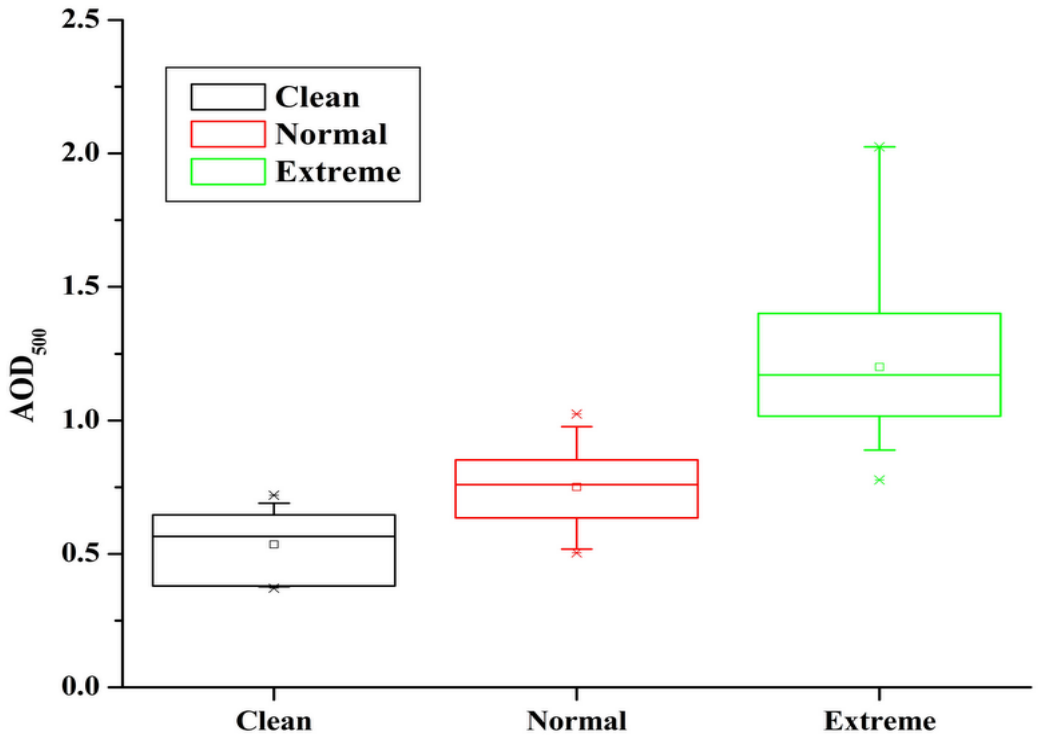

Figure 4.2 Box plot of AOD at 500 nm wavelength during the 'relatively clean', 'normal' and 'extreme' aerosol days at Delhi NCR.

The relative contributions of each aerosol species to AOD are displayed in Figure 4.3. Relative contribution of insoluble component to AOD remains low (<0.1%), while that of water-soluble component remains in the range 12-14% (as compared to a mass fraction of

1-2% as shown in Figure 4.3) during the measurement period. BC contributes 30.1% during the relatively 'clean' days, which decreases to 20.9% and 13.1% during the 'normal' and 'extreme' pollution days respectively. 20.5% (35.0%) relative contribution of accumulation mode dust (coarse mode dust) to AOD during the 'relatively clean' days decreases (increases) to 13.1% (52.8%) and further to 2.5% (70.8%) during the 'normal' and 'extreme' days respectively.

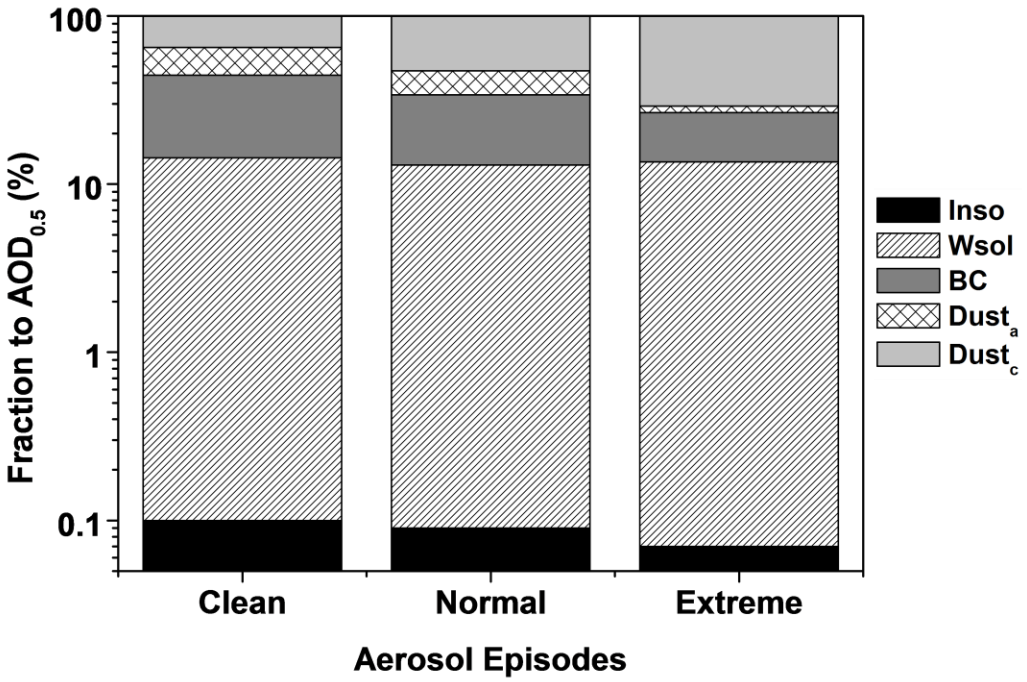

Figure 4.3 Relative contributions of aerosol species to AOD at 500 nm wavelength during the 'relatively clean', 'normal' and 'extreme' aerosol days at Delhi NCR.

Mean SSA spectrum during the 'relatively clean', 'normal' and 'extreme' aerosol days as simulated from the reported aerosol composition is shown in Figure 4.4. During the entire observation period, SSA shows an increasing trend with wavelength, implying the dominance of dust in the aerosol composition. Dust particles scatter large wavelength more efficiently and absorb wavelength closer to UV, thereby exhibiting an increasing SSA spectrum with wavelength (Dey et al., 2004). Overall, aerosols are highly absorbing during the summer.

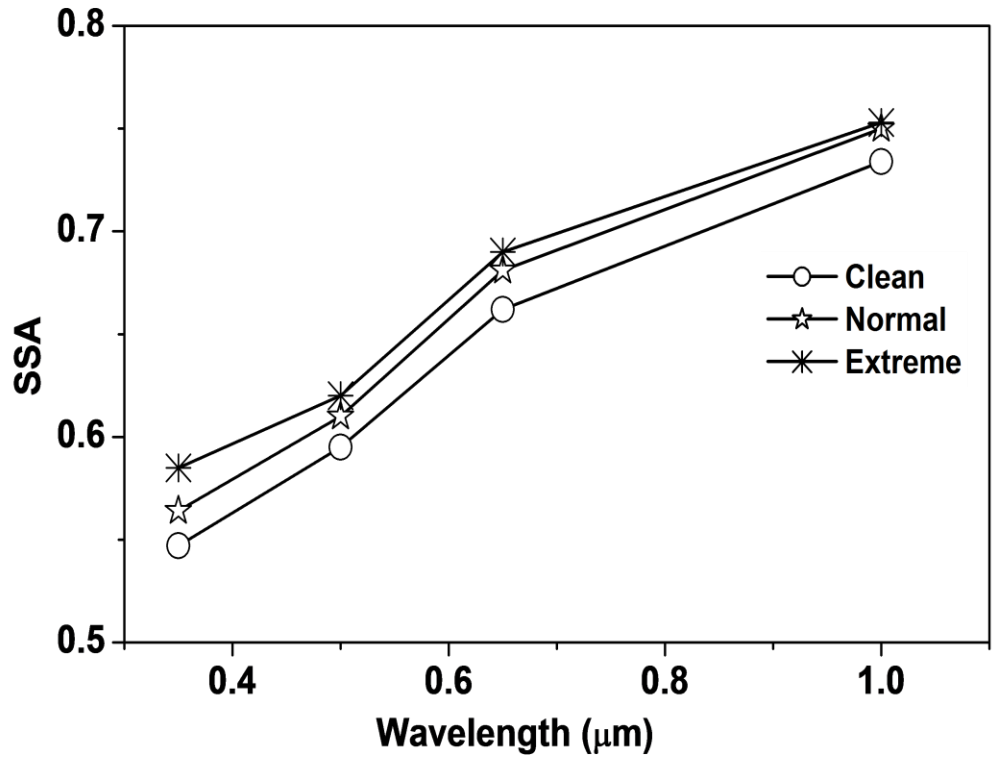

Figure 4.4 SSA spectrum during the relatively 'clean', 'normal' and 'extreme' aerosol episodes at Delhi NCR.

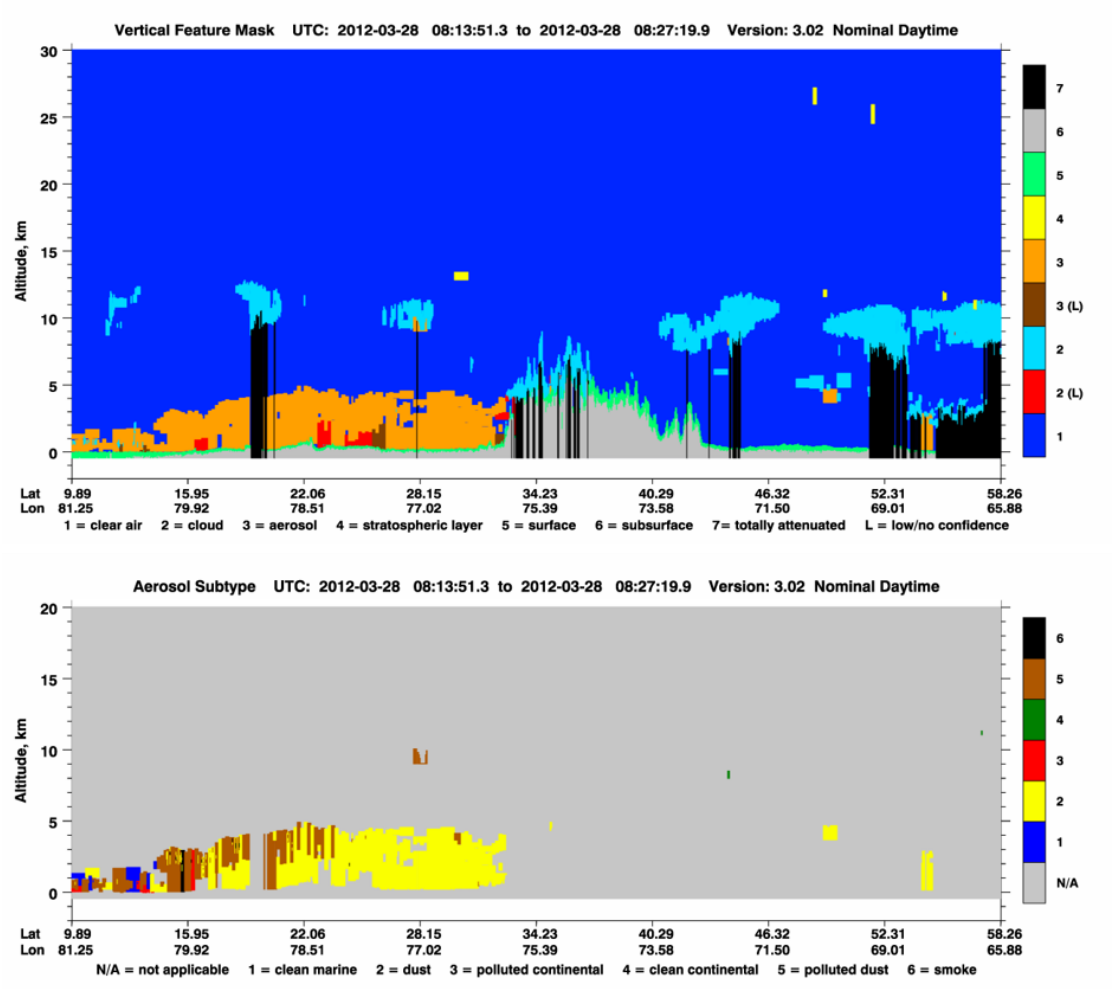

Figure 4.5 CALIOP-retrieval during its overpass on 28th March 2012 indicates presence of thick layer of aerosols over Delhi NCR spread up to 5 km. Aerosol sub-type identified is 'dust' and 'polluted dust'.

This is consistent with previous studies by Singh et al. (2005) at Delhi. Increasing dominance of coarse mode dust (to both mass and AOD) during the 'normal' and extreme' Aerosol episodes are reflected by an increase in SSA at all the wavelengths, implying enhanced scattering of solar radiation. CALIOP aerosol retrieval during its pass over Delhi on 28th March 2012 is shown in Figure 4.5. Based on the measurement, the day is characterized as an 'extreme' aerosol day. Aerosol layer can be easily noticed all the way up to 5 km over the Indo-Gangetic Basin. Aerosol sub-type retrieval indicates presence of 'dust' and 'polluted dust' in this region (bottom panel of Figure 4.5). In the CALIOP algorithm, polluted dust is detected when natural mineral dust is transported from the

source regions to urban areas and gets mixed with other species (Omar et al., 2009). CALIOP aerosol sub-type provides support to aerosol composition inferred from the measurements, suggesting the robustness of the hybrid approach as described earlier.

4.3 Aerosol Direct Radiative Forcing (ADRF)

ADRF is defined as the change in net radiation due to aerosols. ADRF is calculated by Santa Barbara DISORT Atmospheric Radiative Transfer model (SBDART) developed by (Ricchiazzi et al., 1998). We have used the aerosol spectral properties (SSA, asymmetry parameter and AOD) simulated by OPAC as input to SBDART. Other input parameters - total column ozone and surface albedo data have been taken from OMI Level 2G data products and water vapour has been taken from MODIS. Radiative fluxes at the TOA and surface have been calculated as function of solar zenith angle. Finally, diurnally averaged ADRF has been estimated following standard procedure demonstrated earlier by numerous researchers (Dey and Tripathi, 2008; Srivastava et al., 2011).

The mean TOA ADRF has been estimated to be 21.25 W m^{-2} during the 'relatively clean' days, which increases to 27.29 W m^{-2} and further to 56.56 W m^{-2} during the 'normal' and 'extreme' aerosol days (Figure 4.6). Large warming at the TOA is attributed to large aerosol load and highly absorbing aerosols present in the atmosphere of Delhi during the summer. The corresponding value for surface ADRF are -99.47, -122.01 and -153.5 W m^{-2} respectively. This results in a large atmospheric warming of 120.72, 149.3 and 210.06 W m^{-2} for the 'relatively clean', 'normal' and 'extreme' aerosol days, which translates into heating rates of 1.7, 2.1 and 2.96 K/day respectively. Results suggest that the aerosol induced heating is enhanced by ~75.1% for a corresponding increase of 133.3% increase in AOD from the 'relatively clean' to 'extreme' aerosol days. In terms of relative contribution of individual aerosol species, water-soluble components contribute to only 3-4% to estimated surface aerosol DRF (Figure 4.7). BC contribution is highest (57.7%) for the 'relatively clean' days, followed by coarse (26.3%) and accumulation mode dust (11.9%). During the 'normal' aerosol days, contributions of BC and accumulation mode dust reduce to 45.3% and 8.6% respectively. They further reduce to 33.5% and 1.9% during the 'extreme' aerosol days. Relative contribution of coarse mode dust to surface

DRF enhances to 42.1% and then to 60.3% during the 'normal' and 'extreme' aerosol days.

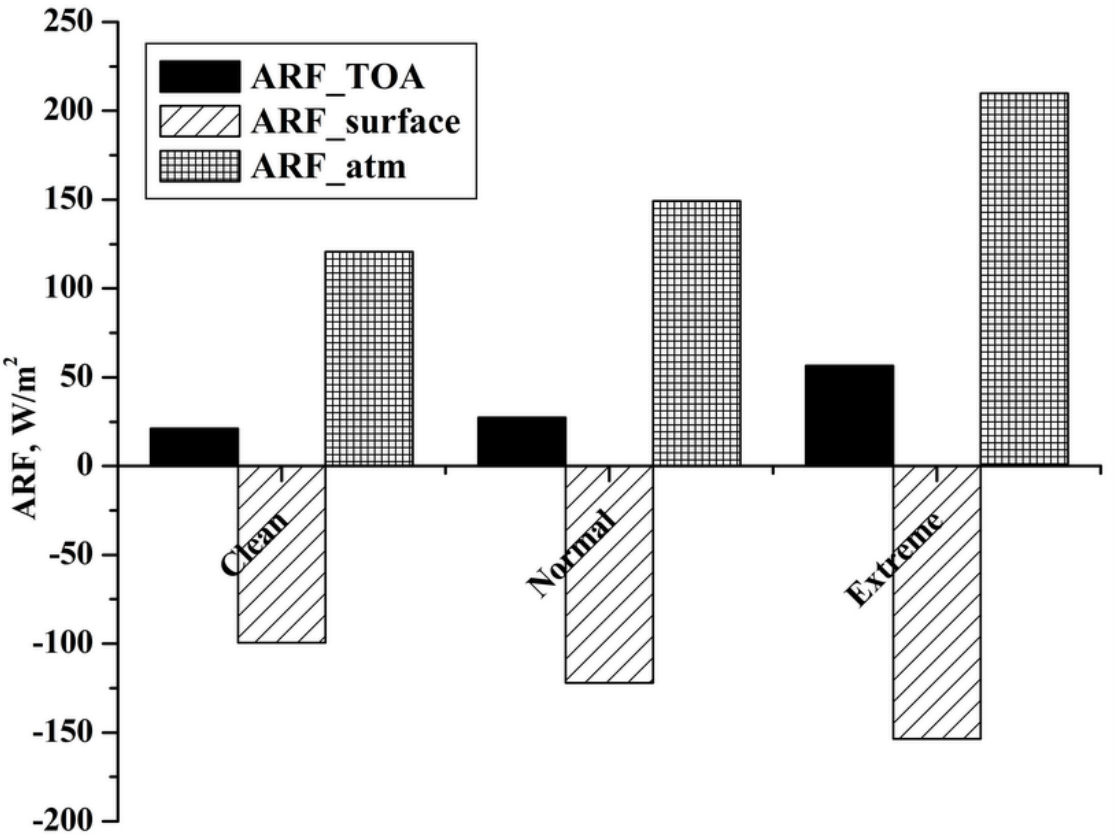

Figure 4.6 Mean aerosol DRF at the TOA, surface and atmosphere during relatively 'clean', 'normal' and 'extreme' aerosol days.

The results presented here have implications for the regional climate. Aerosol loading and ADRF are very large in Delhi NCR. Mean AOD of 0.51 in the 'relatively clean' condition (based on 12-year climatology) suggests that the background aerosol concentration is enormous in Delhi NCR during the summer months. Aerosol direct radiative forcing efficiency (per unit AOD) at the TOA is estimated to be 41.7 W m^{-2}, 36.9 W m^{-2} and 47.1 W m^{-2} respectively for the 'relatively clean', 'normal' and 'extreme' aerosol days. Since mostly accumulation mode dust fraction to bulk aerosol reduces and that of coarse mode dust increases during the transition from 'relatively clean' to 'extreme' aerosol days; the TOA aerosol direct radiative forcing efficiency (related more to aerosol composition rather than total aerosol load) does not show drastic change. The

corresponding values for the surface are -195.0, -164.9 and -127.9 W m^{-2} respectively. While TOA ADRF change from 'relatively clean' to 'normal' aerosol days is small (~ 6 W m^{-2}) for a 45% increase in AOD, the enhancement is large (29.3 W m^{-2}) for a 60.8% increase in AOD during the transition from 'normal' to 'extreme' aerosol days.

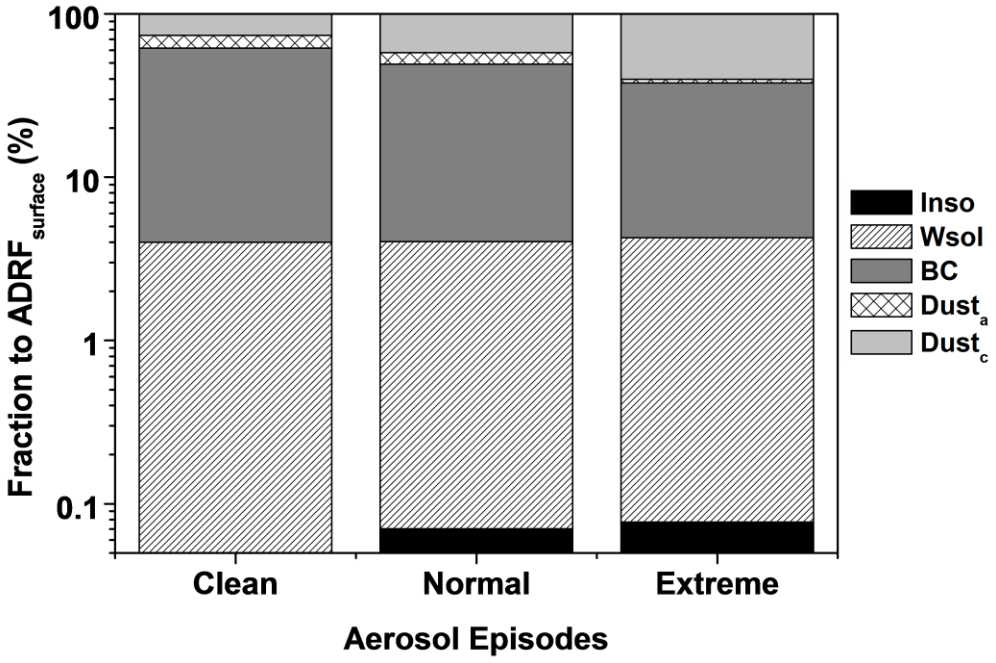

Figure 4.7 Relative contribution of aerosol species to total surface ADRF during relatively 'clean', 'normal' and 'extreme' aerosol days.

Such large surface dimming and atmospheric heating would suppress energy transfer from surface to atmosphere, thereby leading to a stable boundary layer. We note that our estimates assume external mixing of aerosols. During the summertime, dusts transported from the arid regions to the IGB mix with the anthropogenic species, further enhancing the absorption (Dey and Tripathi, 2008). In that case, enhancement in ADRF would have been larger than the values reported here during the 'extreme' aerosol days. Another critical issue, not considered here, is the particle non-sphericity. Dust particles are non-spherical in shape and therefore, the ADRF may differ when the bulk aerosol composition is dominated by dust particles. Mishra et al. (2008) have shown that the

deviation in TOA ADRF due to particle non-sphericity may be as large as 10-15% relative to spherical particle in the IGB. Hence the enhancement of AOD and subsequent ADRF presented here may be considered as conservative estimates.

5.1 General

The present study is planned to develop linear, multi-linear, and log-linear (logistic) regression models to the given knowledge sets and checking out that of those models is best work once analyzing their results to own the reliable estimates of $PM_{2.5}$. For developing the multi-linear regression models, meteorological parameters are used as regressor addionally to the $AOD_{MODIS.}$ Meteorological parameter is used in this study and in other such type of study to get better correlative estimation of PM with the assistance of AOD. Recently Chitranshi et al. (2015) have developed simple multi-linear regression model by using AOD_{MODIS}, RH, WS, and AT as regressors to estimate PM_{10} levels in Agra City. Previously Gupta et al. (2006) have used meteorological and other additional data sets to evaluate the effect of the wind speed, cloud cover, and mixing height (MH) on PM air quality. Their study demonstrated that $PM_{2.5}$- AOD association was powerfully captivated on aerosol concentration, ambient RH, fractional cloud cover, and MLH. Their study accomplished that these data were obligatory to further apply satellite data for air quality investigation (Gupta et al., 2006). The weather conditions can significantly influence the aerosol loading. RH and dew point directly impact the size of the particle, while the wind speed effects the mixing of aerosols (Kumar et al., 2011). Based on that type of study, this study used solely three meteorological parameters, namely, RH, WS, and AT that were used usually in the above studies. Since MH is directly or indirectly associated with meteorological parameters, hence it was not considered in this study.

All the data sets is obtained for six year time period (2007-2012), in which five year (2007-2011) data sets are used for development of models and one year (2012) for the reason of validation studies. This study first intended to evaluate the linear regression models and then after logistic regression models as presented below:

Linear regression models

In this model correlation of hourly average $PM_{2.5}$ data with AOD_{MODIS} was checked with the help of simplest form of regression model (a) below.

Hourly $PM_i = \alpha + \beta_1 AOD_i + e_i$ (a)

Where suffix *i* represents the *i*th observation, PM is $PM_{2.5}$ measured by AAQMS along with meteorological parameters, AOD is AOD_{MODIS}, α and β are the estimators, and e_i is the residual error in the estimation.

For the betterment of the above associations, meteorological parameter is added in successive steps for the estimation of $PM_{2.5}$. First, the effect of RH was considered through association (b) and then after meteorological parameters WS and AT were added in succeeding steps through association (c) and (d) given below. These associations were predicted to show some incremental improvement in the correlation as a result of the addition of specific meteorological parameters.

$$PM_i=\alpha + \beta_1 AOD_i + \beta_2 RH_i + e_i \quad (b)$$

$$PM_i = \alpha + \beta_1 AOD_i + \beta_2 RH_i + \beta_3 WS_i + e_i \quad (c)$$

$$PM_i = \alpha + \beta_1 AOD_i + \beta_2 RH_i + \beta_3 WS_i + \beta_4 AT_i + e_i \quad (d)$$

Since observed value of $PM_{2.5}$, AOD, and meteorological parameters showed some substantial skewness (more than 1) in their variations about their mean values. So we have applied logistic regression models for some development in the correlation over the linear regression models. Previously, some researchers have applied logistic regression models for the better estimates of PM_{10} with the help of AOD_{MODIS} and meteorological parameters (Kumar et al., 2008; Kumar et al., 2011). Therefore logistic models proposed below on the lines of linear models.

Logistic regression models

$$\log (\text{hourly } PM_i) = \alpha + \beta_1 \log (AOD_i) + e_i \quad (a)$$

$$\log (PM_i) = \alpha + \beta_1 \log (AOD_i) + \beta_2 \log (RH_i) + e_i \quad (b)$$

$$\log (PM_i) = \alpha + \beta_1 \log (AOD_i) + \beta_2 \log (RH_i) + \beta_3 \log (WS_i) + e_i \quad (c)$$

$$\log (PM_i) = \alpha + \beta_1 \log (AOD_i) + \beta_2 \log (RH_i) + \beta_3 \log (WS_i) + \beta_4 \log (AT_i) + e_i \quad (d)$$

5.2 Regression Model adequacy check and validation studies

For the suitability of the model generally straight line scatter plots between estimated responses versus observed response is considered. Recently, Chitranshi et al., (2015) have analyzed the usage of scatter plots in detail and found that the information and inferences provided by such plots can be resulting theoretically by the result of regression itself. The intercept and slope of such plots are nothing but coefficient of determination (R^2) and the mean of the observed responses ($\overline{PM_i}$). Further, the correlation between estimated and observed responses has also showed the same as that of developed regression model. The better method for checking the adequacy of the regression model was adopted by Johnson (2005). From this method, the assumptions drawn in in the least square- based classical linear regression essentially make sure the residual errors e_i to be independent of the estimated responses. Thus, the adequacy of the regression model can also be examined by plotting the residuals versus the estimated responses. When model will be adequate, then all the points of residuals will confine within horizontal band around the zero. Any other type of defined distribution patterns of residuals may propose the need of transformation of the proposed regression model/or addition of the square terms of the independent variables in it. Any other undefined trend of the residuals suggest that the model as inadequate (Johnson, 2005).

The model validation studies were carried out by using the data for the year 2012 (validation year) to check whether the models were capable of estimating $PM_{2.5}$ approximately or not. For validation, first, the estimated $PM_{2.5}$ was computed by using the observed AOD_{MODIS} and the meteorological parameters of the year 2012 using the estimators of the corresponding regression model from the data of year 2007-2011. Then validation R^2 was compared with the R^2 of the corresponding regression model. For compare the applicability of the model, the relative standard error (RSE) which is defined as the standard error (SE) when expressed as the percentage of the mean of the observed $PM_{2.5}$ values can be used. Hence, for the validation studies RSE of the regression stage was also compared with that of the validation stage (Chitranshi et al. 2015).

5.3 Descriptive statistics

The descriptive statistics of all the parameters used in the models as mentioned in the approach is revealed in Table 5.1. Mean, standard error, standard deviation, range of values, and total count of the data sets for Delhi capital have been offered in this table for the regression studies as well as validation studies. The data sets from the year 2007-2011 have been used for regression studies and data sets for the year 2012 are used for validation studies. The annual mean (±1 standard deviation) of hourly $PM_{2.5}$ ($\mu g/m^3$) ranged from 37.38-226.75 (±39.79) during regression period, while 52.63-173.75 (±28.28) in the validation period. The minimum value of $PM_{2.5}$ (37.38 $\mu g/m^3$) during the regression period was below the National Ambient Air Quality standards (NAAQ) of 40 $\mu g/m^3$ (annual mean), while during validation period it was slightly greater than annual mean. The annual mean of meteorological parameters, i.e., RH and WS did not have much variation during regression period as well as validation period, and their values centered around 53 % and 8 km/hr, while AT have slight variation in regression period (24^0C) and validation period (20^0C), respectively. These meteorological parameters have significant variation both month wise and season wise in the study region.

Table 5.1 Descriptive Statistics of the data for Delhi capital

Year	Stastical Parameter	Hourly $PM_{2.5}$	AOD	RH (%)	WS (km/hr)	AT (^{0}C)
2007-2011	Mean (μ)	97.46	0.64	52.98	8.04	24.05
	Standard Error	1.57	0.016	0.67	0.17	0.29
	Standard deviation (σ)	39.79	0.41	17.11	4.34	7.39
	Range	37.38-226.75	0.06-3.22	15-95	2-24	7-42
	Count	636	636	636	636	636
2012	Mean (μ)	95.86	0.77	53.97	7.47	19.87
	Standard error	2.96	0.053	1.82	0.38	0.68
	Standard deviation (σ)	28.28	0.50	17.44	3.65	6.48
	Range	52.63-173.75	0.19-2.41	14-97	2-19	9-36
	Count	91	91	91	91	91

Box plot of MODIS derived deep blue monthly AOD_{550} from 2005 to 2014 is shown in figure 5.1. The minimum mean monthly values of AOD_{MODIS} was obtained during the month of September as 0.33 ± 0.30 and March as 0.35 ± 0.26. The maximum value of AOD_{MODIS} was obtained during the month of July as 1.06 ± 0.59 and November as 1.05 ± 0.67. Detailed explanation of MODIS derived deep blue AOD is given in chapter III. Recently that type of result were also reported by Chitranshi et al., (2015) for AOD_{MODIS} variation at Agra, a nearby city of Delhi wherein they reported the decrease in AOD_{MODIS} during February/March and high AOD_{MODIS} in the month of June. Similar type of studies were also carried out by Ahmad et al. (2012), who studied AOD_{MODIS} variation for Aligarh, and found that decrease in AOD_{MODIS} during February/March to the changed weather conditions and high AOD_{MODIS} in May/June due to dust events. Box plot of hourly $PM_{2.5}$ from 2007 to 2012 and estimated $PM_{2.5}$ from 2005 to 2014 is shown in figure 5.2. In this figure first box plot indictaes observed value and adjacent one is estimated value. The mean monthly concentration of observed $PM_{2.5}$ ($\mu g/m^3$) was noticed to be lowest as 41.92 ± 20.30 in the month of August and highest as 156.84 ± 99.45 in the month of December. The higher concentration of $PM_{2.5}$ was also obtained during the month of November as 155.48 ± 96.72 and January as 150.91 ± 103.29. The descriptive statistics of AOD_{MODIS}, $PM_{2.5}$ and $PM_{2.5}$/AOD at Delhi from the years 2005 to 2014 is shown in table 2.

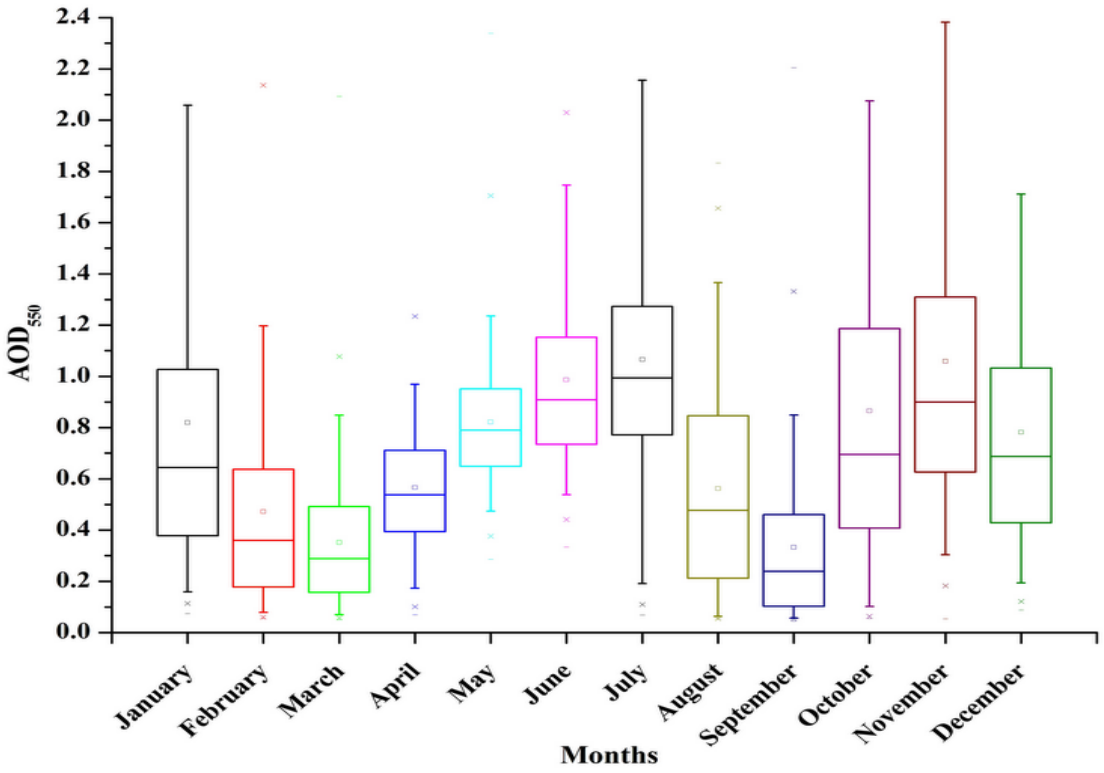

Figure 5.1 Box plot of AOD at 550 nm wavelength from 2005 to 2014 at Delhi NCR.

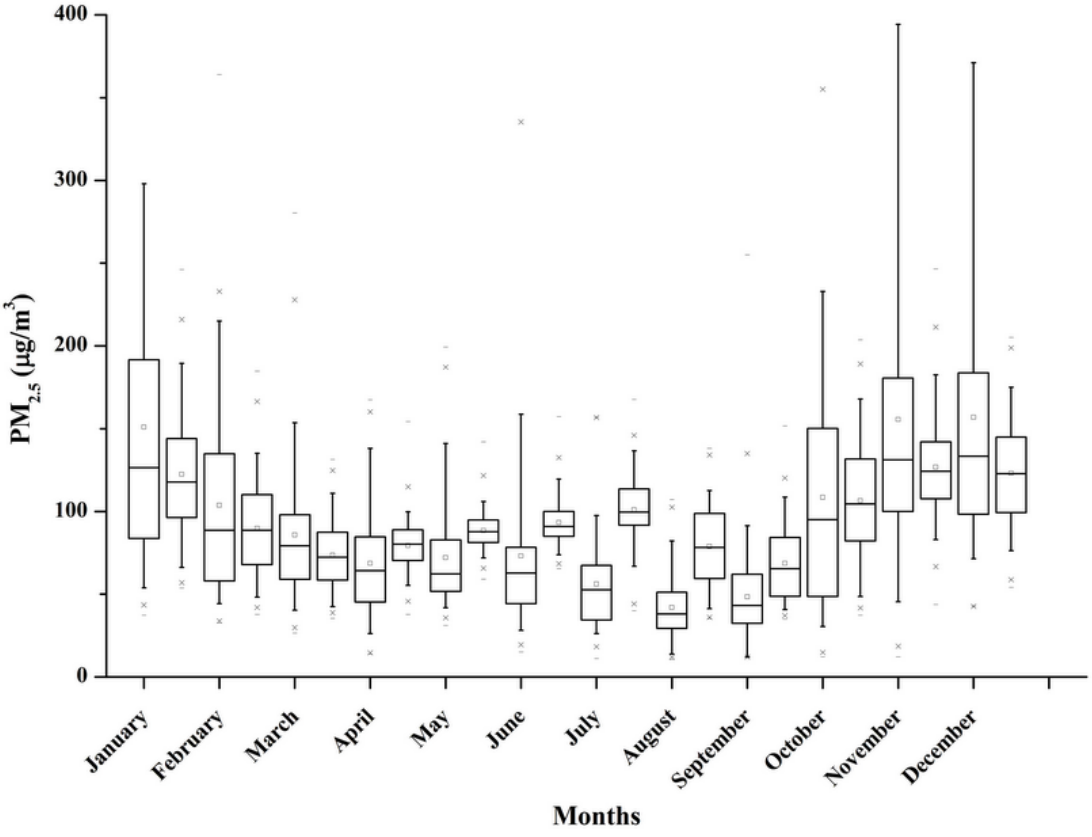

Figure 5.2 Observed $PM_{2.5}$ (2007-2012) and estimated $PM_{2.5}$ (2005-2014) during different months. Note: first box plot is observed value and adjacent one is estimated value month wise.

Table 5.2 Descriptive statistics AOD_{MODIS}, $PM_{2.5}$ and $PM_{2.5}$/AOD at Delhi from the years 2005 to 2014

	AOD_{MODIS}	$PM_{2.5}$ ($\mu g/m^3$)	$PM_{2.5}$/AOD
January	0.82 ± 0.63	122.49 ± 37.71	149.38
February	0.47 ± 0.41	89.77 ± 29.09	190.05
March	0.35 ± 0.26	73.56 ± 20.66	209.39
April	0.56 ± 0.28	79.28 ± 14.63	140
May	0.82 ± 0.26	88.40 ± 11.13	107.52
June	0.98 ± 0.37	93.28 ± 14.32	94.53
July	1.06 ± 0.59	101.12 ± 21.92	94.88
August	0.56 ± 0.41	78.77 ± 24.06	140.23
September	0.33 ± 0.30	68.58 ± 22.95	205.90
October	0.86 ± 0.62	106.43 ± 35.35	123.02
November	1.05 ± 0.67	126.67 ± 30.67	119.90
December	0.78 ± 0.48	123.15 ± 31.83	157.56
Annual	0.72 ± 0.52	97.43 ± 32.84	134.91

5.4 Estimation of $PM_{2.5}$ using linear regression models

The results of regression models are presented in Table 5.3. From these four types of linear regression model, it was evident that hourly $PM_{2.5}$ had moderate correlation with AOD_{MODIS} alone. The coefficient of correlation (R) between them was 0.65 ($p \leq 0.05$). When additional regressors such as RH, WS and AT were added in subsequent steps, which increases the correlative power to some extent. It has been found that the WS had the maximum incremental impact of 0.05 on the coefficient of correlation, whereas RH and AT has the near similar least impact of 0.03. The R values for set I (b), (c), and (d) was 0.65, 0.70, and 0.73 respectively. Earlier Wang and Chirstopher (2003) had correlated the AOD from the Terra and Aqua satellites with both hourly and 24-h averaged $PM_{2.5}$. They found that coefficient of correlation (R) increased from 0.70 to 0.98 when hourly $PM_{2.5}$ was linearly related with AOD_{MODIS} for the aggregated data of all sites and aggregated for daily means of $PM_{2.5}$. Recently Chitranshi et al. (2015) found that both hourly and 24-h average PM_{10} had weak correlation with AOD_{MODIS} alone. However, hourly PM_{10} showed better correlation with AOD_{MODIS} (R~0.45) than 24-h average PM_{10} (R~0.24). On the other hand, Justice et al. (2009) studied the impact of diurnal variation of $PM_{2.5}$ on R^2 and found that R^2

values from hourly $PM_{2.5}$ were higher than those from the daily averages. Though, all the linear regression models as studied above were found to be significant ($p \leq 0.05$). The estimators of all these four models were also found to be significant ($p \leq 0.05$), except estimator of RH in set (d). The optical properties of the aerosols are changed when RH is added to the $PM_{2.5}$ and AOD_{MODIS} association. The greater the RH, the larger proportion of light is scattered and, hence, the larger AOD. Hence, the slope should be smaller with larger RH (Zhang et al., 2009). The surface wind speed in model types (c) and (d), were found to be significant but negative sign of its estimators showed that AOD_{MODIS} estimated lower $PM_{2.5}$ concentration at high wind speed. Ambient temperature was also found to be significant, but its impact on the estimation of $PM_{2.5}$ concentration is relatively small. The negative sign of its estimators also showed that AOD_{MODIS} estimated lower $PM_{2.5}$ concentration at higher temperature, which becomes very unstable at smaller sample size (Liu et al., 2007). In set (d) when all meteorological regressors is added, then RH become insignificant ($p \geq 0.05$). Thus, these additions did not result in any specific trend in the variation of the estimators. The model adequacy checks and its validation studies had applied to all the models because of moderate to good R values.

Table 5.3 Statistical result of linear regression models

Model reference	Statistical parameters						
	R (sig.)	RSE (%)	α (sig.)	β_1 (sig.)	β_2 (sig.)	β_3 (sig.)	β_4 (sig.)
Set I (a)	0.62 (0.00)	31.75	58.16 (0.00)	60.91 (0.00)	-	-	-
Set I (b)	0.65 (0.00)	30.77	34.91 (0.00)	59.80 (0.00)	0.45 (0.00)	-	-
Set I (c)	0.70 (0.00)	28.93	60.97 (0.00)	57.46 (0.00)	0.35 (0.00)	-2.40 (0.00)	-
Set I (d)	0.73 (0.00)	27.83	108.22 (0.00)	61.34 (0.00)	-0.008 (0.91)	-2.06 (0.00)	-1.38 (0.00)

Model adequacy checks were applied to the all the models (a), (b), (c), and (d) of set I which had moderate to good R value. Figure 3 shows the residual plot between residual errors and estimated $PM_{2.5}$ for these models. From these figure it was cleared that increasing trend of residual error (positive/negative) with increasing $PM_{2.5}$ values need model transformation for better estimation of $PM_{2.5}$.

The validations of these models were carried out with the data of 2012. Table 4 depicted that the coefficient of correlation for the validation period were close to the regression stage for all these models. Also, the RSE values of the validation stage were found to be close to the regression stage. The model set (d) had the maximum R (0.73) and slight greater RSE than previous one. Therefore, it could be claimed to provide a better estimate of $PM_{2.5}$ with the help of AOD_{MODIS}, RH, WS, and AT.

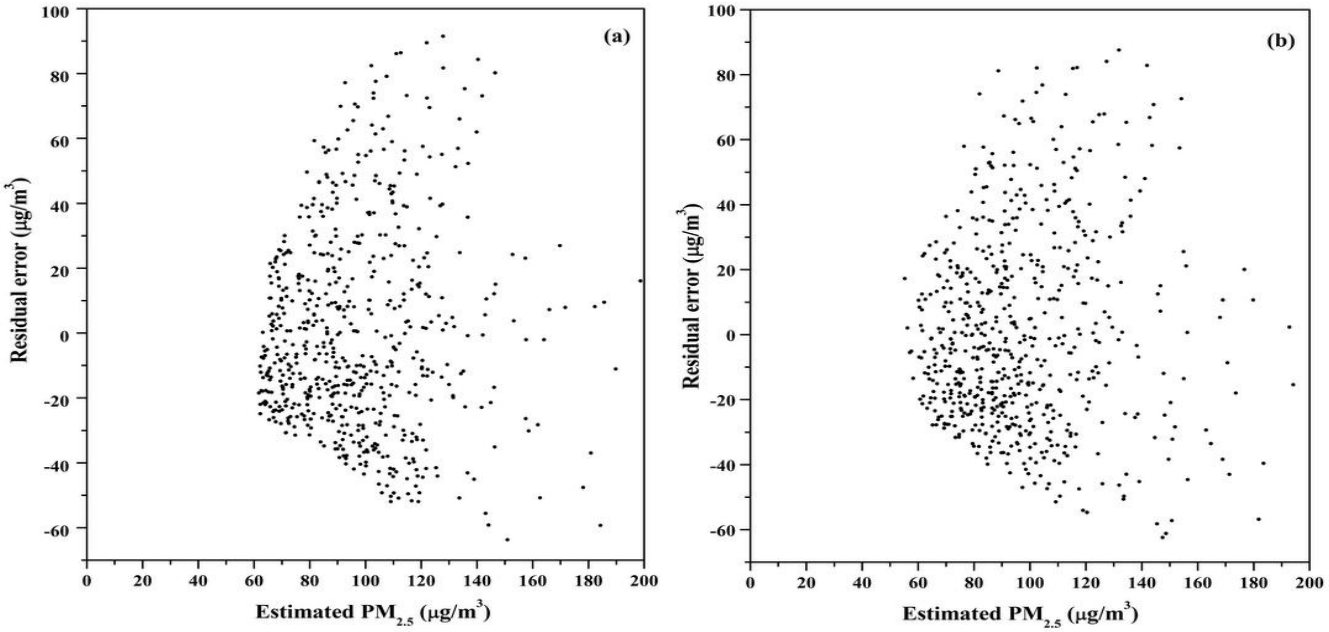

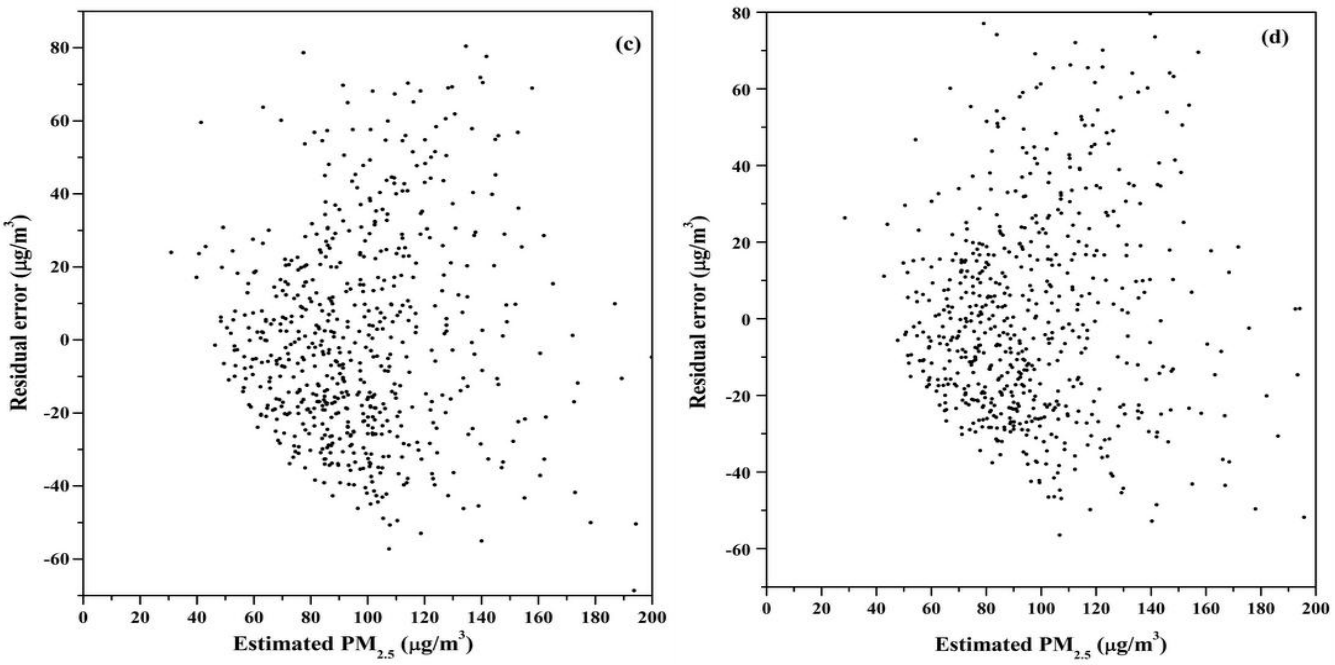

Figure 5.3. Residual plots of linear regression model of set I.

5.5 Estimation of $PM_{2.5}$ using logistic regression models

The results of the log-linear models of set II are presented in Table 5.4 which showed improved results than set I models. After log transformation skewness in the data distribution was reduced, consequently increasing the accuracy of the estimated regression coefficient (estimators) and their standard error (Liu et al., 2007). AOD_{MODIS} has been found to be moderate log-linear correlation with $PM_{2.5}$ (R= 0.65). This study showed improved results in respect to linear regression model when RH, WS, and AT were added successively to AOD_{MODIS} as regressors for the estimation of $PM_{2.5}$. All the regressors as well as estimator was found to be significant ($p \leq 0.05$). RH and WS have been found to have similar incremental effect of 0.04 and AT having the least impact of 0.02. In this case all the models have moderate value of R which was 0.65, 0.69. 0.73, and 0.75, respectively. Here, also the impact of meteorological parameters and of their estimators is experienced and analyzed in similar manner as that of multi-linear regression model above.

Figure 5.3 shows the residual plots between residual errors vs. estimated $PM_{2.5}$ for set II. These figure shows some improvement from (a) to (d) but none of these plots showed an ideal scatter. The fusion of constant band and divergent trend of residuals need further transformation in these models may facilitate a better estimation of $PM_{2.5}$ concentration. Nevertheless, these plots suggested the better adequacy of the log-linear regression models over the linear regression models.

The validation results of these models are presented in Table 5.5 The coefficient of correlation for validation results for all these models shows increasing trend as that of regression and also not much different from regression R. The RSE was nearly same for regression as well as validation. The model (d) of set II had the maximum R and the least RSE, and thus, it was able to provide the best estimates of $PM_{2.5}$ among the models presented in this study. However, the validation results were found to be satisfactory for all these models.

Table 5.4 Statistical result of logistic regression models

Model reference	Statistical parameters						
	R (sig.)	RSE (%)	α (sig.)	β_1 (sig.)	β_2 (sig.)	β_3 (sig.)	β_4 (sig.)
Set I (a)	0.65 (0.00)	6.65	2.05 (0.00)	0.35 (0.00)	-	-	-
Set I (b)	0.69 (0.00)	6.34	1.63 (0.00)	0.36 (0.00)	0.25 (0.00)	-	-
Set I (c)	0.73 (0.00)	5.98	1.85 (0.00)	0.33 (0.00)	0.20 (0.00)	-0.16 (0.00)	-
Set I (d)	0.75 (0.00)	5.78	2.41 (0.00)	0.35 (0.00)	0.07 (0.04)	-0.14 (0.00)	-0.26 (0.00)

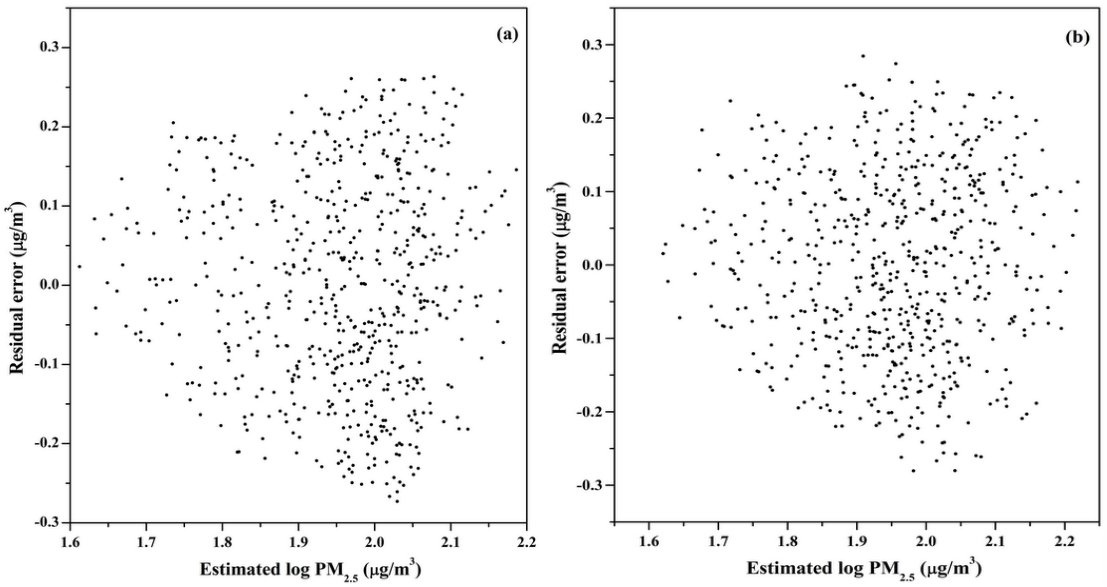

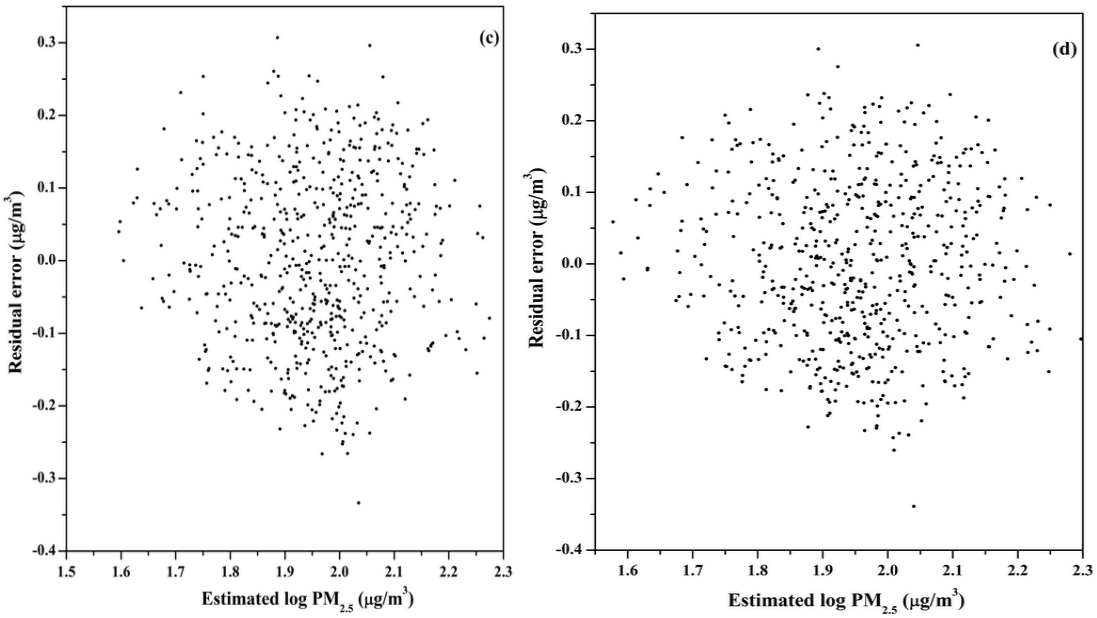

Figure 5.4 Residual plots of log linear regression model of set II.

Table 5.5 Brief comparison of regression and validation results

Model equation	Coefficient of correlation, R		RSE (in %)	
	Regression	Validation	Regression	Validation
Set I (a)	0.62	0.61	31.75	23.31
Set I (b)	0.65	0.71	30.77	20.84
Set I (c)	0.70	0.75	28.93	19.84
Set I (d)	0.73	0.75	27.83	19.91
Set II (a)	0.65	0.61	6.65	5.09
Set II (b)	0.69	0.72	6.34	4.45
Set II (c)	0.73	0.76	5.98	4.24
Set II (d)	0.75	0.76	5.78	4.23

6.1 Variation of $PM_{2.5}$ concentrations

Box plot of $PM_{2.5}$ four days before and four days after Diwali from 2009 to 2013 is shown in figure 6.1. The mean values of $PM_{2.5}$ during these periods were varied between 211.23±102.97 to 265.02±193.68 µg/m^3. The maximum value was obtained on Diwali days (265.02 µg/m^3). On Diwali day its concentration was 2.65 times higher than 24 hour average value of National Ambient Air Quality (NAAQ) standard of 100 µg/m^3. The average concentration of $PM_{2.5}$ before Diwali was 2.27 times higher and after Diwali its concentration was 2.26 times higher than NAAQ standard. The higher concentration of $PM_{2.5}$ on Diwali day indicates festive event. Generally festival of Diwali comes every year in between 3rd week of October to first week of November, during this period extensive burning of fireworks and crackers produces large amount of aerosol in the atmosphere (Attri et al., 2001; Singh et al., 2003). Figure 3.1 shows the average values of temperature, relative humidity, and wind speed, respectively during four days before and after Diwali from 2009 to 2014. The increase in concentration of $PM_{2.5}$ after one day of Diwali was attributed due to low wind speed.

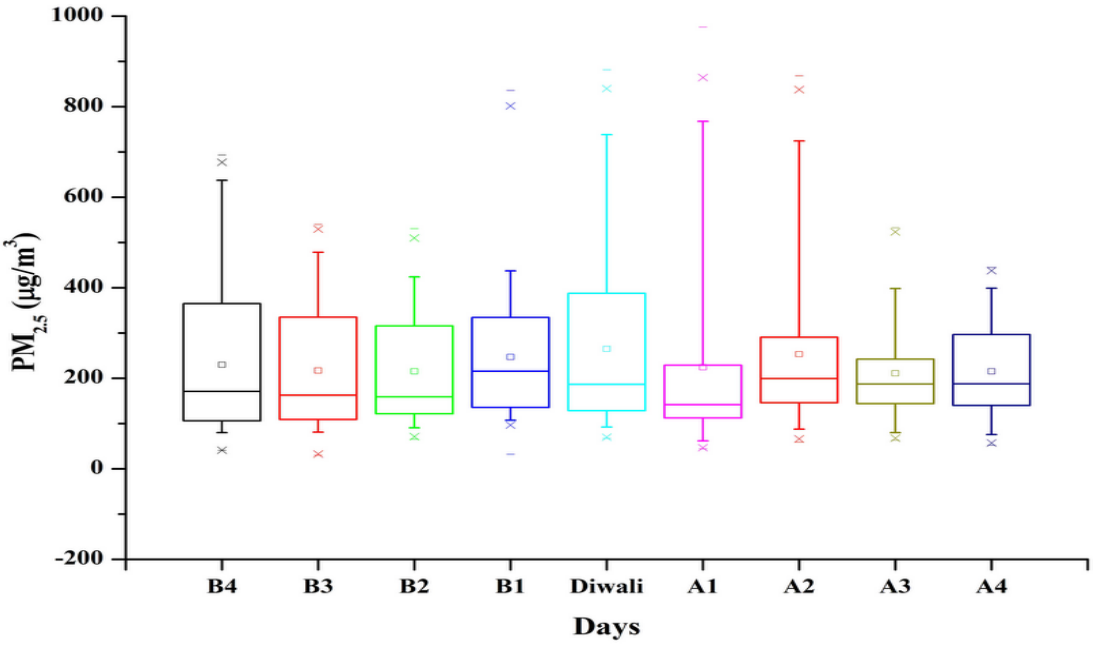

Figure 6.1 Box plot of $PM_{2.5}$ from 2009 to 2013 four days before and four days after Diwali. Here B1-B4 represent days before Diwali and A1-A4 represent days after Diwali.

6.2 Variation of BC and PM

The daily average value of BC in µg/m^3 with standard deviation from 21st to 25th October is shown in figure 6.2. The concentration of BC starts increasing from day one and minimum at the end of the day. We have measured BC concentration from 09:30 to 00:30. The concentration of BC at first day of this period was 8.69 ± 1.08 and last day, it was 9.25 ± 0.95. The highest concentration was obtained on the day of festival of light (14.6 ± 3.09). The daily average value during this study was 11.24 ± 1.55. It was due to celebration practices by the people and heavy traffic all around the sampling site and also Gas Turbine Power Station. Earlier Babu and Moorthy (2001) had reported 3 to 4 fold increase in BC concentration during festival event in respect to unperturbed background level at a tropical coastal station, Thiruvananthapuram.

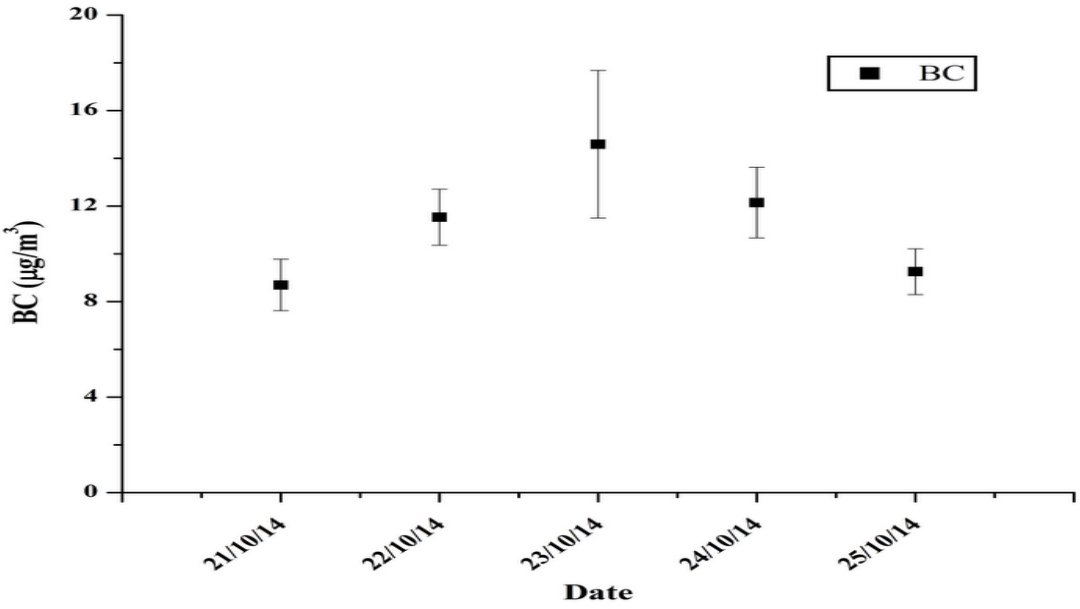

Figure 6.2 Daily average value of BC with standard deviation.

The diurnal average variability of BC is shown in figure 6.3. During this sampling period the concentration of BC was greater in morning hours (09:30 to 10:30) then after start decreasing up to 17:30 and again it start increasing up to 22:30, after that start decreasing. But on 22nd October (one day before Diwali) after morning hours, its concentration starts increasing from 14:30 because of vechuilar activities for shoping purposes. The maximum concentration (22.05 ± 6.83) was obtained on day of festival of light and minimum (10.16 ± 2.55) was obtained on last day of this period during morning hours. In

this period maximum concentration was obtained in morning hours but on Diwali day its concentration cross the maximum value of morning hour concentration (22.05µg/m3) at night. At night between 21:30 to 23:30, its concentration reached up to 26.75- 24.83 µg/m^3. It was due to accumulation of BC in the atmosphere because of burning of crackers and fireworks, then after it start decreasing. The morning hour's peak was due to traffic, local anthropogenic effect, accumulated BC concentration of night and low boundary layer.

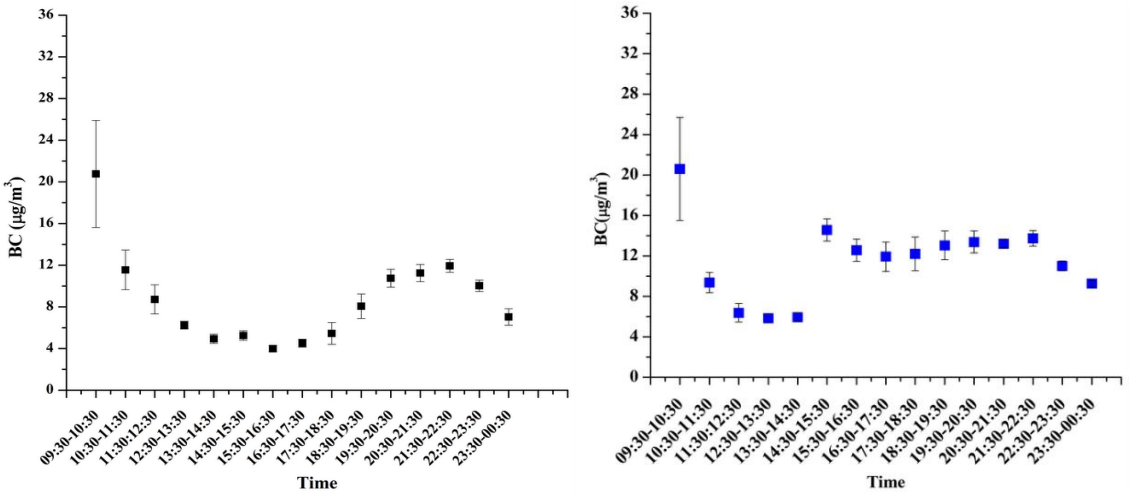

(a) (b)

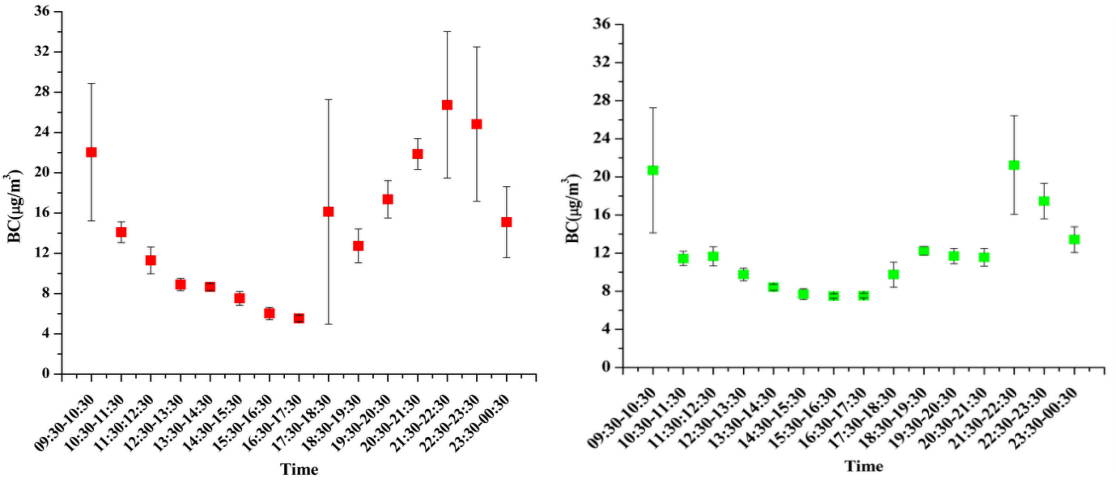

(c) (d)

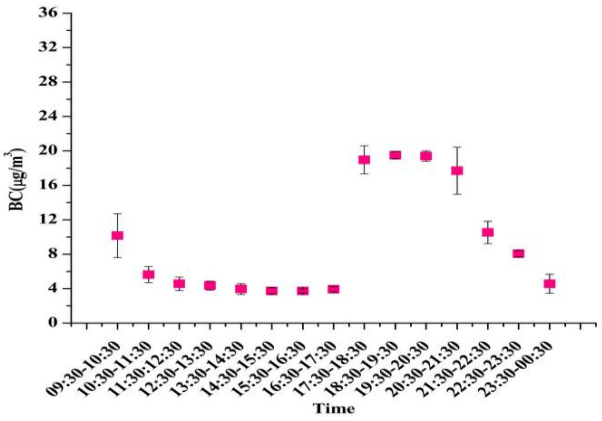

(e)

Figure 6.3 Diurnal variation of BC from 21st to 25th October.

The different size of particles are divided into two parts, namely fine (<1 and 1-2.5) and coarse (2.5-10 and >10). Figure 6.4 shows the daily variation of fine and coarse particles. During this period the concentration of fine particles were varied between 195.08 to 633.09 µg/m^3 and coarse particles varied between 117.78 to 209.80 µg/m^3. The maximum concentration of fine particles were obtained on Diwali day (633.09 µg/m^3), which indicate festive event and minimum concentration were obtained after two days of Diwali. The concentration of coarse particles on Diwali day was 206.12 µg/m^3. The

percentage contribution of fine and coarse particles is shown in figure 6.5. The percentage contribution of fine particle during this period was greater than those of coarse particle and its contribution was highest on Diwali day. This increased trend of smaller size particle concentration support the celebration practice by the people and heavy traffic all around the sampling site. Earlier Tiwari et al. (2012) had reported the concentration of PM_{10}, $PM_{2.5}$ and PM_1 as 723, 588, and 536 µg/m^3 in 2007 and 501, 389, and 346 µg/m^3 in 2008, respectively at Indian Institute of Tropical Meteorology (IITM), Delhi (residential site) on Diwali day. The concentration PM_{10} and $PM_{2.5}$ have been measured by CPCB (www.cpcb.nic.in) in 2014 which was 442 and 323 µg/m^3 on Diwali day at Pragati Maidan, which is near to Laxminagar. Table 6.1 shows the ambient aerosol mass concentration of PM_{10} and $PM_{2.5}$ at various locations measured by CPCB in 2014. Figure 6.6 shows the regression analysis between BC with fine and coarse mode particles. BC is in good correlation with fine mode particles ($R^2 = 0.76$) than coarse mode particles, which support the extensive burning of fireworks and crackers.

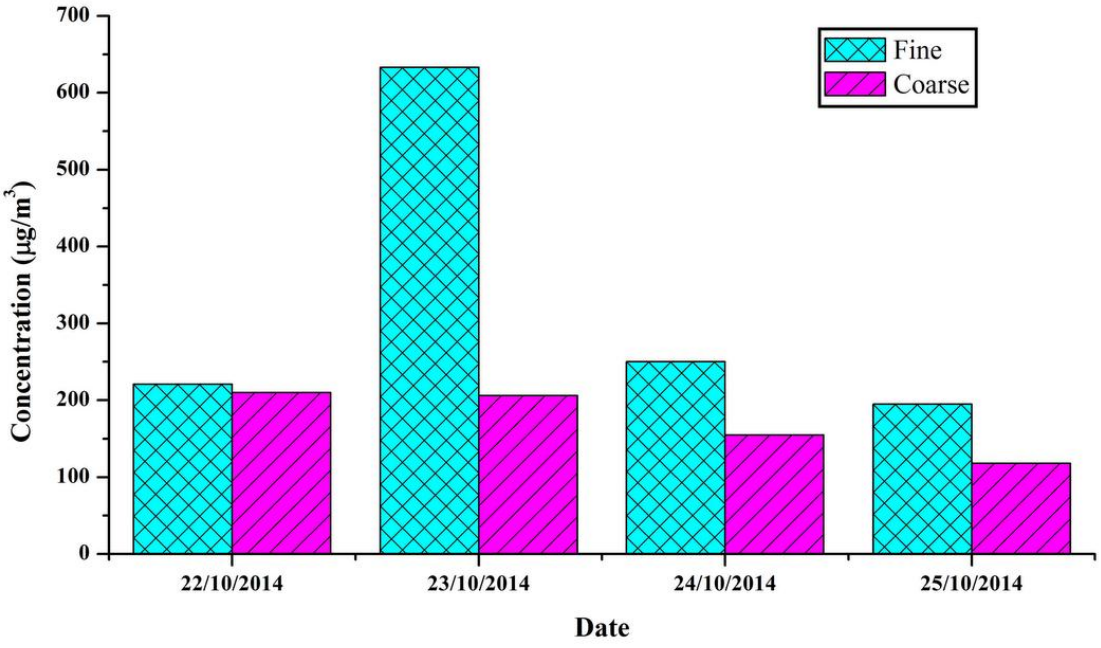

Figure 6.4 Daily variation of fine and coarse particles.

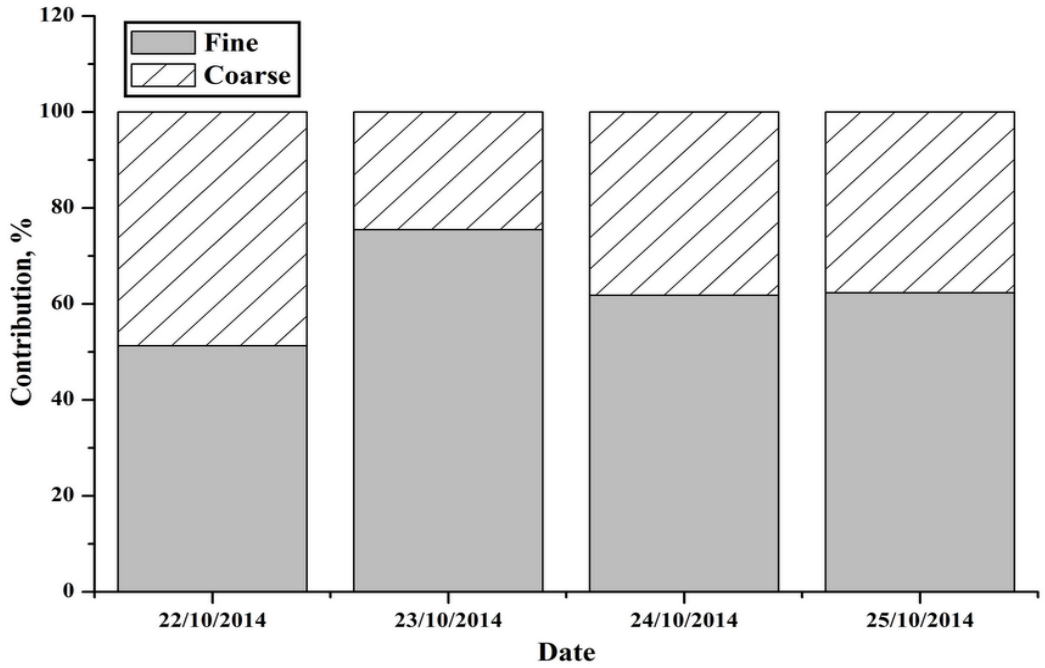

Figure 6.5 Percentage contribution of fine and coarse particles.

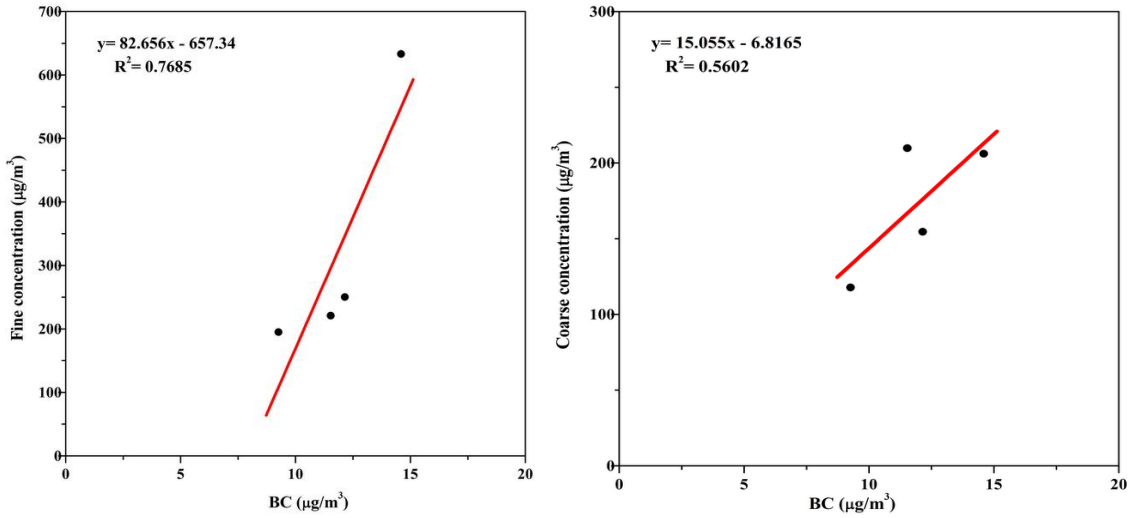

(a) (b)

Figure 6.6 Linear regression between BC and PM (a) fine and (b) coarse particles.

Table 6.1 Ambient aerosol mass concentrations of PM_{10} and $PM_{2.5}$ in $\mu g/m^3$at various locations measured by CPCB in 2014, on Diwali day.

Monitoring Location	PM_{10}	$PM_{2.5}$
1 Pragati Maidan	442	323
2 Pitampura	756	678
3 Janakpuri	648	510

6.3 Variation of AOD and Angstrom Parameter

Figure 6.7 shows the daily average variability of AOD at 500 nm wavelength, Ångstrom exponent (α), computed for the wavelength from 380-1020 nm and derivatives of Angstrom wavelength exponent (α′) computed for the wavelength pairs 380-500 nm and 500-675 nm with standard deviation during the festival of light. AOD starts escalating from day one of the festival and end at the maximum value during the festival. The value of AOD_{500} on Diwali day was 1.49 ± 0.38. AOD shows maximum value of 1.85 ± 0.14 at 500 nm wavelength on 24th October and 2.52 ± 0.16 on 25th October. It was due to burning of crackers, fireworks, local anthropogenic effect and persistence of aerosol in the atmosphere. When people start playing with the firecrackers, their values start increasing especially in urban cities. These firecrackers continuously contribute to the level of the anthropogenic aerosols. These types of anthropogenic activities produces shoot particles and organic carbon compounds, which is responsible for high AOD after festival (Singh et al., 2003). Babu and Moorthy (2001) had also reported the increased value of AODs during fireworks. The derivative of Angstrom exponent, α′ is an indicator of types of aerosol in the population of aerosol. Positive value of α′ is an indicator of dominance of fine/accumulation-mode particles and negative values of α′ indicate coarse-mode particles (Lodhi et al., 2013). α′ is positive during this period which indicates dominance of fine/accumulation-mode particles. However, it was lowest on one day before Diwali. This indicates that this period was dominated with fine mode particles; but

also inclusion of other fine mode particles due to fireworks. Singh et al 2014 had also reported the positive value of α′ during Diwali at Varanasi.

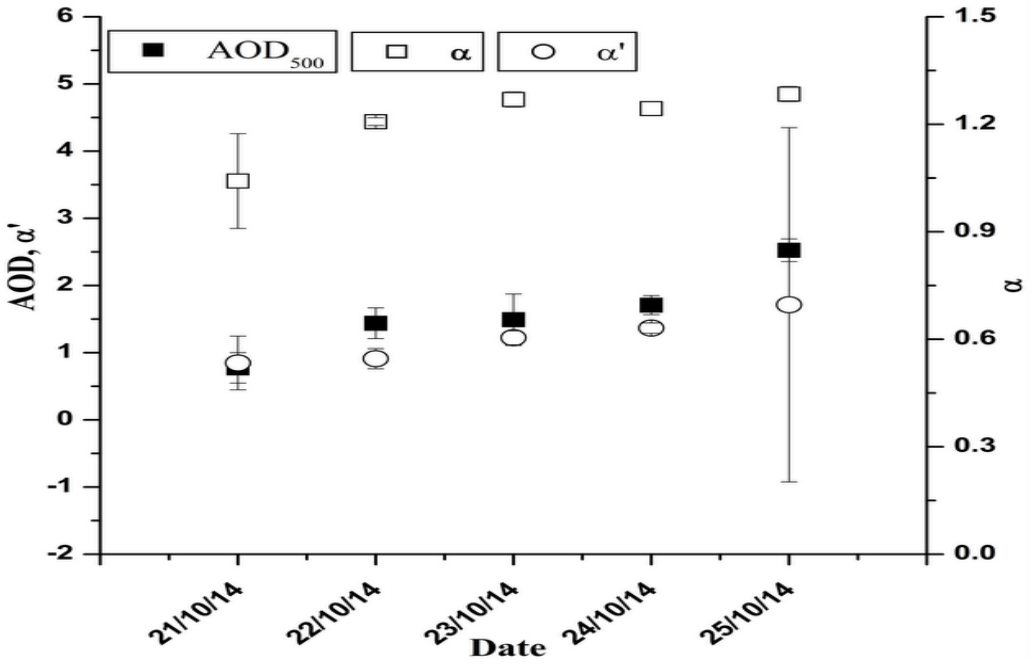

Figure 6.7 Daily average value of AOD_{500}, α and α′ with standard deviation.

Figure 6.8 shows the spectral variation of AOD at different wavelength. The continuous increment in AOD at all wavelengths and highest value of AOD at shorter wavelength was due to celebration practices during the festival. There was a larger variation in AOD at 380 nm and 500 nm as compared to 1020 nm because of interaction of aerosol with shorter wavelength than longer wavelength. The maximum variability has been seen on 25th October and then 22nd October. Singh et al 2003 had also found enhancement of 5.7% and 5.5% AODs at 340 and 500 nm wavelength respectively, during Diwali at Kanpur.

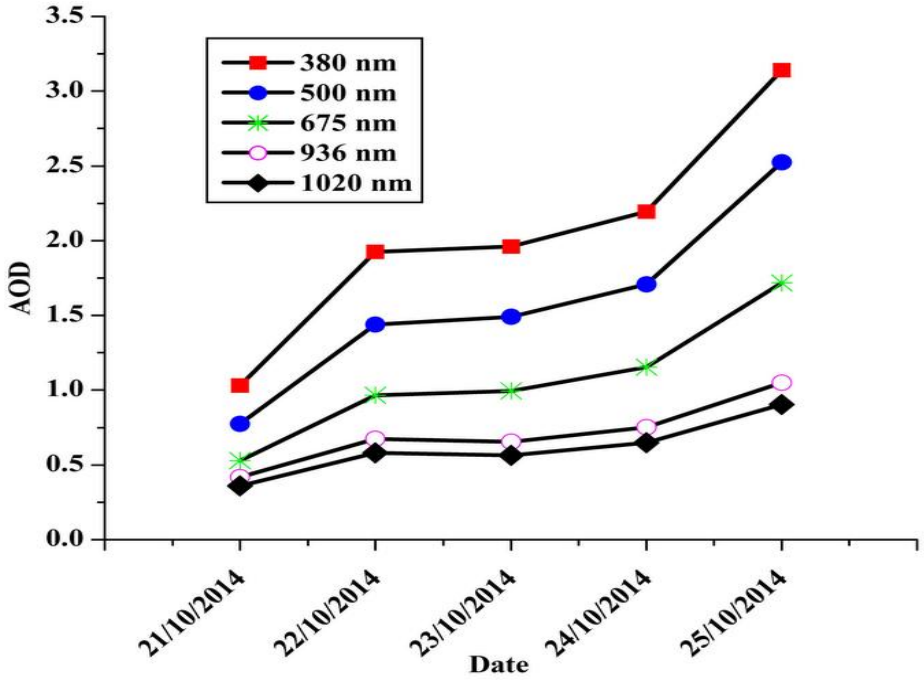

Figure 6.8 AOD variability at different wavelength.

Major findings of the present study are as follows:

- Long term climatology of MODIS derived deep blue AOD_{550} shows that its value was highest during post-monsoon season (0.96), decreases throughout the winter (0.69) to reach a low value in March (0.35), afterwards increase continuously up to pre-monsoon (0.68) and reaches to a lowest values in September (0.33) i.e. monsoon season (0.65).
- Daily variation of AOD 500 for the year 2014 shows that its value was maximum on 25th October (2.52) and minimum on 24th September (0.276). There was a consistent increase in average value of AOD_{500} as month progress from April to June (0.575, 0.684 and 0.796).
- Daily variation of BC shows that its average value was maximum on 19th December (19.32 µg/m^3) and 22nd December (18.65 µg/m^3) and minimum concentration was obtained on 25th September (0.86 µg/m^3) and 26th September (0.68 µg/m^3). The maximum average BC concentration is obtained in the month of December (8.18 µg/m^3) and January (9.82 µg/m^3) and lowest in the month of September (1.07 µg/m^3).
- Linear regression analysis of AOD with meteorological parameters (temperature, wind speed and RH) shows that AOD has insignificant negative correlation with temperature and wind speed and positive insignificant correlation with RH.
- Linear regression analysis of BC with meteorological parameter shows that BC has significant negative correlation with temperature and WS and significant positive correlation with RH.
- During the campaign period in 2012, 33.3%, 40.5% and 26.2% days are categorized as ‘relatively clean’, ‘normal’ and ‘extreme' aerosol days. AOD increases from 0.51 to 1.2 during the 'relatively clean' to 'extreme' aerosol days along with a decrease of Angstrom Exponent from 0.54 ± 0.09 to 0.22 ± 0.12.
- Relative contribution of coarse mode dust to aerosol mass increased from 76.8% ('relatively clean') to 96.8% ('extreme' events), while the corresponding contribution to $AOD_{0.5}$ increased from 35.0% to 70.8%. Spectrally increasing

single scattering albedo and CALIPSO aerosol sub-type information support the dominant presence of dust during the 'extreme' aerosol days.

- Aerosol direct radiative forcing (ADRF) at the top-of-the-atmosphere increases from 21.2 W m^{-2} ('relatively clean') to 56.6 W m^{-2} ('extreme'), while the corresponding change in surface ADRF is from -99.5 W m^{-2} to -153.5 W m^{-2}.
- Coarse mode dust contributes 60.3% to the surface ADRF during the 'extreme' days. The atmospheric heating rate induced by aerosols is enhanced by 75.1% (from 1.7 K/day to 2.96 K/day) during the 'extreme' aerosol days.
- Log-linear regression models (set II) shows better estimates of $PM_{2.5}$ in respect to linear regression models of set I. When RH, WS, and AT, respectively is added as a regressor R value is increased successively.
- The model (d) of set II had the highest R as 0.75 and minimum RSE as 5.78% and thus was declared as the best model to estimate hourly $PM_{2.5}$.
- Long term data of $PM_{2.5}$ four days before and four days after Diwali from 2009 to 2013 revealed that, its concentration was highest on Diwali day (265.02 μg/m^3), which indicates festive event. On Diwali day its concentration was 2.65 times higher than 24 hour average value of National Ambient Air Quality (NAAQ) standards of 100 μg/m^3.
- The daily average value of BC during this period was 11.15 ± 1.6 and maximum value was obtained on Diwali day (14.6 ± 3.09). Diurnal variation shows that concentration of BC was greater during morning hours (22.05 μg/m^3) but on Diwali day it crosses the maximum value of morning hour's peak at night (26.75-24.83 μg/m^3).
- On Diwali day concentration of fine particles were maximum, which indicates festive event. The percentage contribution of fine particle during this period was greater than those of coarse particle and its contribution was highest on Diwali day. Good correlation between BC and fine particles (R^2 = 0.76) support the extensive burning of fireworks and crackers.
- AOD starts escalating from day one of the festival and end at the maximum value during the festival. The positive value of α′ during this period indicates dominance of fine/accumulation-mode particles. The continuous increment in

AOD at all wavelengths and highest value of AOD at shorter wavelength was due to celebration practices during the festival.

- Ahmad, S., Khan, M.A., Husain, A., Matloob, H., Warsi, T., 2012. Monitoring of the air quality in Aligarh City, India using spot: VGT data. Journal of Environmental Research And Development Vol 6.
- Akeredolu, F., 1996. Environmental Engineering Notebook. Department of Chemical Engineering, Obafemi Awolowo University, Ile-Ife, Nigeria.
- Attri, A.K., Kumar, U., Jain, V., 2001. Microclimate: Formation of ozone by fireworks. Nature 411, 1015-1015.
- Babu, S.S., Moorthy, K.K., 2001. Anthropogenic impact on aerosol black carbon mass concentration at a tropical coastal station: A case study. Current Science 81, 1208-1214.
- Babu, S.S., Satheesh, S., Moorthy, K.K., 2002. Aerosol radiative forcing due to enhanced black carbon at an urban site in India. Geophysical Research Letters 29.
- Bano, T., Singh, S., Gupta, N., Soni, K., Tanwar, R., Nath, S., Arya, B., Gera, B., 2011. Variation in aerosol black carbon concentration and its emission estimates at the mega-city Delhi. International journal of remote sensing 32, 6749-6764.
- Bates, T.S., Huebert, B.J., Gras, J.L., Griffiths, F.B., Durkee, P.A., 1998. International Global Atmospheric Chemistry (IGAC) project's first aerosol characterization experiment (ACE 1): Overview. Journal of Geophysical Research: Atmospheres 103, 16297-16318.
- Bellouin, N., Boucher, O., Haywood, J., Reddy, M.S., 2005. Global estimate of aerosol direct radiative forcing from satellite measurements. Nature 438, 1138-1141.
- Boucher, O., Tanré, D., 2000. Estimation of the aerosol perturbation to the Earth's radiative budget over oceans using POLDER satellite aerosol retrievals. Geophysical research letters 27, 1103-1106.
- Cao, J., Wu, F., Chow, J., Lee, S., Li, Y., Chen, S., An, Z., Fung, K., Watson, J., Zhu, C., 2005. Characterization and source apportionment of atmospheric organic

and elemental carbon during fall and winter of 2003 in Xi'an, China. Atmospheric Chemistry and Physics 5, 3127-3137.

- Chin, M., Ginoux, P., Kinne, S., Torres, O., Holben, B.N., Duncan, B.N., Martin, R.V., Logan, J.A., Higurashi, A., Nakajima, T., 2002. Tropospheric aerosol optical thickness from the GOCART model and comparisons with satellite and Sun photometer measurements. Journal of the atmospheric sciences 59, 461-483.
- Chitranshi, S., Sharma, S.P., Dey, S., 2015. Satellite-based estimates of outdoor particulate pollution (PM10) for Agra City in northern India. Air Quality, Atmosphere & Health 8, 55-65.
- Chu, D., Kaufman, Y., Ichoku, C., Remer, L., Tanré, D., Holben, B., 2002. Validation of MODIS aerosol optical depth retrieval over land. Geophysical research letters 29.
- Chung, C.E., Ramanathan, V., Kim, D., Podgorny, I., 2005. Global anthropogenic aerosol direct forcing derived from satellite and ground-based observations. Journal of Geophysical Research: Atmospheres 110.
- Clarke, A.D., Kapustin, V.N., 2002. A Pacific aerosol survey. Part I: A decade of data on particle production, transport, evolution, and mixing in the troposphere*. Journal of the atmospheric sciences 59, 363-382.
- Conant, W.C., Seinfeld, J.H., Wang, J., Carmichael, G.R., Tang, Y., Uno, I., Flatau, P.J., Markowicz, K.M., Quinn, P.K., 2003. A model for the radiative forcing during ACE-Asia derived from CIRPAS Twin Otter and R/V Ronald H. Brown data and comparison with observations. Journal of Geophysical Research: Atmospheres 108.
- Cros, B., Durand, P., Cachier, H., Drobinski, P., Frejafon, E., Kottmeier, C., Perros, P., Peuch, V.-H., Ponche, J.-L., Robin, D., 2004. The ESCOMPTE program: an overview. Atmospheric Research 69, 241-279.
- Deuzé, J., Bréon, F., Devaux, C., Goloub, P., Herman, M., Lafrance, B., Maignan, F., Marchand, A., Nadal, F., Perry, G., 2001. Remote sensing of aerosols over

land surfaces from POLDER-ADEOS-1 polarized measurements. Journal of Geophysical Research: Atmospheres 106, 4913-4926.

- Dey, S., Tripathi, S., 2007. Estimation of aerosol optical properties and radiative effects in the Ganga basin, northern India, during the wintertime. Journal of Geophysical Research: Atmospheres 112.
- Dey, S., Tripathi, S., 2008. Aerosol direct radiative effects over Kanpur in the Indo-Gangetic basin, northern India: Long-term (2001–2005) observations and implications to regional climate. Journal of Geophysical Research: Atmospheres 113.
- Dey, S., Tripathi, S.N., Singh, R.P., Holben, B., 2004. Influence of dust storms on the aerosol optical properties over the Indo-Gangetic basin. Journal of Geophysical Research: Atmospheres 109.
- Di Girolamo, L., Bond, T., Bramer, D., Diner, D., Fettinger, F., Kahn, R., Martonchik, J., Ramana, M., Ramanathan, V., Rasch, P., 2004. Analysis of Multi-angle Imaging SpectroRadiometer (MISR) aerosol optical depths over greater India during winter 2001–2004. Geophysical Research Letters 31.
- Diner, D.J., Beckert, J.C., Bothwell, G.W., Rodriguez, J.I., 2002. Performance of the MISR instrument during its first 20 months in Earth orbit. IEEE Transactions on Geoscience and Remote Sensing 40, 1449-1466.
- Dockery, D.W., Pope, C.A., Xu, X., Spengler, J.D., Ware, J.H., Fay, M.E., Ferris Jr, B.G., Speizer, F.E., 1993. An association between air pollution and mortality in six US cities. New England journal of medicine 329, 1753-1759.
- Dubovik, O., Holben, B., Eck, T.F., Smirnov, A., Kaufman, Y.J., King, M.D., Tanré, D., Slutsker, I., 2002. Variability of absorption and optical properties of key aerosol types observed in worldwide locations. Journal of the atmospheric sciences 59, 590-608.
- Eck, T., Holben, B., Ward, D., Mukelabai, M., Dubovik, O., Smirnov, A., Schafer, J., Hsu, N., Piketh, S., Queface, A., 2003. Variability of biomass burning aerosol optical characteristics in southern Africa during the SAFARI 2000 dry

season campaign and a comparison of single scattering albedo estimates from radiometric measurements. Journal of Geophysical Research: Atmospheres 108.

- Eldering, A., Larson, S.M., Hall, J.R., Hussey, K.J., Cass, G.R., 1993. Development of an improved image processing based visibility model. Environmental science & technology 27, 626-635.
- Finlayson-Pitts, B., Pitts, J.N., 2000. Chemistry of the upper and lower troposphere. Academic Press: New York.
- Flanner, M.G., Zender, C.S., Randerson, J.T., Rasch, P.J., 2007. Present-day climate forcing and response from black carbon in snow. Journal of Geophysical Research: Atmospheres 112.
- Forster, P., Ramaswamy, V., Artaxo, P., Berntsen, T., Betts, R., Fahey, D.W., Haywood, J., Lean, J., Lowe, D.C., Myhre, G., 2007. Changes in atmospheric constituents and in radiative forcing. Chapter 2, Climate Change 2007. The Physical Science Basis.
- Fruin, S.A., Winer, A.M., Rodes, C.E., 2004. Black carbon concentrations in California vehicles and estimation of in-vehicle diesel exhaust particulate matter exposures. Atmospheric Environment 38, 4123-4133.
- Ganguly, D., Jayaraman, A., Gadhavi, H., 2006a. Physical and optical properties of aerosols over an urban location in western India: Seasonal variabilities. Journal of Geophysical Research: Atmospheres 111.
- Ganguly, D., Jayaraman, A., Rajesh, T., Gadhavi, H., 2006b. Wintertime aerosol properties during foggy and nonfoggy days over urban center Delhi and their implications for shortwave radiative forcing. Journal of Geophysical Research: Atmospheres 111.
- Gautam, R., Hsu, N., Lau, K.-M., Kafatos, M., 2009. Aerosol and rainfall variability over the Indian monsoon region: distributions, trends and coupling, Annales Geophysicae. Copernicus GmbH, pp. 3691-3703.

- Gautam, R., Hsu, N.C., Kafatos, M., Tsay, S.C., 2007. Influences of winter haze on fog/low cloud over the Indo-Gangetic plains. Journal of Geophysical Research: Atmospheres 112.
- Griffiths, F., Bates, T., Quinn, P., Clementson, L., Parslow, J., 1999. Oceanographic context of the First Aerosol Characterization Experiment (ACE 1): A physical, chemical, and biological overview. Journal of Geophysical Research: Atmospheres 104, 21649-21671.
- Gupta, P., Christopher, S.A., Wang, J., Gehrig, R., Lee, Y., Kumar, N., 2006. Satellite remote sensing of particulate matter and air quality assessment over global cities. Atmospheric Environment 40, 5880-5892.
- Hansen, A., Rosen, H., Novakov, T., 1984. The aethalometer—an instrument for the real-time measurement of optical absorption by aerosol particles. Science of the Total Environment 36, 191-196.
- Hansen, J., Nazarenko, L., 2004. Soot climate forcing via snow and ice albedos. Proceedings of the National Academy of Sciences of the United States of America 101, 423-428.
- Hansen, J., Sato, M., Ruedy, R., 1997. Radiative forcing and climate response. Journal of Geophysical Research: Atmospheres 102, 6831-6864.
- Hansen, J.E., Travis, L.D., 1974. Light scattering in planetary atmospheres. Space Science Reviews 16, 527-610.
- Harrison, L., Michalsky, J., Berndt, J., 1994. Automated multifilter rotating shadow-band radiometer: an instrument for optical depth and radiation measurements. Applied Optics 33, 5118-5125.
- Haywood, J., Boucher, O., 2000. Estimates of the direct and indirect radiative forcing due to tropospheric aerosols: A review. Reviews of geophysics 38, 513-543.
- Hegg, D.A., Livingston, J., Hobbs, P.V., Novakov, T., Russell, P., 1997. Chemical apportionment of aerosol column optical depth off the mid-Atlantic

coast of the United States. Journal of Geophysical Research: Atmospheres 102, 25293-25303.

- Herman, J., Bhartia, P., Torres, O., Hsu, C., Seftor, C., Celarier, E., 1997. Global distribution of UV-absorbing aerosols from Nimbus 7/TOMS data. Journal of Geophysical Research: Atmospheres 102, 16911-16922.
- Herrmann, P., Hänel, G., 1997. Wintertime optical properties of atmospheric particles and weather. Atmospheric Environment 31, 4053-4062.
- Hess, M., Koepke, P., Schult, I., 1998. Optical properties of aerosols and clouds: The software package OPAC. Bulletin of the American meteorological society 79, 831-844.
- Hess, M., Wiegner, M., 1994. COP: a data library of optical properties of hexagonal ice crystals. Applied optics 33, 7740-7746.
- Hignett, P., Taylor, J., 1997. Aircraft observations of direct aerosol forcing during TARFOX. EOS, Trans. Amer. Geophys. Union 78, S88.
- Holben, B., Tanre, D., Smirnov, A., Eck, T., Slutsker, I., Abuhassan, N., Newcomb, W., Schafer, J., Chatenet, B., Lavenu, F., 2001. An emerging ground-based aerosol climatology: Aerosol optical depth from AERONET. Journal of Geophysical Research: Atmospheres 106, 12067-12097.
- Houghton, J., Ding, Y., Griggs, D., Noguer, M., Van der Linden, P., Dai, X., Maskell, K., Johnson, C., 2001. IPCC 2001: Climate Change 2001. The Climate change Contribution of Working Group I to the Third Assessment Report of the Intergovemmental Panel on Climate Change 159.
- Husar, R.B., Prospero, J.M., Stowe, L.L., 1997. Characterization of tropospheric aerosols over the oceans with the NOAA advanced very high resolution radiometer optical thickness operational product. Journal of Geophysical Research: Atmospheres 102, 16889-16909.
- Jacobson, M.Z., 2004. Climate response of fossil fuel and biofuel soot, accounting for soot's feedback to snow and sea ice albedo and emissivity. Journal of Geophysical Research: Atmospheres 109.

- Jayaraman, A., Gadhavi, H., Ganguly, D., Misra, A., Ramachandran, S., Rajesh, T., 2006. Spatial variations in aerosol characteristics and regional radiative forcing over India: Measurements and modeling of 2004 road campaign experiment. Atmospheric Environment 40, 6504-6515.
- Jayaraman, A., Lubin, D., Ramachandran, S., Ramanathan, V., Woodbridge, E., Collins, W., Zalpuri, K., 1998. Direct observations of aerosol radiative forcing over the tropical Indian Ocean during the January-February 1996 pre-INDOEX cruise. Journal of Geophysical Research: Atmospheres 103, 13827-13836.
- Jin, Z., Charlock, T.P., Rutledge, K., Cota, G., Kahn, R., Redemann, J., Zhang, T., Rutan, D.A., Rose, F., 2005. Radiative transfer modeling for the CLAMS experiment. Journal of the atmospheric sciences 62, 1053-1071.
- Johnson, R., 2005. Miller and Freund's Probability and Statistics for Engineers:: Pearson Prentice Hall. Upper Saddle River, New Jersey.
- Justice, E., Huston, L., Krauth, D., Mack, J., Oza, S., Strawa, A.W., Skiles, J., Legg, M., Schmidt, C., 2009. INVESTIGATING CORRELATIONS BETWEEN SATELLITE-DERIVED AEROSOL OPTICAL DEPTH AND GROUND PM2. 5 MEASUREMENTS IN CALIFORNIA'S SAN JOAQUIN VALLEY WITH MODIS DEEP BLUE, American Society of Photogrammetry and Remote Sensing Annual Conference, pp. 9-13.
- Kahn, R., Anderson, J., Anderson, T.L., Bates, T., Brechtel, F., Carrico, C.M., Clarke, A., Doherty, S.J., Dutton, E., Flagan, R., 2004. Environmental snapshots from ACE-Asia. Journal of Geophysical Research: Atmospheres 109.
- Kasten, F., 1965. A new table and approximation formula for the relative optial air mass. Archiv für Meteorologie, Geophysik und Bioklimatologie, Serie B 14, 206-223.
- Kaufman, Y., Boucher, O., Tanré, D., Chin, M., Remer, L., Takemura, T., 2005. Aerosol anthropogenic component estimated from satellite data. Geophysical Research Letters 32.

- Kaufman, Y., Gitelson, A., Karnieli, A., Ganor, E., Fraser, R., Nakajima, T., Mattoo, S., Holben, B., 1994. Size distribution and scattering phase function of aerosol particles retrieved from sky brightness measurements.
- Kaufman, Y., Hobbs, P., Kirchhoff, V., Artaxo, P., Remer, L., Holben, B., King, M., Ward, D., Prins, E., Longo, K., 1998a. Smoke, Clouds, and Radiation-Brazil (SCAR-B) experiment. Journal of Geophysical Research: Atmospheres 103, 31783-31808.
- Kaufman, Y.J., Holben, B.N., Tanré, D., Slutsker, I., Smirnov, A., Eck, T.F., 2000. Will aerosol measurements from Terra and Aqua polar orbiting satellites represent the daily aerosol abundance and properties? Geophysical Research Letters 27, 3861-3864.
- Kaufman, Y.J., Justice, C.O., Flynn, L.P., Kendall, J.D., Prins, E.M., Giglio, L., Ward, D.E., Menzel, W.P., Setzer, A.W., 1998b. Potential global fire monitoring from EOS-MODIS. Journal of Geophysical Research: Atmospheres 103, 32215-32238.
- Keil, A., Haywood, J.M., 2003. Solar radiative forcing by biomass burning aerosol particles during SAFARI 2000: A case study based on measured aerosol and cloud properties. Journal of Geophysical Research: Atmospheres 108.
- Kiehl, J.T., Trenberth, K.E., 1997. Earth's annual global mean energy budget. Bulletin of the American Meteorological Society 78, 197-208.
- Kim, D.H., Sohn, B., Nakajima, T., Takamura, T., 2005. Aerosol radiative forcing over East Asia determined from ground-based solar radiation measurements. Journal of Geophysical Research: Atmospheres 110.
- Kimani, N., 2007. Environmental Pollution and Impact to Public Health. Implication of the Dandora Municipal Dumping Site in Nairobi, Kenya. a pilot study report In cooperation with The United Nations Environment Programme (UNEP).

- King, M.D., Kaufman, Y.J., Tanré, D., Nakajima, T., 1999. Remote sensing of tropospheric aerosols from space: Past, present, and future. Bulletin of the American Meteorological society 80, 2229-2259.
- Krishnamurti, T., Jha, B., Prospero, J., Jayaraman, A., Ramanathan, V., 1998. Aerosol and pollutant transport and their impact on radiative forcing over the tropical Indian Ocean during the January–February 1996 pre-INDOEX cruise. Tellus B 50.
- Kumar, N., Chu, A., Foster, A., 2008. Remote sensing of ambient particles in Delhi and its environs: estimation and validation. International Journal of Remote Sensing 29, 3383-3405.
- Kumar, N., Chu, A.D., Foster, A.D., Peters, T., Willis, R., 2011. Satellite remote sensing for developing time and space resolved estimates of ambient particulate in Cleveland, OH. Aerosol Science and Technology 45, 1090-1108.
- Kumar, S., Dey, S., Srivastava, A., 2016. Quantifying enhancement in aerosol radiative forcing during 'extreme aerosol days' in summer at Delhi National Capital Region, India. Science of The Total Environment 550, 994-1000.
- Latha, K.M., Badarinath, K., Moorthy, K.K., 2004. Impact of diesel vehicular emissions on ambient black carbon concentration at an urban location in India. Current Science 86, 451-453.
- Liu, Y., Franklin, M., Kahn, R., Koutrakis, P., 2007. Using aerosol optical thickness to predict ground-level PM 2.5 concentrations in the St. Louis area: a comparison between MISR and MODIS. Remote sensing of Environment 107, 33-44.
- Lodhi, N.K., Beegum, S.N., Singh, S., Kumar, K., 2013. Aerosol climatology at Delhi in the western Indo-Gangetic Plain: Microphysics, long-term trends, and source strengths. Journal of Geophysical Research: Atmospheres 118, 1361-1375.
- Lohmann, U., Feichter, J., 2005. Global indirect aerosol effects: a review. Atmospheric Chemistry and Physics 5, 715-737.

- Magi, B.I., Hobbs, P.V., Kirchstetter, T.W., Novakov, T., Hegg, D.A., Gao, S., Redemann, J., Schmid, B., 2005. Aerosol properties and chemical apportionment of aerosol optical depth at locations off the US east coast in July and August 2001. Journal of the atmospheric sciences 62, 919-933.
- Mallet, M., Roger, J., Despiau, S., Dubovik, O., Putaud, J., 2003. Microphysical and optical properties of aerosol particles in urban zone during ESCOMPTE. Atmospheric Research 69, 73-97.
- Malm, W.C., Day, D.E., 2001. Estimates of aerosol species scattering characteristics as a function of relative humidity. Atmospheric Environment 35, 2845-2860.
- Malm, W.C., Day, D.E., Kreidenweis, S.M., 2000. Light scattering characteristics of aerosols as a function of relative humidity: Part I—a comparison of measured scattering and aerosol concentrations using the theoretical models. Journal of the Air & Waste Management Association 50, 686-700.
- Malm, W.C., Sisler, J.F., Huffman, D., Eldred, R.A., Cahill, T.A., 1994. Spatial and seasonal trends in particle concentration and optical extinction in the United States. Journal of Geophysical Research: Atmospheres 99, 1347-1370.
- Matthias, V., Balis, D., Bösenberg, J., Eixmann, R., Iarlori, M., Komguem, L., Mattis, I., Papayannis, A., Pappalardo, G., Perrone, M., 2004. Vertical aerosol distribution over Europe: Statistical analysis of Raman lidar data from 10 European Aerosol Research Lidar Network (EARLINET) stations. Journal of Geophysical Research: Atmospheres 109.
- Menon, S., Hansen, J., Nazarenko, L., Luo, Y., 2002. Climate effects of black carbon aerosols in China and India. Science 297, 2250-2253.
- Mishra, A., Srivastava, A., Jain, V., 2013. Spectral dependency of aerosol optical depth and derived aerosol size distribution over Delhi: an implication to pollution source. Sustainable Environ. Res 23, 113-128.

- Mishra, S., Dey, S., Tripathi, S., 2008. Implications of particle composition and shape to dust radiative effect: A case study from the Great Indian Desert. Geophysical Research Letters 35.
- Moorthy, K., Niranjan, K., Narasimhamurthy, B., Agashe, V., Murthy, B.K., 1999. Aerosol Climatology over India, 1, ISRO GBP MWR network and data base. ISRO GBP SR-03 99.
- Moorthy, K.K., Babu, S.S., Satheesh, S., 2005. Aerosol characteristics and radiative impacts over the Arabian Sea during the intermonsoon season: Results from ARMEX field campaign. Journal of the atmospheric sciences 62, 192-206.
- Murayama, T., Sugimoto, N., Uno, I., Kinoshita, K., Aoki, K., Hagiwara, N., Liu, Z., Matsui, I., Sakai, T., Shibata, T., 2001. Ground-based network observation of Asian dust events of April 1998 in east Asia. Journal of Geophysical Research: Atmospheres 106, 18345-18359.
- Noble, C.A., Prather, K.A., 1998. Single particle characterization of albuterol metered dose inhaler aerosol in near real-time. Aerosol science and technology 29, 294-306.
- Novakov, T., Hegg, D.A., Hobbs, P.V., 1997. Airborne measurements of carbonaceous aerosols on the East Coast of the United States. Journal of Geophysical Research: Atmospheres 102, 30023-30030.
- Omar, A.H., Winker, D.M., Vaughan, M.A., Hu, Y., Trepte, C.R., Ferrare, R.A., Lee, K.-P., Hostetler, C.A., Kittaka, C., Rogers, R.R., 2009. The CALIPSO automated aerosol classification and lidar ratio selection algorithm. Journal of Atmospheric and Oceanic Technology 26, 1994-2014.
- Pandithurai, G., Dipu, S., Dani, K., Tiwari, S., Bisht, D., Devara, P., Pinker, R., 2008. Aerosol radiative forcing during dust events over New Delhi, India. Journal of Geophysical Research: Atmospheres 113.
- Pandithurai, G., Pinker, R., Takamura, T., Devara, P., 2004. Aerosol radiative forcing over a tropical urban site in India. Geophysical research letters 31.

- Petzold, A., Kopp, C., Niessner, R., 1997. The dependence of the specific attenuation cross-section on black carbon mass fraction and particle size. Atmospheric Environment 31, 661-672.
- Pincus, R., Baker, M.B., 1994. Effect of precipitation on the albedo susceptibility of clouds in the marine boundary layer. Nature 372, 250-252.
- Pope III, C.A., Burnett, R.T., Thun, M.J., Calle, E.E., Krewski, D., Ito, K., Thurston, G.D., 2002. Lung cancer, cardiopulmonary mortality, and long-term exposure to fine particulate air pollution. Jama 287, 1132-1141.
- Prasad, A.K., Singh, R.P., Kafatos, M., 2006. Influence of coal based thermal power plants on aerosol optical properties in the Indo-Gangetic basin. Geophysical Research Letters 33.
- Quenzel, H., Müller, H., 1978. Optical Properties of Single Mie Particles: Diagrams of Intensity-extinction-scattering-and Absorption Efficiencies. Münchener Universitäts-Schriften.
- Quinn, P., Bates, T., Coffman, D., Miller, T., Johnson, J., Covert, D., Putaud, J.P., Neusüß, C., Novakov, T., 2000. A comparison of aerosol chemical and optical properties from the 1st and 2nd Aerosol Characterization Experiments. Tellus B 52, 239-257.
- Ramachandran, S., Rajesh, T., 2007. Black carbon aerosol mass concentrations over Ahmedabad, an urban location in western India: comparison with urban sites in Asia, Europe, Canada, and the United States. Journal of Geophysical Research: Atmospheres 112.
- Ramachandran, S., Rengarajan, R., Jayaraman, A., Sarin, M., Das, S.K., 2006. Aerosol radiative forcing during clear, hazy, and foggy conditions over a continental polluted location in north India. Journal of Geophysical Research: Atmospheres 111.
- Ramanathan, V., Crutzen, P., 2003. New directions: Atmospheric brown "clouds". Atmospheric Environment 37, 4033-4035.

- Ramanathan, V., Crutzen, P., Kiehl, J., Rosenfeld, D., 2001. Aerosols, climate, and the hydrological cycle. science 294, 2119-2124.
- Ramaswamy, V., Boucher, O., Haigh, J., Hauglustaine, D., Haywood, J., Myhre, G., Nakajima, T., Shi, G., Solomon, S., Betts, R.E., 2001. Radiative forcing of climate change. Pacific Northwest National Laboratory (PNNL), Richland, WA (US).
- Remer, L.A., Gassò, S., Hegg, D.A., Kaufman, Y.J., Holben, B.N., 1997. Urban/industrial aerosol: Ground-based Sun/sky radiometer and airborne in situ measurements. Journal of Geophysical Research: Atmospheres 102, 16849-16859.
- Remer, L.A., Kaufman, Y., Tanré, D., Mattoo, S., Chu, D., Martins, J.V., Li, R.-R., Ichoku, C., Levy, R., Kleidman, R., 2005. The MODIS aerosol algorithm, products, and validation. Journal of the atmospheric sciences 62, 947-973.
- Ricchiazzi, P., Yang, S., Gautier, C., Sowle, D., 1998. SBDART: A research and teaching software tool for plane-parallel radiative transfer in the Earth's atmosphere. Bulletin of the American Meteorological Society 79, 2101.
- Russell, P., Livingston, J., Hignett, P., Kinne, S., Wong, J., Chien, A., Bergstrom, R., Durkee, P., Hobbs, P., 1999. Aerosol-induced radiative flux changes off the United States mid-Atlantic coast: Comparison of values calculated from Sunphotometer and in situ data with those measured by airborne pyranometer. Journal of Geophysical Research: Atmospheres 104, 2289-2307.
- Satheesh, S., Ramanathan, V., 2000. Large differences in tropical aerosol forcing at the top of the atmosphere and Earth's surface. Nature 405, 60-63.
- Seinfeld, J.H., Kahn, R.A., Anderson, T.L., Charlson, R.J., 2004. Scientific objectives, measurement needs, and challenges motivating the PARAGON aerosol initiative. Bulletin of the American Meteorological Society 85, 1503.
- Seinfeld, J.H., Pandis, S.N., 2016. Atmospheric chemistry and physics: from air pollution to climate change. John Wiley & Sons.

- Sikka, D., 1997. Desert climate and its dynamics. CURRENT SCIENCE-BANGALORE- 72, 35-46.
- Singh, R., Dey, S., Holben, B., 2003. Aerosol behaviour in Kanpur during Diwali festival. Current Science 84, 1302-1304.
- Singh, R., Dey, S., Tripathi, S., Tare, V., Holben, B., 2004. Variability of aerosol parameters over Kanpur, northern India. Journal of Geophysical Research: Atmospheres 109.
- Singh, S., Nath, S., Kohli, R., Singh, R., 2005. Aerosols over Delhi during pre-monsoon months: Characteristics and effects on surface radiation forcing. Geophysical Research Letters 32.
- Singh, S., Soni, K., Bano, T., Tanwar, R., Nath, S., Arya, B., 2010. Clear-sky direct aerosol radiative forcing variations over mega-city Delhi, Annales Geophysicae. European Geosciences Union, pp. 1157-1166.
- Solomon, S., 2007. Climate change 2007-the physical science basis: Working group I contribution to the fourth assessment report of the IPCC. Cambridge University Press.
- Srivastava, A., Tiwari, S., Devara, P., Bisht, D., Srivastava, M.K., Tripathi, S., Goloub, P., Holben, B., 2011. Pre-monsoon aerosol characteristics over the Indo-Gangetic Basin: implications to climatic impact, Annales Geophysicae. European Geosciences Union, pp. 789-804.
- Srivastava, P., Dey, S., Agarwal, P., Basil, G., 2014. Aerosol characteristics over Delhi national capital region: a satellite view. International Journal of Remote Sensing 35, 5036-5052.
- Stamnes, K., Tsay, S.-C., Wiscombe, W., Jayaweera, K., 1988. Numerically stable algorithm for discrete-ordinate-method radiative transfer in multiple scattering and emitting layered media. Applied optics 27, 2502-2509.
- Stern, A., Boubel, R., Turner, D., Fox, D., 1984. Fundamental of air pollution. Ed. ke-2. Orlando: Academic Press, Inc.

- Tanré, D., Kaufman, Y., Herman, M., Mattoo, S., 1997. Remote sensing of aerosol properties over oceans using the MODIS/EOS spectral radiances. Journal of Geophysical Research: Atmospheres 102, 16971-16988.
- Tanré, D., Kaufman, Y., Holben, B.e.a., Chatenet, B., Karnieli, A., Lavenu, F., Blarel, L., Dubovik, O., Remer, L., Smirnov, A., 2001. Climatology of dust aerosol size distribution and optical properties derived from remotely sensed data in the solar spectrum. Journal of Geophysical Research: Atmospheres 106, 18205-18217.
- Tiwari, S., Chate, D., Srivastava, M., Safai, P., Srivastava, A., Bisht, D., Padmanabhamurty, B., 2012. Statistical evaluation of PM10 and distribution of PM1, PM2. 5, and PM10 in ambient air due to extreme fireworks episodes (Deepawali festivals) in megacity Delhi. Natural hazards 61, 521-531.
- Tiwari, S., Srivastava, A., Bisht, D., Parmita, P., Srivastava, M.K., Attri, S., 2013. Diurnal and seasonal variations of black carbon and PM 2.5 over New Delhi, India: influence of meteorology. Atmospheric Research 125, 50-62.
- Torres, O., Bhartia, P., Herman, J., Ahmad, Z., Gleason, J., 1998. Derivation of aerosol properties from satellite measurements of backscattered ultraviolet radiation: Theoretical basis. Journal of Geophysical Research: Atmospheres 103, 17099-17110.
- Torres, O., Bhartia, P., Sinyuk, A., Welton, E., Holben, B., 2005. Total Ozone Mapping Spectrometer measurements of aerosol absorption from space: Comparison to SAFARI 2000 ground-based observations. Journal of Geophysical Research: Atmospheres 110.
- Trijonis, J., Malm, W., Pitchford, M., White, W., 1991. Visibility: Existing and Historical Conditions–Causes and Effects, u: Acidic Deposition: State of Science and Technology, Volume III: Terrestrial, Materials. Health and Visibility Effects.
- Tripathi, S., Pattnaik, A., Dey, S., 2007. Aerosol indirect effect over Indo-Gangetic plain. Atmospheric Environment 41, 7037-7047.

- Twomey, S., 1974. Pollution and the planetary albedo. Atmospheric Environment (1967) 8, 1251-1256.
- Twomey, S., 1977. The influence of pollution on the shortwave albedo of clouds. Journal of the atmospheric sciences 34, 1149-1152.
- Verver, G., Raes, F., Vogelezang, D., Johnson, D., 2000. The 2nd aerosol characterization experiment (ACE-2): Meteorological and chemical context. Tellus B 52.
- Wang, J., Christopher, S.A., 2003. Intercomparison between satellite-derived aerosol optical thickness and PM2. 5 mass: implications for air quality studies. Geophysical research letters 30.
- Yu, H., Kaufman, Y., Chin, M., Feingold, G., Remer, L., Anderson, T., Balkanski, Y., Bellouin, N., Boucher, O., Christopher, S., 2006. A review of measurement-based assessments of the aerosol direct radiative effect and forcing. Atmospheric Chemistry and Physics 6, 613-666.
- Zhang, H., Hoff, R.M., Engel-Cox, J.A., 2009. The relation between Moderate Resolution Imaging Spectroradiometer (MODIS) aerosol optical depth and PM2. 5 over the United States: a geographical comparison by US Environmental Protection Agency regions. Journal of the Air & Waste Management Association 59, 1358-1369.

Science of the Total Environment 550 (2016) 994–1000

Contents lists available at ScienceDirect

Science of the Total Environment

journal homepage: www.elsevier.com/locate/scitotenv

Quantifying enhancement in aerosol radiative forcing during 'extreme aerosol days' in summer at Delhi National Capital Region, India

Sumant Kumar [a], Sagnik Dey [b,*], Arun Srivastava [a]

[a] School of Environmental Sciences, Jawaharlal Nehru University, New Delhi 110067, India
[b] Centre for Atmospheric Sciences, IIT Delhi, New Delhi 110016, India

HIGHLIGHTS

- Change in aerosol forcing in 'extreme' aerosol days at Delhi are quantified.
- Mean AOD increases >107% during the 'extreme' aerosol days.
- Coarse-mode dust is the dominant (70.8%) contributor to AOD during 'extreme' days.
- Aerosol-induced heating rate increased by 75.1% from 1.7 K/day to 2.96 K/day.

GRAPHICAL ABSTRACT

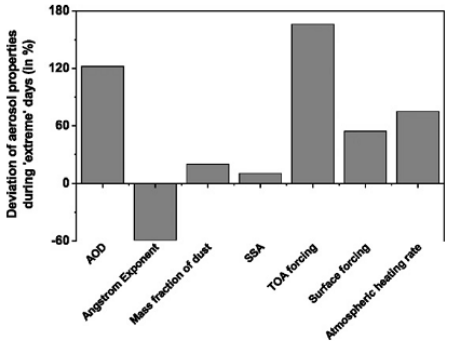

Deviation (in %) of aerosol properties from 'relatively clean' days to 'extreme' aerosol days.

ARTICLE INFO

Article history:
Received 11 November 2015
Received in revised form 13 January 2016
Accepted 27 January 2016
Available online 6 February 2016

Editor: D. Barcelo

Keywords:
Aerosol radiative forcing
Extreme aerosol events
Delhi NCR

ABSTRACT

Changes in aerosol characteristics (spectral aerosol optical depth, AOD and composition) are examined during the transition from 'relatively clean' to 'extreme' aerosol days in the summer of 2012 at Delhi National Capital Region (NCR), India. AOD smaller than 0.54 (i.e. 12-year mean AOD $-$ 1σ) represents 'relatively clean' days in Delhi during the summer. 'Extreme' days are defined by the condition when $AOD_{0.5}$ exceeds 12-year mean AOD + 1 standard deviation (σ). Mean ($\pm 1\sigma$) AOD increases to 1.2 $\pm$ 0.12 along with a decrease of Angstrom Exponent from 0.54 $\pm$ 0.09 to 0.22 $\pm$ 0.12 during the 'extreme' days. Aerosol composition is inferred by fixing the number concentrations of various individual species through iterative tweaking when simulated (following Mie theory) AOD spectrum matches with the measured one. Contribution of coarse mode dust to aerosol mass increased from 76.8% (relatively clean) to 96.8% (extreme events), while the corresponding contributions to $AOD_{0.5}$ increased from 35.0% to 70.8%. Spectrally increasing single scattering albedo (SSA) and CALIPSO aerosol sub-type information support the dominant presence of dust during the 'extreme' aerosol days. Aerosol direct radiative forcing (ADRF) at the top-of-the-atmosphere increases from 21.2 W m^{-2} (relatively clean) to 56.6 W m^{-2} (extreme), while the corresponding change in surface ADRF is from -99.5 W m^{-2} to -153.5 W m^{-2}. Coarse mode dust contributes 60.3% of the observed surface ADRF during the 'extreme' days. On the contrary, 0.4% mass fraction of black carbon (BC) translates into 13.1% contribution to $AOD_{0.5}$ and 33.5% to surface ADRF during the 'extreme' days. The atmospheric heating rate increased by 75.1% from 1.7 K/day to 2.96 K/day during the 'extreme' days.

* Corresponding author.

http://dx.doi.org/10.1016/j.scitotenv.2016.01.191
0048-9697/